NTNU – Trondheim
Norwegian University of
Science and Technology

The UNIS Borehole Jack;

Description, fieldwork and new classification system

Joar Aspenes Justad

Civil and Environmental Engineering
Submission date: June 2012
Supervisor: Knut Vilhelm Høyland, BAT

Norwegian University of Science and Technology
Department of Civil and Transport Engineering

NORWEGIAN UNIVERSITY OF SCIENCE AND TECHNOLOGY
DEPARTMENT OF CIVIL AND TRANSPORT ENGINEERING

Report Title: The UNIS Borehole Jack; Description, fieldwork and new classification system	Date:10.06.12 Number of pages (incl. appendices): 114			
	Master Thesis	X	Project Work	
Name: Joar Aspenes Justad				
Professor in charge/supervisor: Knut V. Høyland				
Other external professional contacts/supervisors:				

Abstract:

The increasing interest in the Arctic region due to exploitation of natural resources requires methods for estimating design loads on offshore structures. The borehole jack (BHJ) is an ISO approved tool for assessing the in-situ confined compressive strength of ice. On request from the Norwegian University of Science and Technology (NTNU), a BHJ was made by M-Tech and delivered to the University Centre in Svalbard (UNIS) in 2010. This work presents a technical description of the UNIS-BHJ as well as calibration instructions and experimental setup. A classification system of stress – time curves has been developed with focus on post-peak stress behavior. Three field campaigns have been conducted, two in Van Mijenfjorden (first-year level ice) and one in the Barents Sea (young and rafted ice) in March and April 2012. The new classification system proved convenient when used for classifying the results of these experiments. An advantage is that the system is applicable for all BHJs, hence allowing comparisons of different works to be made regardless of the BHJ used. Investigations of the spatial variation of borehole (BH) strength were also done. Sampling areas of sizes 100 by 100 m and 10 by 10 meters were established in Van Mijenfjorden, where both concluded mean BH strength of 16.8 MPa with STD of the larger area 1.9 MPa and the smaller 0.3 MPa. Another three sampling areas of sizes 20 by 20, 4 by 4 and 4 by 4 m were established in the Barents Sea, with BH strengths 13.0, 11.1 and 14.0 MPa and STDs 3.2, 2.0 and 2.4 MPa.

Keywords:

1. Borehole jack
2. Classification system
3. Technical description
4. Spatial variation

NTNU
Fakultet for ingeniørvitenskap og teknologi
Institutt for bygg, anlegg og transport

MASTER DEGREE THESIS

Spring 2012
for
Joar Aspenes Justad

The UNIS Borehole Jack;
Description, fieldwork and new classification system

BACKGROUND

In 2010 M-Tech made a uniquely designed borehole jack (BHJ) on request from NTNU. It was handed over to the University Centre in Svalbard (UNIS) to be used as a tool for education and research purposes at the Department of Arctic Technology. A thorough study of the UNIS-BHJ has not been done before, and this work is therefore its first comprehensive evaluation.

TASK DESCRIPTION

With an increasing interest in the Arctic due to exploitation of natural resources, the necessity of calculating the design loads of ice-structure interaction becomes essential. The borehole jack (BHJ) is an ISO approved tool for assessing the confined compressive strength of ice. Such a device was made by M-Tech on request from NTNU in 2010. Justad is to give a technical description of the BHJ as well as calibration instructions and experimental setup. A refinement of an existing classification system for analyzing and interpreting the results is to be developed. Justad is further to conduct field work on Svalbard, in Van Mijenfjorden in March and in the Barents Sea in April. The results are to be discussed and classified according to the new suggested classification system. Finally, recommendations for further work both regarding improvements of the BHJ and interpretation of data will be addressed.

General about content, work and presentation

The text for the master thesis is meant as a framework for the work of the candidate. Adjustments might be done as the work progresses. Tentative changes must be done in cooperation and agreement with the professor in charge at the Department.

In the evaluation thoroughness in the work will be emphasized, as will be documentation of independence in assessments and conclusions. Furthermore the presentation (report) should be well organized and edited; providing clear, precise and orderly descriptions without being unnecessary voluminous.

The report shall include:

- Standard report front page (from DAIM, http://daim.idi.ntnu.no/)

- Title page with abstract and keywords.(template on: http://www.ntnu.no/bat/skjemabank)
- Preface
- Summary and acknowledgement. The summary shall include the objectives of the work, explain how the work has been conducted, present the main results achieved and give the main conclusions of the work.
- Table of content including list of figures, tables, enclosures and appendices.
- If useful and applicable a list explaining important terms and abbreviations should be included.
- The main text.
- Clear and complete references to material used, both in text and figures/tables. This also applies for personal and/or oral communication and information.
- Text of the Thesis (these pages) signed by professor in charge as Attachment 1.
- The report musts have a complete page numbering.

Advice and guidelines for writing of the report is given in: "Writing Reports" by Øivind Arntsen. Additional information on report writing is found in "Råd og retningslinjer for rapportskriving ved prosjekt og masteroppgave ved Institutt for bygg, anlegg og transport" (In Norwegian). Both are posted on http://www.ntnu.no/bat/skjemabank

Submission procedure

Procedures relating to the submission of the thesis are described in DAIM (http://daim.idi.ntnu.no/). Printing of the thesis is ordered through DAIM directly to Skipnes Printing delivering the printed paper to the department office 2-4 days later. The department will pay for 3 copies, of which the institute retains two copies. Additional copies must be paid for by the candidate / external partner.

On submission of the thesis the candidate shall submit a CD with the paper in digital form in pdf and Word version, the underlying material (such as data collection) in digital form (eg. Excel). Students must submit the submission form (from DAIM) where both the Ark-Bibl in SBI and Public Services (Building Safety) of SB II has signed the form. The submission form including the appropriate signatures must be signed by the department office before the form is delivered Faculty Office.

Documentation collected during the work, with support from the Department, shall be handed in to the Department together with the report.

According to the current laws and regulations at NTNU, the report is the property of NTNU. The report and associated results can only be used following approval from NTNU (and external cooperation partner if applicable). The Department has the right to make use of the results from the work as if conducted by a Department employee, as long as other arrangements are not agreed upon beforehand.

Tentative agreement on external supervision, work outside NTNU, economic support etc.
Separate description to be developed, if and when applicable. See http://www.ntnu.no/bat/skjemabank for agreement forms.

Health, environment and safety (HSE) http://www.ntnu.edu/hse
NTNU emphasizes the safety for the individual employee and student. The individual safety shall be in the forefront and no one shall take unnecessary chances in carrying out the work. In particular, if the student is to participate in field work, visits, field courses, excursions etc. during the Master Thesis work, he/she shall make himself/herself familiar with " Fieldwork HSE

Guidelines". The document is found on the NTNU HMS-pages at
http://www.ntnu.no/hms/retningslinjer/HMSR07E.pdf

The students do not have a full insurance coverage as a student at NTNU. If you as a student want the same insurance coverage as the employees at the university, you must take out individual travel and personal injury insurance.

Start and submission deadlines
The work on the Master Thesis starts on January 16, 2012

The thesis report as described above shall be submitted digitally in DAIM at the latest at 3pm June 11, 2012

Professor in charge: Knut V. Høyland

Other supervisors:

Trondheim, January 16, 2012. (revised: 11.06.2012)

_____
Professor in charge (sign)

Preface

This paper is the result of the last 20 weeks of effort put into the 5 years Master's Degree Program at the Department of Civil and Transport Engineering at NTNU. In collaboration with UNIS the fieldwork and the majority of report writing have been done on Svalbard.

The purpose of the work is to give students of Arctic Technology an introduction to the UNIS-BHJ. It will act as a reference point when it comes to technical description, calibration and experimental setup. Fieldwork data was collected in Van Mijenfjorden and in the Barents Sea during March and April and the results are analyzed based on a classification system introduced in the paper. The BHJ has been in UNIS' possession since 2010, but never thoroughly studied. The need for a reference work that could be utilized by students was therefore required, and this paper is the result.

I thank R. Yulmetov for helping with the calibration of the UNIS-BHJ and the students and supervisors of AT307f and AT208 who assisted in BHJ testing and collecting valuable data for the thesis. A special thanks to P. Kildahl and K. Sigbjørnsen for their good spirits and help in both Van Mijenfjorden and the Barents Sea. Thanks also to the crew aboard R/V Lance for their hospitality on the voyage to (and from) the Barents Sea and the Logistics at UNIS for providing equipment and snowmobiles. Thanks also to O. C. Ekeberg for explaining how the UNIS-BHJ works and C. Lønøy for allowing me to develop his Matlab scripts. I would further like to acknowledge the support from the SAMCoT CRI through the Research Council of Norway and all the SAMCoT partners. Last but not least, thanks to K. V. Høyland for the interesting discussions and giving me the opportunity to live and work in the Arctic.

Trondheim, June 10th, 2012

Joar A. Justad

Abstract

The increasing interest in the Arctic region due to exploitation of natural resources requires methods for estimating design loads on offshore structures. The borehole jack (BHJ) is an ISO approved tool for assessing the in-situ confined compressive strength of ice. On request from the Norwegian University of Science and Technology (NTNU), a BHJ was made by M-Tech and delivered to the University Centre in Svalbard (UNIS) in 2010. This work presents a technical description of the UNIS-BHJ as well as calibration instructions and experimental setup. A classification system of stress – time curves has been developed with focus on post-peak stress behavior. Three field campaigns have been conducted, two in Van Mijenfjorden (first-year level ice) and one in the Barents Sea (young and rafted ice) in March and April 2012. The new classification system proved convenient when used for classifying the results of these experiments. An advantage is that the system is applicable for all BHJs, hence allowing comparisons of different works to be made regardless of the BHJ used. Investigations of the spatial variation of borehole (BH) strength were also done. Sampling areas of sizes 100 by 100 m and 10 by 10 meters were established in Van Mijenfjorden, where both concluded mean BH strength of 16.8 MPa with STD of the larger area 1.9 MPa and the smaller 0.3 MPa. Another three sampling areas of sizes 20 by 20, 4 by 4 and 4 by 4 m were established in the Barents Sea, with BH strengths 13.0, 11.1 and 14.0 MPa and STDs 3.2, 2.0 and 2.4 MPa.

Sammendrag

En økende interesse i Arktiske områder på grunn av naturressurser krever forbedret kunnskap for å dimensjonere laster på offshore konstruksjoner. Borehullsjekken (BHJ) er et ISO godkjent verktøy for å beregne in-situ kompresjonssyrk av is. I 2010 leverte M-Tech en BHJ til Universitetssenteret på Svalbard (UNIS) på oppdrag fra Norges Teknisk Naturvitenskapelige Universitet (NTNU). Dette arbeidet gir en presentasjon av UNIS'-BHJ i form av en teknisk beskrivelse, instrukser for kalibrering og eksperimentelt oppsett. Tre fetlarbeid har blitt gjort, hvorav to i Van Mijenfjorden (førsteårs-flat is) og ett i Barentshavet (ung og skrudd is) iløpet av mars og april 2012. Det nye klassifikasjonssystemet viste seg å være beleilig da det ble brukt for å klassifisere resultatene fra feltarbeidene. En fordel med systemet er at det er anvendelig for alle BHJer og at det derfor tillater sammenligninger av resultater uavhengig av hvilken BHJ som ble brukt. Undersøkelser av romlig variasjon av borehullsstyrken (BH-styrken) ble også gjort. Prøvetakingsområder av størrelser 100 ganger 100 m og 10 ganger 10 m ble opprettet i Van Mijenfjorden, hvor begge konkluderte med gjennomsnittlig BH-styrke på 16.8 MPa og STD for det større området på 1.9 MPa og det mindre 0.3 MPa. Enda tre prøvetakingsområder av størrelser 20 ganger 20, 4 ganger 4 og 4 ganger 4 m ble opprettet i Barentshavet med BH-styrker 13.0, 11.1 og 14.0 MPa og STD 3.2, 2.0 og 2.4 MPa.

Contents

List of Figures

List of Tables

Nomenclature

Abbreviations

AARI	Arctic and Antarctic Research Institution
AS	Asymptotic
AT208	Thermo-Mechanical Properties of Materials, Undergraduate course at UNIS
AT307f	Arctic Offshore Engineering fieldwork, Graduate course at UNIS
BH	Borehole
BHJ	Borehole jack
c	perfect-plastic
C_{min}	Minimal vertical confinement
e	elastic
FB	Freeboard
FS	Flow stress
FT	Failure type
FYLI	First-year level ice
h	hardening plasticity
h_i	Ice thickness
h_s	Snow depth
ID	Indentor depth
LVDT	Linear variable displacement transducer
NRC	National Research Council
NTNU	Norwegian University of Science and Technology
NPI	Norwegian Polar Institute
P	Premature
s	softening plasticity
STD	Standard deviation
T	Temperature
t_f	Time to failure
UNIS	University Centre in Svalbard
UY	Upper yield
U/D	Indentation rate

Greek symbols

σ	Stress
$\dot{\sigma}_{af}$	Average stress rate to failure
σ_f	Failure stress
$\frac{d\sigma}{dt}$	Stress rate

1 Introduction

The University Centre in Svalbard (UNIS) is located in Longyearbyen at 78.2°N, 15.3°E, making a perfect springboard for fieldwork in the Arctic. It was founded in 1993 based on the idea of bringing classrooms into nature and introduces 350 students yearly to the waste nature of the Svalbard archipelago. Snow mobile trips to Van Mijenfjorden are done in both undergraduate and graduate courses as the fjord traditionally provides reliable fieldwork conditions. Collaborating with the Norwegian Polar Institute (NPI), UNIS students are also invited to join the research vessel R/V Lance's yearly expeditions to the Barents Sea. Figure 1 shows the location of Svalbard among other European Arctic islands and seas.

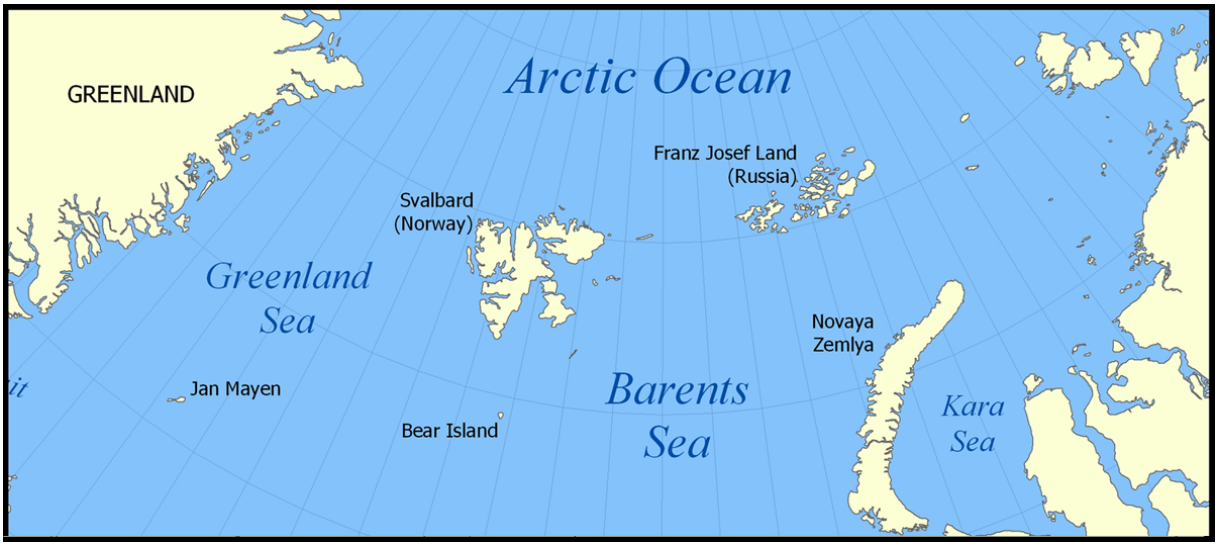

Figure 1: Map of the European Arctic islands and seas (Norman Einstein, 2012).

With the increased activity in the Arctic regions due to the exploitation of natural resources and a growing interest for the shipping route through the North East Passage, the necessity of understanding the designing loads on offshore structures and vessels becomes essential. Extensive testing on the unconfined compressive strength of ice has been done in laboratory and its behavior under controlled boundary conditions is therefore well understood. However, the unconfined strength of ice found in laboratories may not carry the properties of what is encountered in nature, hence the need for investigate the in-situ confined compressive strength, also referred to as the borehole (BH) strength. This parameter can be obtained through a borehole jack (BHJ) experiment.

In short, a BHJ works as follows; a hole is drilled in the ice in which a piston is lowered to a desired test depth. An electric motor runs a hydraulic pump, which in turn provides an oil pressure to the piston that compresses the ice. Pressure, displacement and time are recorded throughout the experiment.

Today, the unconfined strength is considered a reference parameter in ISO/DIS 19906:2010 Petroleum and natural gas industries standard - Arctic offshore structures, where it is proposed that the BH strength is 3 times greater than the unconfined strength. It further claims that this parameter varies between 2 and 4, though in other papers reported to reach a value of 5 (Shkhinek et al., 2010). Traditionally the BH strength has been obtained at certain displace-

ments or the greatest stress (σ) recorded during indentation. A classification system that distinguishes between the different stress - time curves, and consequently also different ice features, may contribute to a reduction of the unconfined and BH strength ratio. By implication this means introducing one parameter for each ice feature.

The purpose of this work is primarily to provide a guideline for students working with the BHJ at UNIS in terms of;

1. A technical description
2. Experimental setup
3. Calibration
4. Provide relevant theory on ice mechanics and physics and interpretation of BHJ data
5. Introducing a quantitative development of the classification system established by Sinha (2011), which was recently agreed upon by the National Research Council (NRC), Canada and Arctic and Antarctic Research Institute (AARI), Russia as a suitable approach for classifying BHJ records.

Secondarily, data collected in Van Mijenfjorden and the Barents Sea in March and April 2012 have been classified by the system in 6) and thus becomes the first test of its applicability. Finally, the report gives recommendations on possible improvements of 6) and the mechanical components of the UNIS-BHJ.

The interest of finding the BH strength of ice emerged in the early 1970s as oil and gas companies encountered ice loads in search for offshore reservoirs in the Canadian Arctic. From a Norwegian perspective, the activity in the Barents Sea is expected an increase after the agreement on the Grey Zone issue with Russia in April 2010 along with major findings of oil reservoirs in the Barents Sea; Skrugard in April 2011 and Havis in January 2012. Another aspect is the expected shipping growth through the North East Passage. A realization of a trade route here will require emergency stations and lighthouses along the northern coastline of Russia designed for coping with ice actions.

As temperature, salinity and crystal structure of ice changes with depth, so does its strength. An instrument capable of measuring the confined strength throughout an ice sheet emerged as a consequence of the exploration of the Canadian Arctic, and in 1971 the first approach of finding the BH strength was made by Dr. Hans Kivisild (Masterson and Graham, 1994). Originally designed for obtaining the strength and stiffness of soil, the Menard pressure meter turned out to have insufficient capacity when exerted in ice. However, the principle of applying an hydraulic pressure to a BH wall, see Figure 2, turned out to be a step in the right direction. Later, the Goodman Jack was adopted from the field of rock mechanics where it had proven a successful tool. As the stiffness of rock is significantly greater than that of ice, and thus fails at an earlier stage, the jack did not deliver the displacement necessary for ice to fail. However, its capacity of 70 MPa was found adequate. Figure 3 shows the principles of the Goodman Jack where linear variable displacement transducers (LVDTs) are used to record the displacement of the indentors. In 1974 the original BHJ was made, see Figure 4. The potentiometer used as displacement sensor was first installed on top of the BHJ, but was in later versions mounted inside for better protection. The BHJ was designed to fit a 150 mm BH and deliver a total displacement of 50 mm using two indentors, which proved sufficient for observing ice failure. Later

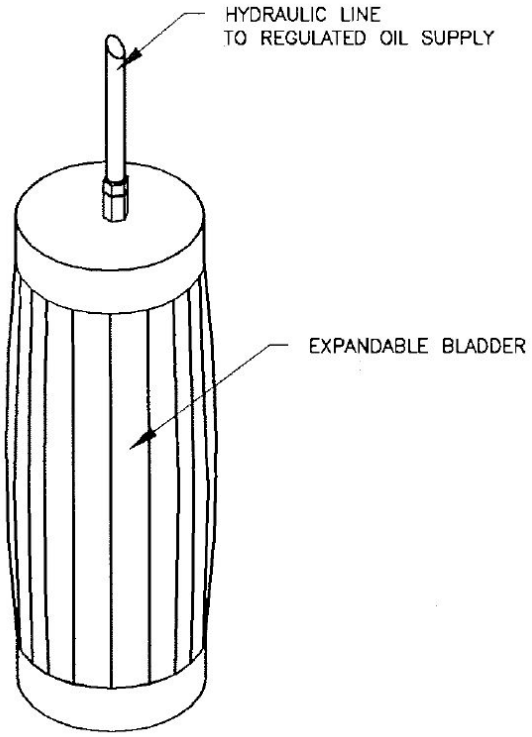

Figure 2: Pressure meter from Masterson and Graham (1994).

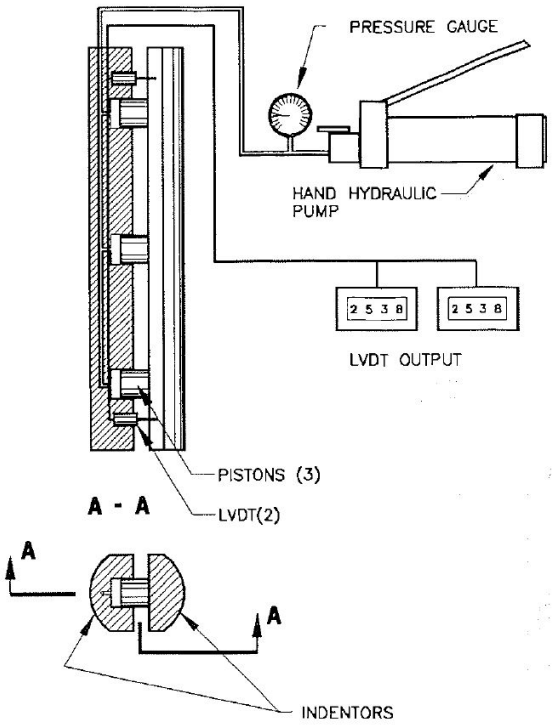

Figure 3: Goodman Jack from Masterson and Graham (1994).

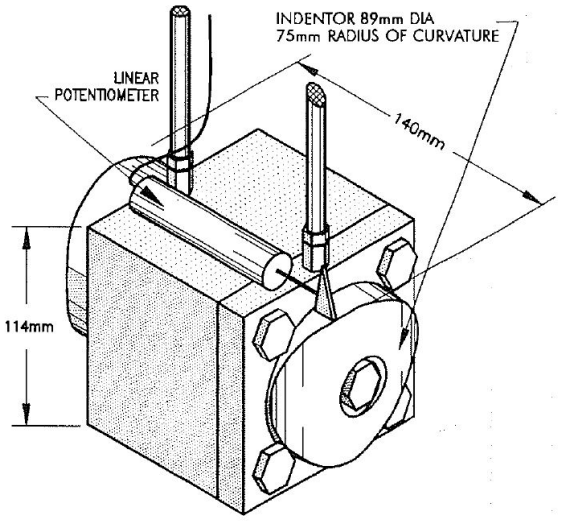

Figure 4: Original BHJ from Masterson and Graham (1994).

improvements have been made and these rely mostly on the design of the equipment, the hydraulic system and improvements of pressure and displacement sensors.

Today, there are a number of BHJs operating in the Arctic with differences on e.g. indentor area and curvature, indentation rate, pump capacity, design, etc. In principle, this implies that data obtained with the various tools is not directly comparable.

A part of the fieldwork was conducted in young sea ice (ice thickness less than 30 cm (Sinha, Shkhinek and Smirnov, 2012)) in the Barents Sea, where the ice thickness was about 20 cm for a significant number of tests. This means that full confinement was not achieved for all tests, and consequently, the term BH strength does not apply and failure stress is therefore used instead. In these tests radial cracking and especially spalling failures were observed frequently, which are typical failure modes observed in ice-structure interaction, see

Figure 5. The failure modes are mainly depending on two factors; aspect ratio, which is ice thickness (h_i) divided by the width of the structure, and the indentation rate (U/D)), velocity of the ice floe divided by the width of the structure. What is comparable to a BHJ test are the parameters ice thickness and velocity of the ice floe (which is equivalent to the velocity of the indentor). The latter is not entirely correct for the UNIS-BHJ since its indentor velocity changes with the stiffness and strength of the ice throughout the experiment. The last parameter, structure width, does not relate to BHJ testing, and direct comparisons between ice-structure and BHJ tests (though both are indentation tests) cannot be made. Typical for radial cracking is high aspect ratios. Spalling failure occurs for low aspect ratios and high indentation rates, where fragments of the ice break upwards and downwards as a result of horizontal cracks growing away from the contact surface.

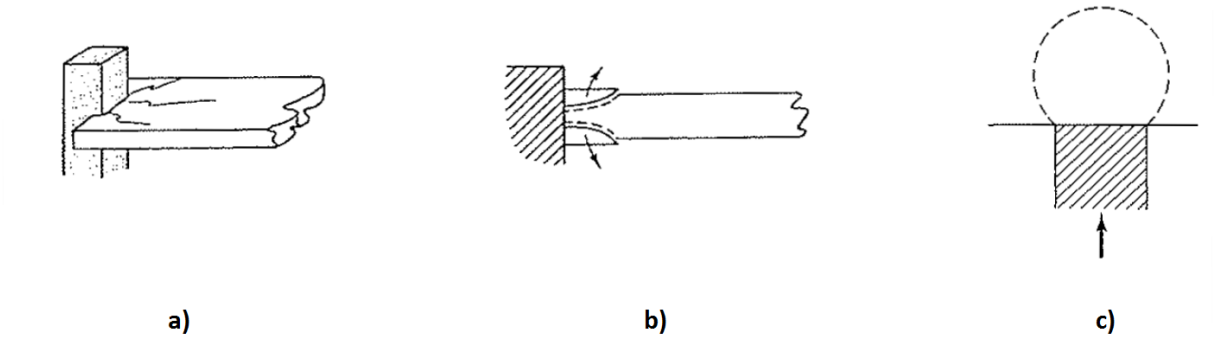

Figure 5: Radial cracking a), vertical b) and horizontal cross-section spalling c) failure modes from Sanderson (1988).

The following list presents possible sources of error and assumptions that were necessary to make upon interpretation of the data presented in this paper;

- The fieldworks in Van Mijenfjorden and Barents Sea were done with first-year UNIS students, from who the data regarding salinity and density of the ice is measured and calculated. Density is a property that has proven difficult to measure accurately. The ice cores are cut by a saw before weighed and dimensions are measured. The sawing process is difficult in the sense that the edges should be parallel to each other and perpendicular to the core center axis. Once the core is extracted from its natural environment it will be affected by e.g. air temperature, sun light and salt drainage. Consequently, the measurements will differ to some extent from what are the original qualities of the ice. Temperature measurements are considered more accurate as there are less sources of error here. With that said, a number of measurements have been done, and indications of the properties of the ice in the area are presented.

- A calibration of the BHJ was done before the field season started and pressure (stress) recordings are therefore considered accurate.

- The fact that the displacement sensor is defect means that indentation was not recorded for any of the tests, which is a major limitation to the processing of the data. In fact,

the average displacement rate to failure is considered the most appropriate quantity to be used for analysis of BHJ records (Sinha, 2011). The data processed in this paper rely only on the two remaining parameters, pressure and time. Though valuable information is omitted, a thorough analyze of stress development with time becomes feasible.

- Another limiting factor is the capacity of the hydraulic system of the UNIS-BHJ, which allows a maximal stress of 18.5 MPa to be induced to the ice.
- The pressure transducer in the UNIS-BHJ calculates the imposed force to/from the indentor. The interpretation of the data is often based on the stress development, which is simply the force divided by the initial contact area. This involves that a reduction in contact area, which was frequently observed in spalling failures, has not been accounted for.
- Stress is calculated from the projected area of the indentor, while the true contact area is slightly larger due to the curvature of the indentor. The difference is considered negligible.
- Shear forces acting on the indentor sides are also considered negligible.
- Grain structure relies only on field investigations, and precise assessments are therefore not available.
- Where the ice thickness was less than 30 cm the jack needed to be held above the ice surface to get the test depth in the center of the floe. The accuracy is estimated to ± 1 cm.
- The vertical confinement of the ice is assumed uniform through the ice floe.
- The pressure has been logged with a frequency of 5 Hz for all results presented in this paper.

2 Equipment

Until 2008 UNIS operated with a dual indentor BHJ that had pistons moving in opposite directions, similar to the original BHJ shown in Figure 4. Unfortunately, the BHJ turned out inconvenient to use as it often got stuck in the borehole. A new BHJ was therefore requested by the Norwegian University of Science and Technology (NTNU), and the task was appointed to M-Tech in Trondheim. As new students are introduced to the BHJ yearly and often use it no more than 10 days in season, certain demands were made to the new BHJ system; 1) it needed to be easily operated, 2) practical and reliable of use in cold temperatures and 3) provide accurate data on the BH strength. Finished in 2010, the result was a 100 kg box of steel containing a uniquely designed BHJ for coping with the Arctic environment. Figure 6 shows the UNIS-BHJ with accompanying equipment on test location.

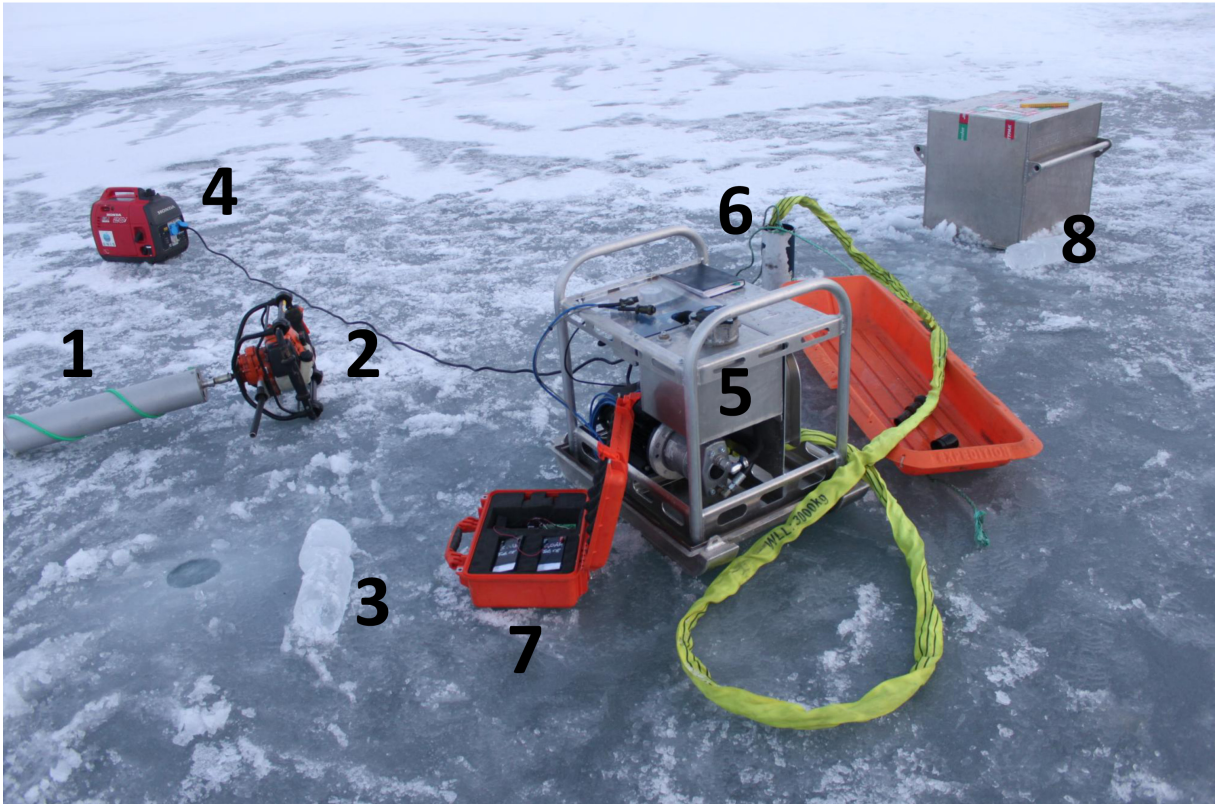

Figure 6: Equipment on test location; 1) 150 mm core drill, 2) Stihl engine, 3) extracted ice core, 4) generator of 2.0 kWh, 5) electric motor and hydraulic pump, 6) “the jack”, a cylinder house containing piston with indentor and displacement sensor, 7) CR1000 Wiring Panel (transducer) with two 12 V batteries and 8) steel cover.

A BHJ experiment is normally conducted by a crew of two persons, but a larger crew may be necessary depending on the ice conditions to be worked in. For example, if an experiment takes place in the sail of an ice ridge, the equipment needs to be carried over blocks of ice and thus more manpower is required. The electric motor and hydraulic pump is mounted on skies, see Figure 9, and the UNIS-BHJ is therefore conveniently handled on level ice between BHs. The steel cover also ensures that snow and water do not enter the electric system and offers

protection when transported for longer distances. This is normally done by snowmobile using a sledge or by a vessel. Transportation by helicopter is not tested yet, but is also a possibility.

The motor requires a power supply of 230 V which is usually provided by a generator with a capacity of 3.6 kWh. This is a generator of significant size and weight and will need transportation by sledge between BHs if extension cords do not reach. Generators of less capacity have been used earlier with limited success in fresh water ice and should be avoided. The power supply may also come directly from a vessel if moored nearby.

The indentor is connected to the piston by bolts, initially leaving holes in the indentor surface. These are filled with silicon in order to obtain a smooth surface, which is important because the roughness of the contact area is one of many factors influencing on the failure mode, and in turn the BH strength. The protective cylinder, piston and indentor are often referred to as "the jack". The jack is connected to the hydraulic pump and the electric system on the surface through a 5 m Kevlar hose, in which the oil tubes and wire for the displacement sensor are located. The length of the hose limits the depth an experiment can be conducted to approximately 4 m. However, as the diameter of the BH only exceeds that of the cylinder by 10 mm, one should be careful at such depths as snow, ice and inaccurate drilling may cause the jack to get stuck.

The piston extracts and retracts as the operator uses a lever to control the oil pressure, see Figures 7 and 8. It has a maximal displacement of 50 mm and is protected by a steel cylinder with outer diameter 140 mm, height 303 mm and wall thickness 5 mm. The indentor itself matches the curvature of the cylinder and has a projected area of 6.36 x 10^3 mm^2, which is significantly less than the opposing cylinder wall. Hence, penetration in the desired direction is assured.

Figure 7: The jack with piston fully retracted.

Figure 8: The jack with piston fully extracted, 50 mm.

There are two pressure gauges mounted in the hydraulic system; a manual reading gauge on the control panel of the BHJ and a digital sensor connected to the transducer. The former provides pressure in the hydraulic system in bar, and the latter raw pressure and pressure on the indentor in mV. Figure 10 gives a view top down on the BHJ control panel with the manual

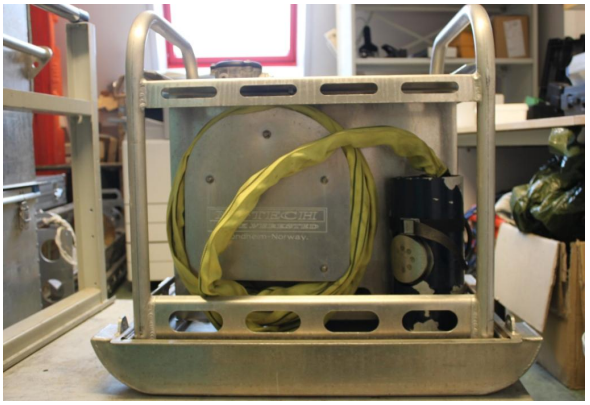

Figure 9: The jack in position during transportation and the bottom acts as a sledge.

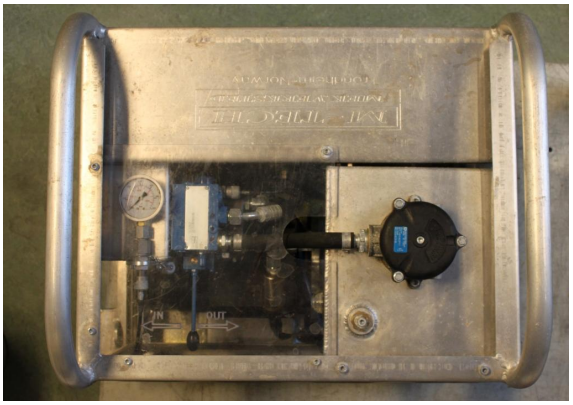

Figure 10: The control panel of the BHJ with manual pressure gauge and lever.

pressure gauge and flow control lever. The displacement sensor is located in the jack connected to the piston. When the CR1000KD (digital display) is connected to the CR1000 Wiring Panel (transducer), see Figure 11 and 12, the operator is able to read the recorded pressure and displacement while running the test. Otherwise, he or she has to rely solely on the manual reading pressure gauge. The CR1000KD and CR1000 Wiring Panel are products of Campbell Scientific Inc., and have usually been logging with a frequency of 5 Hz. The frequency can be changed and increased to a maximal value of 50 Hz when programming the transducer. The data is obtained using the PC200W software installed on field laptops of UNIS.

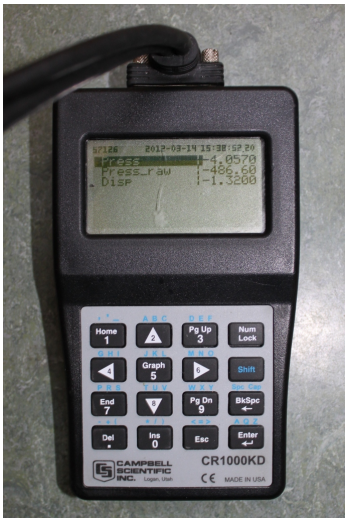

Figure 11: CR1000KD (digital display).

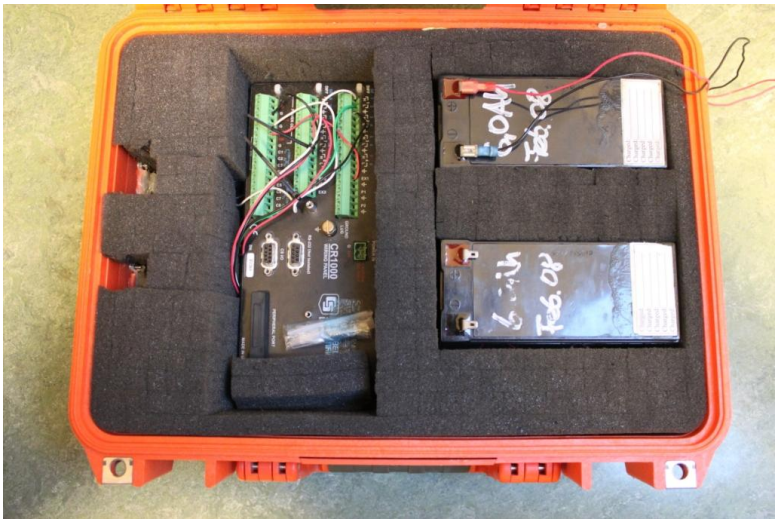

Figure 12: CR1000 Wiring Panel (transducer) with two batteries of 12 V in a shockproof suitcase.

The hydraulic pump is a product of Hawe Hydraulic with a capacity of 2.02 cm^3/U. The time it takes the piston to go from 0 to 50 mm in air is 7.5 seconds. Its maximal velocity is therefore estimated to 6.7 mm/s, equivalent to an ice flow moving at 0.007 m/s. A safety valve is mounted in the hydraulic system to ensure that the pressure does not exceed 300 bar, corresponding to a raw pressure of 2150 mV. The limitation is given by the rubber tubes, where higher pressures

may cause punctures. In order to ensure the safety of the students, a Kevlar hose encloses the rubber tubes (and the wire for the displacement sensor). It has been questioned if the viscosity of the oil changes with low outdoor temperatures or high pressures during testing, and thus leads to corrupted pressure recordings. This has been refused by Scharffcher and Scharffcher (2012), as its viscosity is unchanged down to -45°C and: "A significant number of tests is required to heat the oil so that its viscosity changes." A simplified sketch of the UNIS-BHJ is shown in Figure 13.

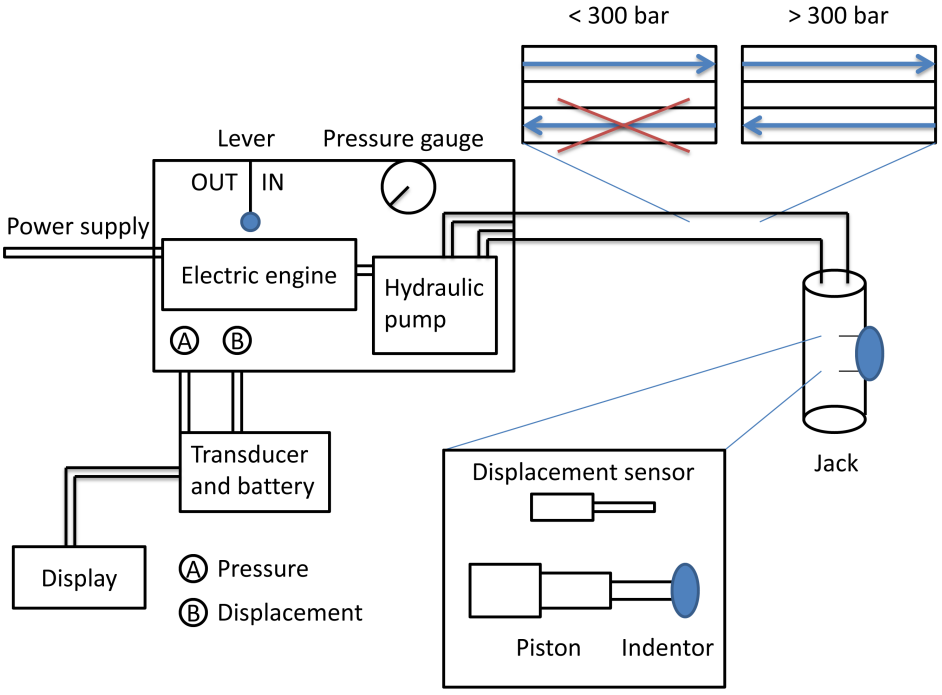

Figure 13: A simplified version of the UNIS-BHJ. The pressure and displacement recordings through connectors A and B are done in mV. It is seen that the safety valve allows backflow of the oil when the pressure exceeds 300 bar.

3 Experimental setup

A full check-list of all necessary equipment for conducting and simplifying a BHJ test is given in Appendix A. A borehole is normally made using a core drill of 15 cm in diameter and 70 cm long which is connected to a Stihl engine, seen as 1) and 2) in Figure 6. The two-stroke engine runs on gasoline mixed with 2% oil and has proven reliable even at low temperatures. Extensions are necessary if the ice exceeds the length of the core drill. For thick ice, as encountered in e.g. ice ridges, it has proven difficult to extract the core. An auger may here be used instead, but will cause loss of valuable data on the properties of the ice as these are measured from the extracted core. The BH is normally drilled in matter of minutes, depending on ice thickness, ice temperature (T), snow depth (h_s) etc. It is however not necessary to drill all the way through the ice sheet. In fact, leaving some ice in the bottom will delay water from entering the hole. The thermal regime of the ice is altered by the water (Sinha, 2011) and is therefore better left out. One wants to have a minimal change in the environment, so the tests should be carried out as quickly as possible after drilling. In case a core is stuck in the BH, pincers and iron bar are useful tools for extraction. The iron bar is used to put a moment on the core and break it loose, and an axe can be used to make cuts in the ice surrounding the BH in order get a grip with the pincers.

Ice temperature, density and salinity affect the mechanical properties of ice. These are parameters that ideally should be measured for each core, but turn out to be given lower priorities as they are more time demanding than the mechanical test. Nevertheless, at least one core within each site should provide information on these parameters. A visual inspection of the core may also give valuable information on the crystal structure and porosity. It also gives the crew the possibility to some extent choose the properties of the ice of which they are testing, by deciding at what depth the test is run. Further, ice thickness, freeboard (FB) and snow depth are of interest. These are parameters found quickly and should be measured for each BH. Bringing cores back to the laboratory for a more thorough investigation on the crystal structure is also of great interest. Figure 14 shows a vertical cross-section of the ice when the drilling is finished. Frederking and Johnston (2002) used a wooden plank, or "straight edge", on top of the BH to measure the freeboard more accurately.

Using pressure sensors in the ice, Barrault and Strub-Klein (2009) concluded that the pressure drops by 98% in a horizontal distance 0.6 m from test location. Therefore, in order preserve the horizontal confinement of the ice, BHs are drilled with a minimum spacing of 1.5 m as recommended by Sinha (2011). If the ice is sufficiently thick, several tests can be conducted in the same hole. A minimum vertical spacing of 37 cm is assumed necessary to ensure full confinement for all tests. For the same reason, this is considered the minimum distance from the indentor center to the ice surface and bottom. Consequently, the ice should have a thickness of at least 74 cm for performing one test, 111 cm for two, and so on.

The first tests at every site should be conducted in air to make sure that the equipment works properly. Here, the deviation (if any) between recorded and manually measured displacement can be found. If the difference turns out to be significant, a dry test may need to be done between each proper one. Such tests were done by Ekeberg and Shestov (2011) and provided valuable information on the displacement recordings on that expedition.

Once a BH is drilled, the jack is lowered by a chain to the desired test depth, often referred to as indentor depth (ID). The Kevlar hose should be kept as straight as possible since every

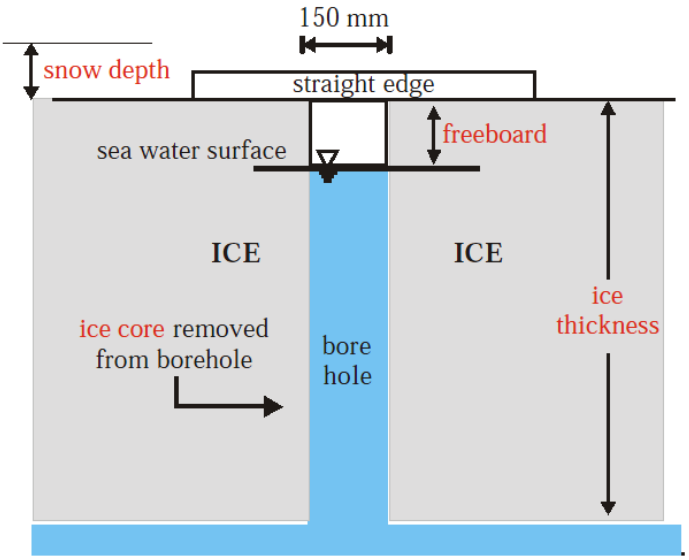

Figure 14: Vertical cross-section of a BHJ test location (Frederking and Johnston, 2002).

turn and twist will cause a drop in the oil pressure, which in turn corrupts the data recorded on indentor pressure (Scharffcher and Scharffcher, 2012). At this point the electric motor can be started and the transducer is ensured connected its battery and the BHJ properly.

The lever has three positions; neutral, *OUT* and *IN*, see also Figure 10. To run a test, the lever is put in its *OUT* position and held there. What happens next, assuming the generator provides sufficient power, is decided by the stiffness and strength of the ice;

1. The indentor penetrates the ice until maximal displacement is reached, at which the pressure gauge shows 300 bar for the first time.

2. The pressure gauge shows 300 bar instantly after contact is established between the indentor and BH wall. In this case, the strength and stiffness of the ice exceeds the capacity of the hydraulic system, and the safety valve allows backflow of the oil. The pressure remains at 300 bar, inducing a constant stress of 18.5 MPa on the BH wall for as long as the operator allows the oil to circulate (that is holding the lever in its *OUT* position). Here, there are two different outcomes;

    a. The stiffness and strength of the ice is of such magnitudes that the indentor is only allowed to penetrate the ice a certain distance or not at all. Maximal displacement is not reached.

    b. The indentor penetrates the ice slowly and in the end reaches the maximal displacement.

Scenario 2a and 2b emphasize the necessity of the digital display, so that the displacement of the piston can be monitored throughout the experiment.

Listening to sounds from the ice should be done carefully during testing. For instance, cracking noises indicate cold ice and brittle failures. Ideally, each test should be filmed. Notes

should always describe the tests progress and contain information on the following; BH number, test number, time at start of test, indentor depth and direction, freeboard, snow depth and ice thickness. Photos and descriptions of the cores should also be included. Further, pictures of the ice surface both before and after each test along with a characterization of the surface deformations are of interest.

When the test is finished, the lever is put in its *IN* position and the jack is either lowered to the next depth or brought to the surface. It should be noted that the wires from the transducer to the UNIS-BHJ are relatively short. Therefore, between BHs the transducer needs either to be carried or disconnected in order to avoid tension in the wires. Alternatively, everything can be transported on one sledge. Depending on the weather, the option of disconnection may also cause snow or rain to enter the plugs and in turn cause electrical problems.

4 Calibration

The UNIS-BHJ has been pressure calibrated three times since its finish in 2010; two times digitally using the transducer and one time relying on its manual pressure gauge. When performing digital calibrations the relation between the applied load and the recorded voltage is established in kN and mV. The transducer is in this case connected to the BHJ, preferably along with the digital display providing live updates of the recorded data. When calibrating the BHJ manually, i.e. without the transducer, one has to solely rely on the pressure gauge on the control panel of the BHJ. This is not considered an accurate calibration, but provides a rough estimate of the ratio between applied load and the response in the hydraulic pressure, here in kg or kN and bar.

A digital calibration can be done using "Knekkis". It is a compression device normally used for frozen soil and ice cores and has a capacity of 10 tons. Knekkis was made in 1996 by the Department of Geotechnics at NTNU and is currently located in the Cold Laboratory at UNIS. It is normally used to perform tests with constant load or constant velocity, where the former option is used for BHJ calibration. Placed in the jaws of Knekkis, the BHJ acts like a "core sample", see Figure 15. As the indentor of the BHJ is curved and the jaws of Knekkis flat, use of a rubber mat is necessary in order to prevent the jack from sliding.

Figure 15: The jack with a rubber mat placed in the jaws of Knekkis during calibration.

Calibrating the BHJ in Knekkis is a two person job. One is in charge of Knekkis where a stepwise compression of the BHJ indentor is done and reads the load exerted by Knekkis. The other person reads the induced pressure on the BHJ indentor on the display. The loads exerted by Knekkis are then compared to the corresponding recordings of the transducer.

The first digital calibration was done 20th of September 2010 using Knekkis by Lønøy (2010). As expected, it was a linear relation between the load exerted by Knekkis and the pressure output from the transducer. The calibration was done at two different temperatures to find if the response from the BHJ was temperature dependent. Temperatures -5°C and -15°C was chosen, as these represent typical working conditions in the field. The results from the calibrations were identical, implying that the BHJ system is unaffected by air temperatures in the tested range. The maximal capacity of the BHJ was here estimated to 120.4 kN corresponding to 18.5 MPa.

The manual calibration is also a two person job. While one person is controlling the mag-

nitude of applied load, the other reads the pressure in the hydraulic system from the manual pressure gauge. 23rd of August 2011 the BHJ was brought to M-Tech's premises in Trondheim, where an oil exchange and a manual calibration were performed by M-Tech and O. C. Ekeberg. When a load of 2000 kg was applied to the indentor, the pressure gauge showed 50 bar. Assuming a linear relation, 300 bar would correspond to a loading of 12 000 kg, about the same as what was found in the digital calibration in 2010.

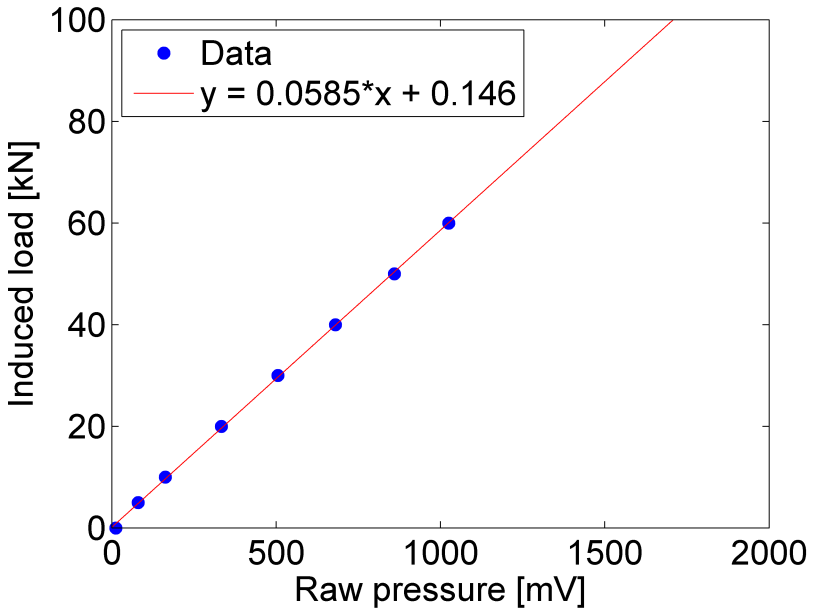

Figure 16: Calibration regression from 6th of March 2012. Load from Knekkis on y-axis and response in the transducer of the UNIS-BHJ on the x-axis.

On the 6th of March 2012 the BHJ was again calibrated using Knekkis, this time by Ph.D. student R. Yulmetov and the author. As Lønøy (2010) showed that the measurements were independent of temperature within normal working conditions, it was decided to run the calibration only at -5°C. The jack was enclosed in a rubber mat before it was put in the jaws of Knekkis. The piston of the BHJ was then exerted to 21 mm, allowing contact only between the load cells of the two devices. While R. Yulmetov operated Knekkis from the control room by applying a chosen load to the indentor, the author was in the Cold Lab reading the raw pressure recorded in the transducer using the digital display. This was repeated for a number of loads, see Figure 16. Exact values are found in Appendix B. As the capacity of the UNIS-BHJ exceeds that of Knekkis, a calibration of the BHJ close to its maximal capacity has yet to be done. It is therefore only assumed that the linear relation also holds for loads greater than 60 kN. The calibration setup is shown in Figure 17.

Figure 17: Calibration setup 6th of March 2012.

5 Literature

5.1 Mechanical and physical properties of sea ice

According to Masterson (1996) the compressive strength of ice is a function of five factors:

- Ice crystal structure
- Temperature and loss of latent heat (i.e. melting ice)
- Brine and gas volume
- Scale
- Stress and strain rate

It is also known that confinement is among the governing factors (Løset et al., 2006). Natural sea ice is a polycrystalline material that acts much like metals. There are mainly two complicating factors that differences the treatment of ice from other materials, 1) the grains are relatively large and 2) ice exists close to its melting point (Løset et al., 2006). The mechanics and physics are extremely complex for high-temperature materials (Sinha et al., 2012), such as ice in its natural state, and brittle and ductile failure modes are not sufficient when describing its behavior. A full mechanical model would need to take linear and non-linear aspects of elasticity, visco-elasticity, visco-plasticity and fracture into account (Løset et al., 2006).

Natural ice contains impurities which affect its mechanical properties as well as its many structural features (Sinha, 2011). The bulk properties can therefore only be found when testing large volumes containing many grains, which are to a great extent preserved in BHJ experiments and therefore of the main advantages with the method. For laboratory testing relatively small samples are collected that may not carry the bulk representative of the ice. For instance, it is known that drainage of salt from sampled cores is inevitable during transportation, even when recovered at extremely cold temperatures (Sinha, 2011). The advantages with laboratory experiments are that they are relatively cheap to perform and the boundary conditions are easily controlled. It is understood that laboratory testing is closer to the theoretical terms, but further from reality (Løset et al., 2006).

Sea ice consists of pure ice, brine, air and sometimes solid salts (Løset et al., 2006). In Figure 18 it is seen that the brine content is a function of temperature, and if the temperatures are sufficiently low, solid salt precipitates. The porosity is equal to the sum of brine volume and air volume, and is therefore also temperature dependent. Further, the temperature has a direct effect on the mechanical behavior of ice. As it decreases, the elastic modulus increases (Løset et al., 2006). The E-modulus is a function of strain rate and brine volume (Masterson, 1996).

In laboratory tests the E-modulus is obtained through uniaxial or triaxial compression tests, where temperature and brine volume can be measured, the crystal structure can be studied in thin sections and the strain rate and the scale of the experiments are controlled parameters. The E-modulus can be calculated directly from the stress - strain curve, as the ice acts as a linear elastic material immediately after the load is applied. Its range is approximately from 4 to 6 MPa for sea ice (Løset et al., 2006).

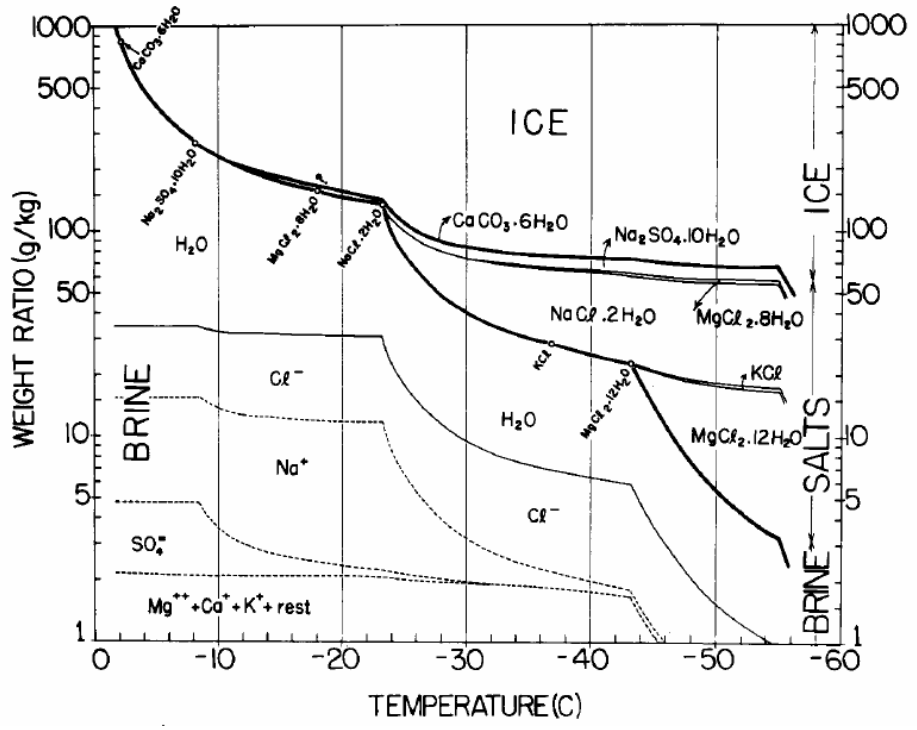

Figure 18: Phase relations for sea ice of salinity 34.325 ppt (parts per thousand). Indications at which temperatures solid salt participates are given on the brine-salt line in small circles (Løset, 1998).

5.2 Interpretation of BHJ records

BHJ experiments are relatively slow, and conducted in ice that exists close to its melting point, it is not possible to evaluate the elastic properties. The reason for this is that the elastic theories of indentation are only applicable for short time (fractions of 1 s) loading (Sinha et al., 2012). The E-modulus can only be obtained in the primary stage of deformation, i.e. the purely elastic deformations within the lattice (Timco and Weeks, 2009). Once the delayed elasticity comes into effect, only the Effective Modulus can be estimated. This value can be significantly less than the true E-modulus (Sinha et al., 2012).

Blanchet et al. (1997) compared the BH and uniaxial strengths and their dependence on temperature for first-year sea ice, see Figure 19. They found that the respective strengths were both decreasing with increasing temperatures, which is in accordance with the temperature effect on the mechanical properties previously mentioned. The relation between the uniaxial and BH strength is non-constant, emphasizing the issue regarding this ratio.

Standardized methods of interpretation are necessary in order to compare the results of BHJ tests, and traditionally, this has been done by evaluating the stress - displacement curves. Mechanical behavior of materials become extremely sensitive to loading rate when existing close to the melting point (Sinha, 2011). In order to draw precise conclusions from BHJ records one need therefore to consider the stress - time and indentation - time development.

One such approach was done by Johnston et al. (2001), where the pressure at 3 mm (σ_{3mm}), was obtained for all tests, regardless of the tendencies of the stress - displacement curve. σ_{3mm} is subsequently divided by the time it takes to reach 3 mm and hence the stress rate of the test is

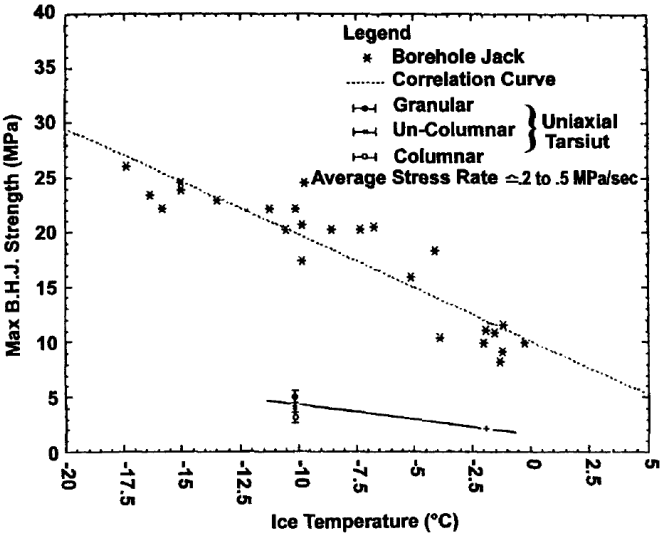

Figure 19: BH and uniaxial strengths plotted vs. temperature (Blanchet et al., 1997).

found. Figure 20 illustrates the process, where σ_M is the maximum stress for an arbitrary test. The parameter have been used in e.g. study of decaying first-year ice, see Johnston et al. (2001). It is noted that σ_{3mm} is obtained regardless of σ_M.

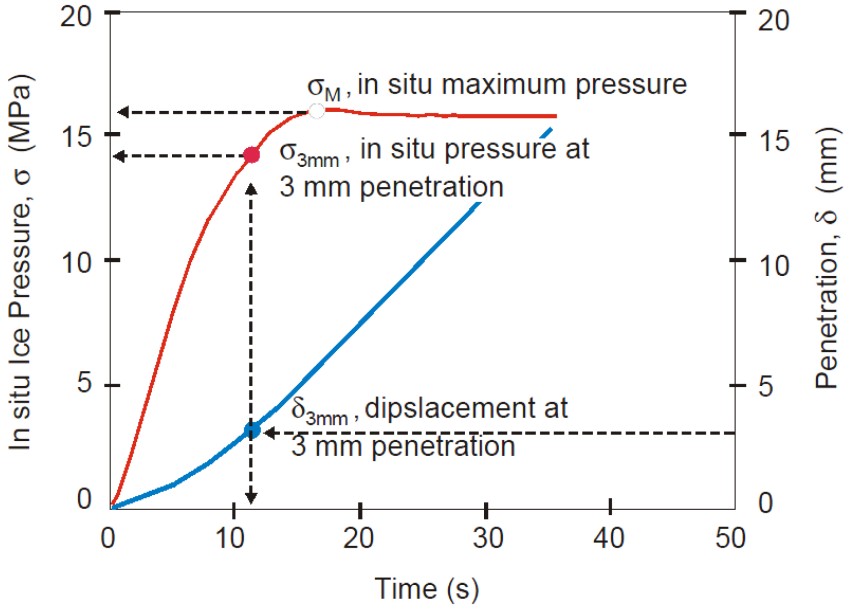

Figure 20: The blue and red line shows respectively displacement and pressure vs. time, for an arbitrary tests (Johnston et al., 2001). The stress rate is here obtained by dividing σ_{3mm} by the time it takes to reach 3 mm displacement.

As the indentation rate is non-constant throughout a test, the average stress rate to failure ($\dot{\sigma}_{af}$), which is failure stress (σ_f) divided by time to time to failure (t_f) and average displace-

ment rate (displacement at failure divided by t_f) becomes feasible approaches of measuring the loading rate. The reason is that both measures are easily obtained in laboratory and in-situ, making comparisons of the data possible (Sinha, 2011). The magnitude of $\dot{\sigma}_{af}$ has been found to vary between 0.01 and 3 MPa/s, see e.g. Sinha (2011) and Johnston, Timco and Frederking (2003), for S1 ice.

Classification of BHJ tests was first done by Shkhinek et al. (2010), where pressure - time curves were divided into four categories, see Figure 21. Type 1 curves occur when cold brittle ice is tested. The pressure reaches a peak after short time, followed by increasing pressure, where crack formation may be observed. Type 2 and 3 pressures are typical for warm ductile ice. The pressure builds up slowly, followed by either decreasing or increasing pressure. Here, the crack formation, if registered at all, will be at very low scale. Type 4 pressures are results of weak zones in the ice. The pressure increases, then stabilize for a short time, before dropping towards zero.

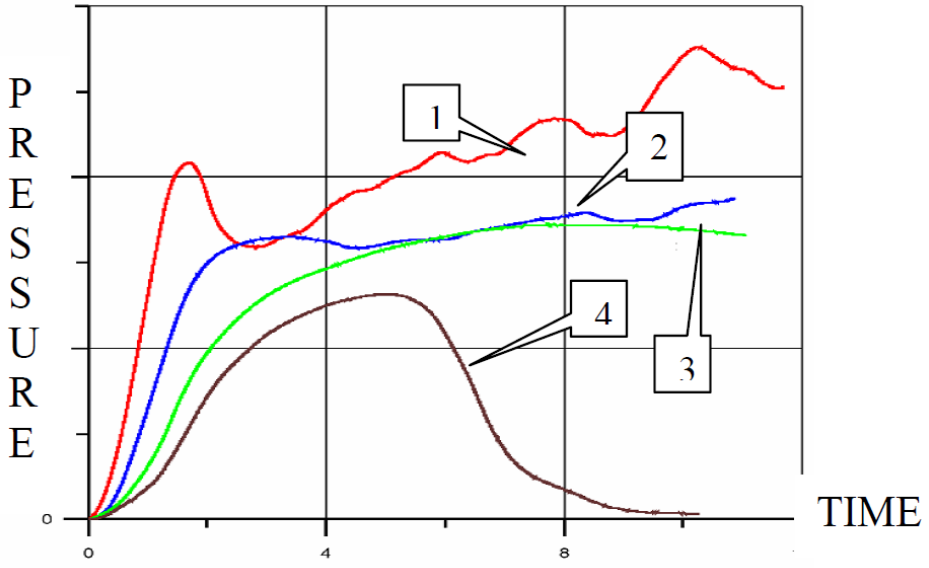

Figure 21: Typical pressure - time curves obtained with a BHJ (Shkhinek et al., 2010).

A similar approach was made by Sinha (2011). Also here, four typical failure types (FT) are classified, see Figure 22.

- Flow stress (FS) failure: The pressure is continually increasing throughout the test. It is typical for warm first year ice, deteriorating first year ice and old decaying sea ice. The flow stress is found from a predefined displacement. Sinha (2011) suggests 2 or 5 mm, comparable to the yield strength ($\sigma_{0.2\%}$) used for metals in tensile tests.

- Asymptotic (AS) failure: The pressure increases to a certain level, and then remains constant throughout the test. This response is typically seen in warm and/or decaying ice. It has also been observed in cold ice, where the design load to the system has reached the upper limits. The pressure at the constant level is classified as the asymptotic strength.

- Upper yield (UY) failure: Pressure increases to a certain level, from where it decreases monotonically as displacement increases. This test is comparable to ductile failure in metals and alloys. Failure occurs at the upper yield strength.
- Premature (P) failure: The pressure increases rapidly before a sudden drop. Several peaks may occur at later stages of the test, resulting in a saw-tooth diagram. The failure mode is classified as brittle, and the fracture strength is found from the first peak.

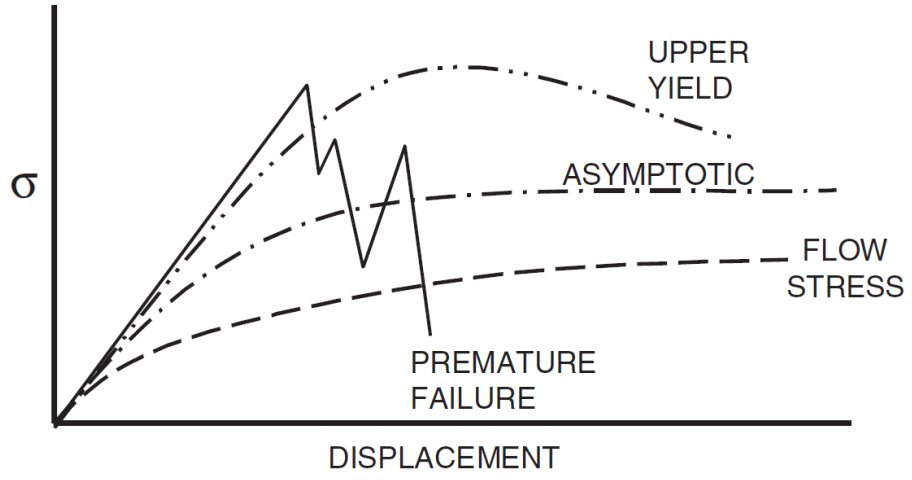

Figure 22: Classification of 4 typical stress - displacement curves obtained through BHJ testing (Sinha, 2011).

6 Classification system

The purpose of classifying BHJ tests is to identify and categorize the behavior of ice upon indentation. An archive of classified BHJ tests could ideally be used to predict the BH strength and failure type of an ice feature where parameters such as thickness, temperature, salinity, density and velocity are known. The failure type of a BHJ test can be determined by the classification model developed by Sinha (2011), which is based on idealized stress – displacement curves from BHJ records. The advantage of classifying failure types relates to weak zone recognition and failure modes (e.g. crushing and radial cracking) and in turn loads on structures. This chapter presents a further development of the model where a quantitative approach is introduced to describe and distinguish the failure types. It is important to classify the tests, and thereby also the ice behavior upon loading, as the response can be fundamentally different from one ice feature to another.

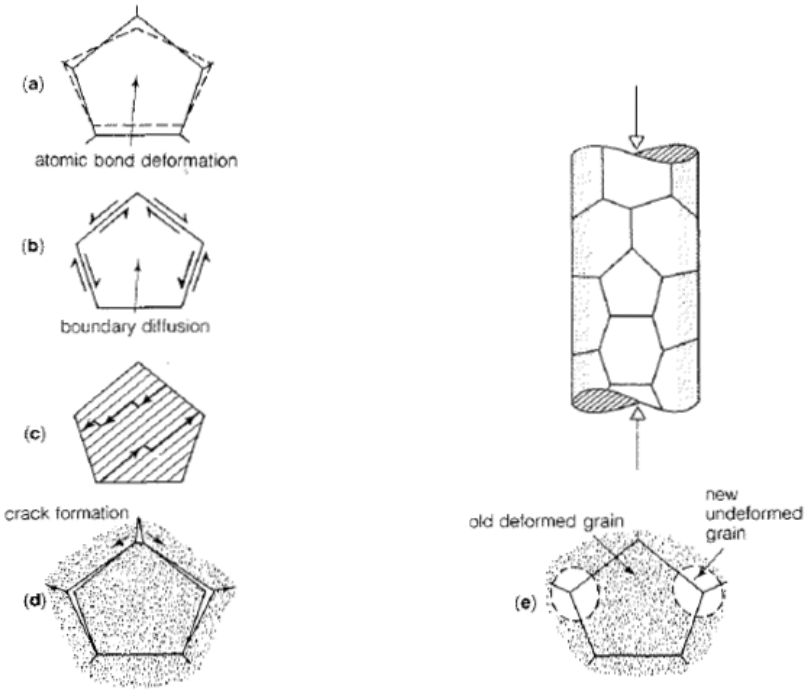

Figure 23: Processes of deformation within and around a grain of a cylindrical sample upon compressive loading (Sanderson, 1988).

Figure 23 from Sanderson (1988) describes the process of deformation within and around a grain under uniaxial compressive loading, where explanations to the stages of deformation are as follows;

(a) Elastic strain: Atomic bonds deform as a response to the strain in which the grain is exposed to. The deformations are purely elastic.

(b) Delayed elastic strain: When the elastic deformation is anisotropic and the different grains have different c-axis, the elastic deformation will create shear stresses and shear strains on the grain boundaries. These shear strains are time dependant (viscous) and cause a delayed elastic response.

(c) Secondary creep: Dislocations within the grain leading to irreversible deformations.

The result of dislocation pile-up at grain boundaries may come to (d) or (e):

(d) Crack formation: Formation of cracks and possibly accelerating strain rates.

(e) Recrystallisation: New grains may start to form from high dislocation density, specifically at high temperatures.

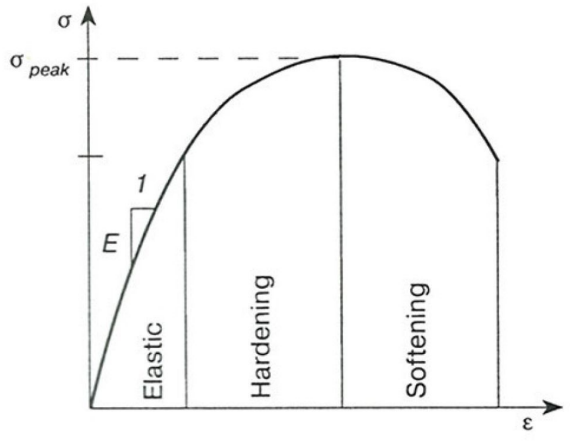

Figure 24: Stress - strain curve for linear-elastic-plastic material (Løset et al., 2006), uniaxial test of constant strain rate.

In short-term loading (fractions of 1 s) the visco-elastic and visco-plastic strains do not have time to develop, and are therefore neglected in linear-elastic-plastic models which is the case for the uniaxial test as seen in Figure 24. The instant response from the material is elastic (*e*) deformation, where Young's modulus can be found by evaluating the tangent of the curve (Masterson, 1996). The material yields in transition to hardening (*h*), from where plastic deformation takes over. The transition zone between hardening and softening (*s*) is called upper or ultimate yield. For a tensile test this is where the necking, or narrowing, of the material starts. The reduction of the true area continues with increasing deformations until fracture occurs. The transition zone can at times be hard to identify, especially for ductile materials e.g. aluminum. In such cases where the strain is increasing under constant loading the material is undergoing perfect-plastic behavior (*c*).

The classification system described in this chapter uses the zones elastic, softening plasticity, hardening plasticity and perfect-plastic behavior from a stress - strain curve as a point of reference when describing what is happening in a BHJ test. It is emphasized that the behavior of the material undergoing a BHJ test is far more complex than the terms suggest. Focus is put on the post-peak stress behavior and as it may contribute to the understanding of the distance to and volume of weak zones.

From a BHJ test it is not possible to identify the elastic zone, first of all because the strain rate is an unknown parameter. Secondly, crushed ice forms at a very early stage of the process followed by subsequent stress concentrations (Masterson, 1996). This implies that the elastic zone has a very short appearance and that the hardening process starts early. It is therefore not known at which stress or displacement the yielding of the ice starts. Considering Figure 22, the BHJ test may never enter a softening zone, which are the cases for flow stress and asymptotic failures. Another term for flow stress is therefore current yield stress (Reyes, 2006). Likewise, asymptotic failures may be referred to as constant yield stress.

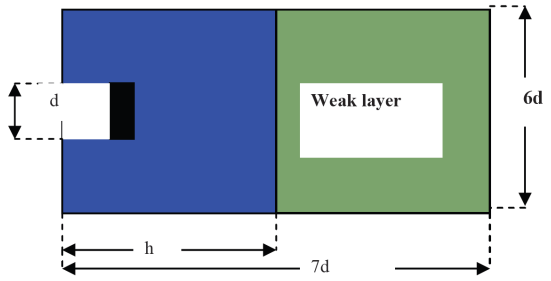

Figure 25: Simulation the distance, h, from BH wall to weak layer in the ice, where d is the indentor diameter (Shkhinek et al., 2010).

Shkhinek et al. (2010) investigated the phenomenon of weak zones by applying numerical models to BHJ records. Simulating a two-layered medium of one strong and one weak layer (Figure 25) they found that the distance from the BH wall to the weak layer affected both the magnitude of failure stress and time to failure. Applying different failure models, among others Mohr-Coloumb and Tresca, they found that the Fish-Zaretsky model fitted the data best (Figure 26). The vertical lines indicate the respective distances to the weak layers as a function of indentor diameter, d. It is understood that flow stress and asymptotic failures are types where upper yield is not reached, indicating that weak layers are not in immediate vicinity of the indentor. Opposed to uniaxial tests, the ice in a BHJ test may fail several times, allowing a cycle of hardening, softening and/or constant stress zones. Depending on the manner of failure, that is brittle or ductile, premature and upper yield are introduced. In either case, it is the first peak that defines the BH strength of the ice.

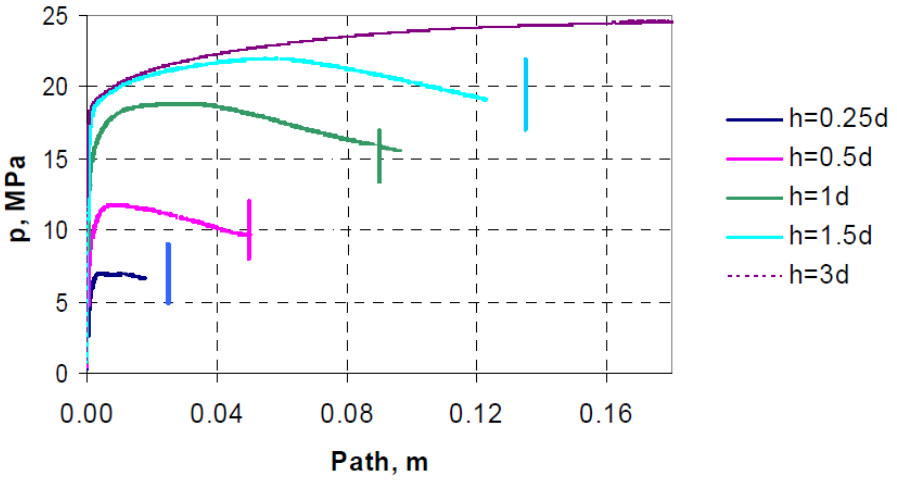

Figure 26: Results from the weak layer simulation by Shkhinek et al. (2010). Y-axis shows the indentor stress divided on compressive strength of uniaxial samples and x-axis the distance from the BH wall, h, as functions of indentor diameter, d.

It is emphasized that the system is based on stress - strain, and not stress - time curves. For validation of the system the strain rate should be constant. This is however not the case since the strain rate is a function of indentation rate, which is previously mentioned to vary throughout the tests. Nevertheless, the tendencies of stress development are the same for both indentation and time, and the stress zones are therefore assumed applicable in both cases.

Based on these four zones of stress development, *e*, *h*, *c* and *s*, a classification chart has been made to categorize the different failure types, see Figure 27. FS corresponds to *e-h* failure, AS corresponds to *e-h-c* and so on. The UY failure has further been divided into four subgroups,

UY1, UY2, UY3 and UY4, depending on the third and fourth term. To distinguish P failure from UY1 the stress rate in the transition zone between hardening and softening required a quantitative explanation. The difference between constant stress and softening/hardening has been evaluated on similar basis. Consequently, it was necessary to establish certain definitions;

1. Premature failure occurs where the stress rate ($\frac{d\sigma}{dt}$) is less than -2.5 MPa/s in transition between hardening and softening.

2. Constant stress is defined where the mean stress rate is in range ± 0.1 MPa/s for a period of at least 3 s. Exceptions are made for tests where the trend clearly changes during the final, i.e. less than 3, seconds. In these cases the tendency of the curve decides if the ice is experiencing a softening, hardening or constant stress.

3. Softening and hardening appears where the stress rate is less than -0.1 MPa/s and greater than 0.1 MPa/s for a period of at least 3 s. Same exception applies as for point 2.

4. Failure occurs if the decrease of stress is equal to or greater than 0.5 MPa during a period of maximal 5 s. In other words, softening of at least 0.5 MPa.

5. The maximal capacity of the hydraulic system is reached if the stress and stress rate reaches minimum values of respectively 18 MPa and 10 MPa/s within the first 5 s of the test, regardless of when contact is established.

where the stress rate is defined as the running derivative of stress with respect to time, see Equation (1).

$$\frac{d\sigma}{dt} = \frac{\sigma_{t+1} - \sigma_t}{\Delta t} \tag{1}$$

with unit MPa/s. This definition will be used on stress rate from here on. Additional comments on the system are listed below:

- Based on over 100 BHJ tests conducted in old level ice in the Fram Strait, 10.5 s was discovered the average duration of an arbitrary test. It was therefore considered appropriate to choose 3 s as the minimum duration of stress level to categorize a *h*, *s* or *c* zone, as this would correspond to about 30% duration of an average test.

- The failure types are indexed max where the maximal capacity of the system is reached.

- The stress may alternate from hardening to softening several times during a test. However, four zones were considered sufficient to describe the development of a test, but the system does allow for further expansions to be made in order to describe each test in greater detail.

- The tests are considered starting when the voltage exceeds 0.10 mV, which corresponds to 0.15 kN or 2.38 x 10^{-2} MPa, for the first time.

- Contact with the BH wall is normally reached at about 2 s. This corresponds to a displacement of approximately 13 mm assuming the velocity is about the same in water as in air (6.7 mm/s).

- It is emphasized that the system is merely a draft of a quantitative approach of classifying BHJ results. Future work will show whether the system needs to be adjusted and how.

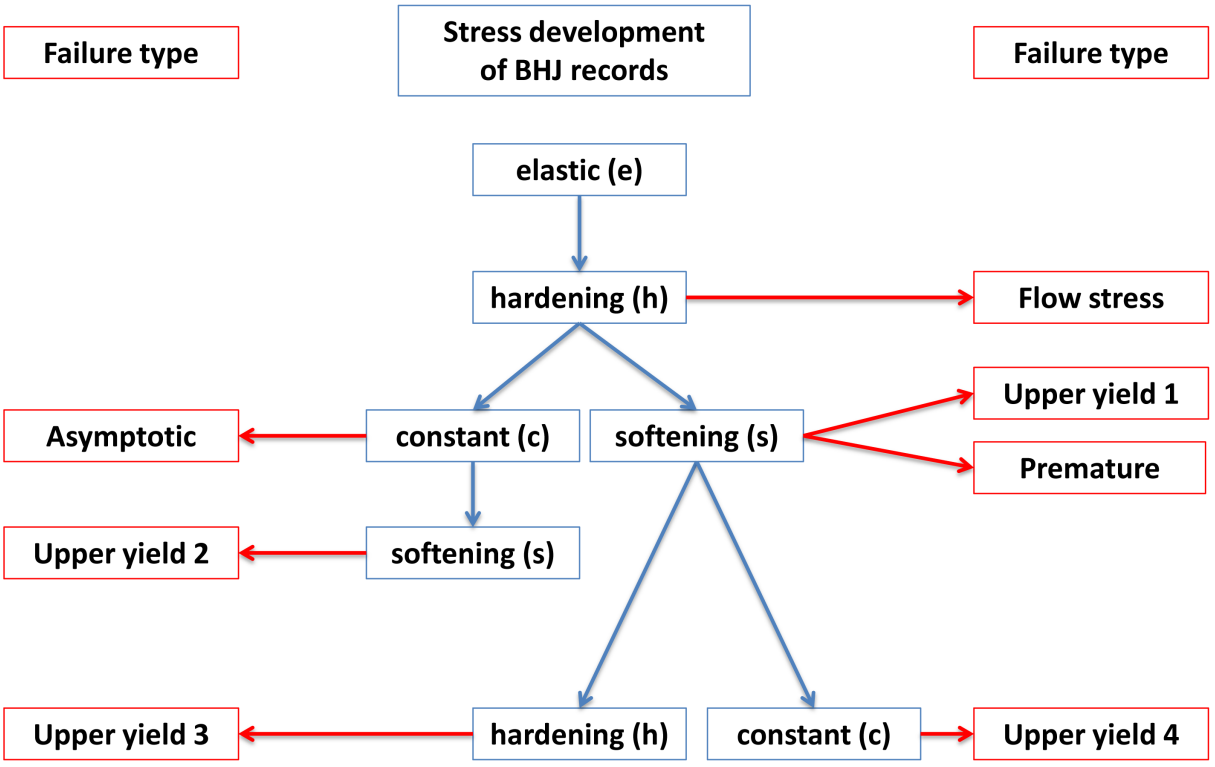

Figure 27: Classification chart of BHJ records.

7 Fieldwork descriptions

The Department of Arctic Technology is responsible for research and education on ice mechanics and physics at UNIS, where an important part of the program is to familiarize the students with fieldwork. The most frequently visited fieldwork locations are the Barents Sea and Van Mijenfjorden. Van Mijenfjorden is known for reliable fieldwork conditions where the main reason is Akseløya, which is situated in the outer parts of the fjord, limiting the currents in the fjord and thus allowing the ice to grow relatively undisturbed. Depending on the weather conditions, a scooter trip from Longyearbyen takes approximately 2 hours, enabling the students to visit the fjord also for shorter periods of time. A small mining town named Sveagruva is found in the inner parts of the fjord, improving its attractiveness regarding longer stays and emergency situations. BHJ tests were performed here during two separate visits during the spring 2012, AT208 from 21st to 23rd and AT307f from 27th to 29th of March. Co-operating with the NPI, the students of AT208 also joined the expedition to the Barents Sea lasting from 16th to 25th of April. This chapter provides a description of the fieldwork conditions in the three mentioned periods.

All tests within each site were consistently conducted in same indentation direction to keep the number of unknown parameters as low as possible, and subsequently simplifying the process of interpreting the data. Thin sections to study the grain structure of the ice have not been done because the UNIS-microtome was out of order. It is however reason to believe that the tests conducted in Van Mijenfjorden were in transition granular to columnar ice. The reason is that considerable amounts of snow have caused submergence of the ice early in the season, which resulted in upward growth in the following cold period. A consistent direction (South) was also kept here regardless of the fact that Sinha (1986) showed that the BH strength in S2 ice is insusceptible to loading direction.

7.1 Van Mijenfjorden

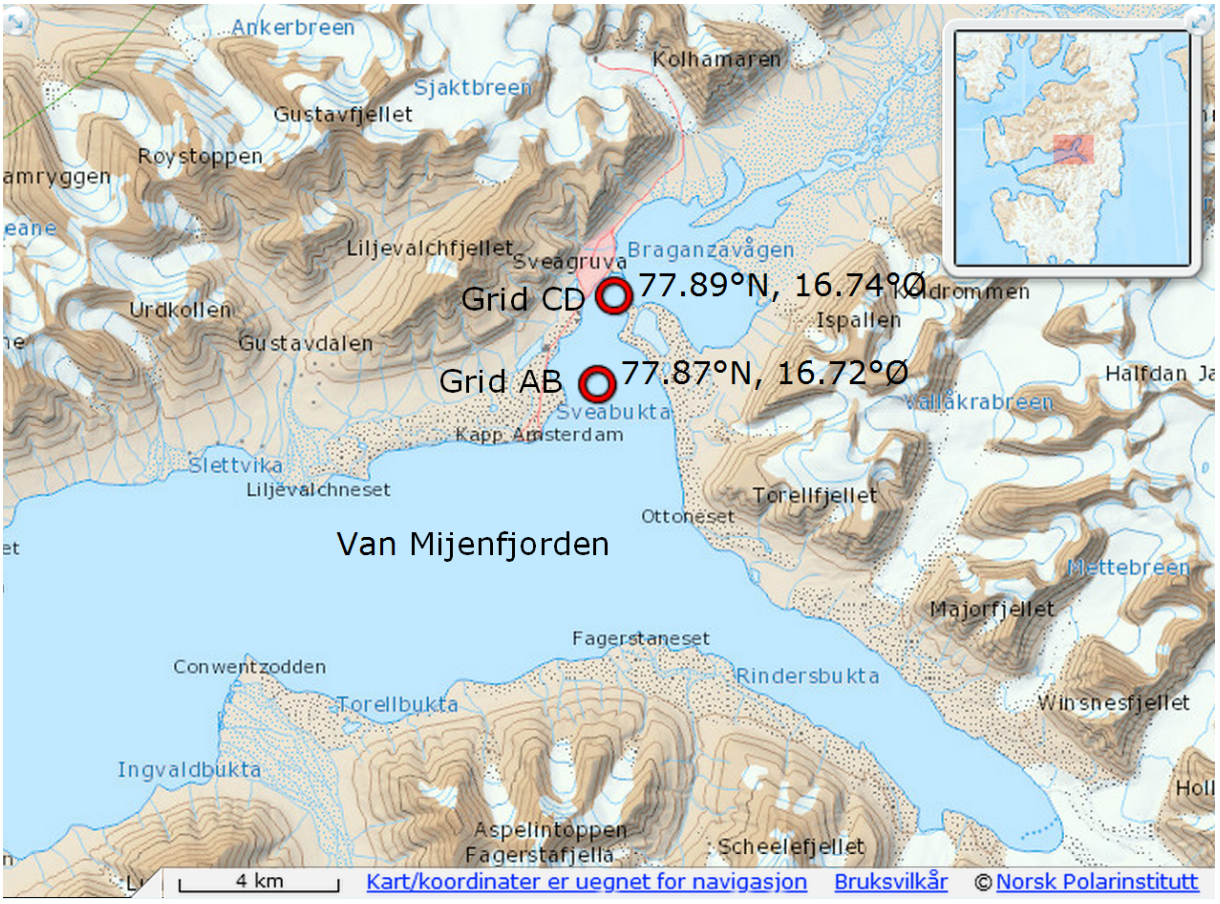

Figure 28: Map of the inner parts of Van Mijenfjorden showing the locations of Grid AB and CD (Norsk Polarinstitutt, 2012).

7.1.1 Grid AB

The weather was mostly clouded during the period with mean temperatures -8 and -9 °C on the 22nd and 23rd of March respectively. Upon arrival in Van Mijenfjorden we decided to establish two grids in the first-year level ice (FYLI) encountered. Grid A was established first, having dimensions 60 by 60 m with internal distance 10 m between BHs. Grid B was later established within Grid A to provide information on the spatial variation, see Figure 29 for grid setups. A picture taken within Grid A is shown in Figure 30. Once the grids were established, one group of students started drilling BHs with the 150 mm core drill and doing measurements on ice thickness, snow depth and freeboard, see Table 1 for main results. Some digging was necessary to get through the snow and to the ice surface. Also, since the freeboard was negative, the snow mixed with water, forming slush in the BHs. This made it difficult for the BHJ crew to observe deformations in the ice during tests. Temperature, salinity and density profiles were found for a number of BHs, where the results are shown in Figure 31, 32 and 33. Relative warm and porous ice was tested. The depths of which BHJ tests were done is marked in the figures as “Test

range", since this is the data of greatest interest here. Further, straight lines are drawn between measured points, and these do not represent the actual measurements at the running depth. The method is also applied for similar measurements throughout this chapter. Once the BHs were drilled, another group of students started performing BHJ tests where the indentor direction in all BHs was consistently kept South.

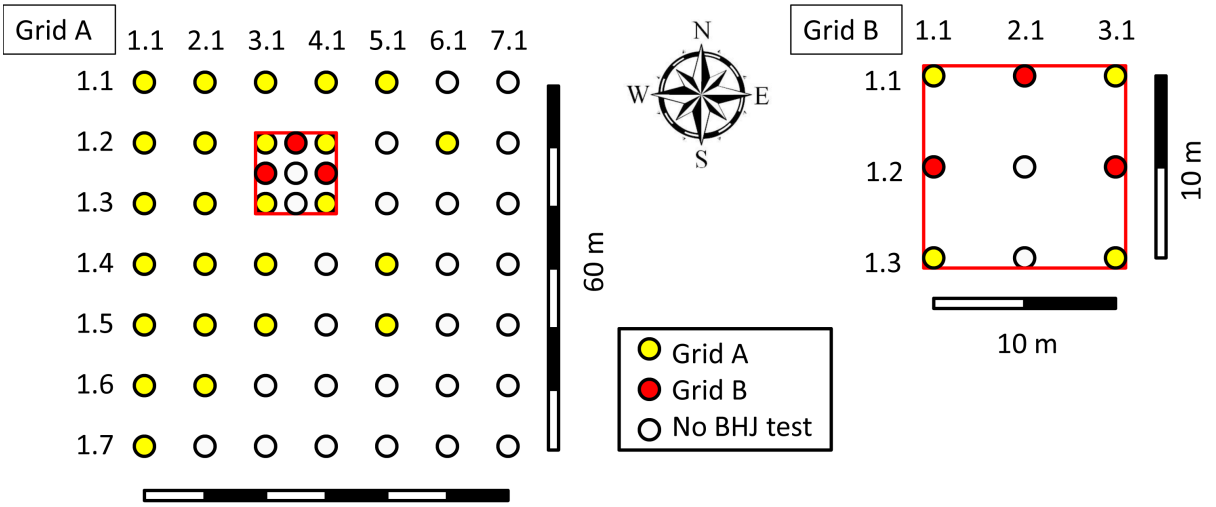

Figure 29: Setup for Grid A (60 by 60 m) and Grid B (10 by 10 m). Yellow and red dots indicate BHs where successful BHJ test were conducted. The white legend marks BHs where no tests were done, either due to mud flooding the BH or lack of time.

Figure 30: Picture of Grid A, direction South-East taken next to BH A4.4.

A photo of the core from A4.3 is shown in Figure 34, with a close-up of the skeleton layer in Figure 35. The ice thickness was here measured to 63 cm where the lower 5 cm (left in the picture) is the skeleton layer. This is a weak layer that fell apart upon touching and is not considered to provide a substantial contribution to the vertical constraint of the ice. However, it is hard to estimate its actual contribution, and the layer is therefore considered to be a part of

the ice floe on equal level as the rest of the ice. It can also be seen from the figures that the ice is relatively porous with brine and gas pockets.

In Test 5 and 17 (A1.5 and A3.3) the indentor twisted about 45°, see Figure 36. This happened for the first time on the 27th of February when using the BHJ in Isdammen, which is a freshwater lake near Longyearbyen. It came as a surprise that this also could happen in the porous FYLI in Van Mijenfjorden. The system may has suffered permanent damage, and thus increased probability for recurrence, but nevertheless we decided to continue the testing, which turned out a success as the piston twisted back in the respective successive tests.

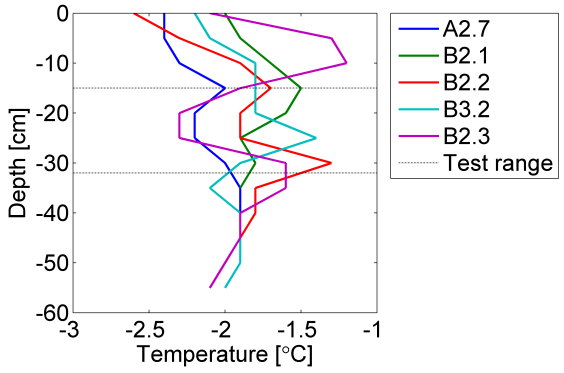

Figure 31: Temperature profiles from Grid A and B with test range from 15 to 32 cm (Karlsen et al., 2012).

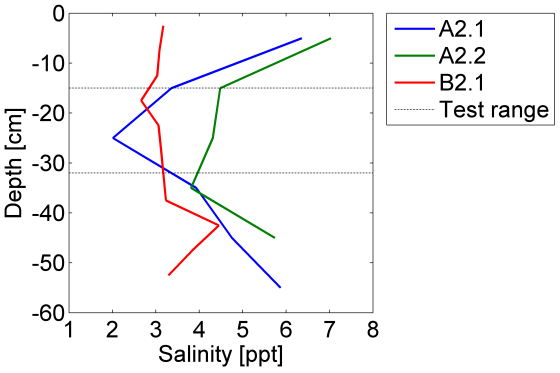

Figure 32: Salinity profiles from Grid A and B with test range from 15 to 32 cm (Karlsen et al., 2012).

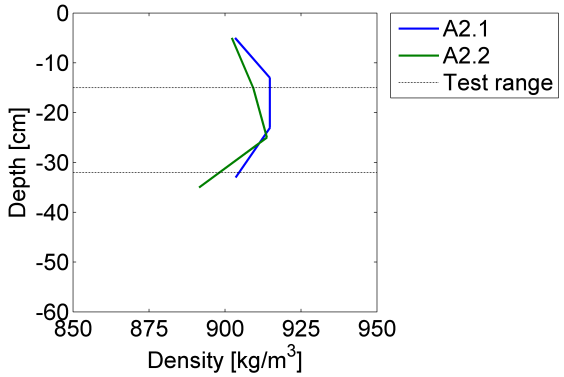

Figure 33: Density profiles from Grid A with test range from 15 to 32 cm (Karlsen et al., 2012).

On several occasions mud was encountered in the BHs, see Figure 37 and 38. In order to avoid putting the equipment at risk, BHJ tests were not conducted at these locations. The initial plan of evaluating the spatial variation became difficult as the tests could not always be conducted where intended. Grid A and B are therefore considered as one grid, Grid AB, from here on. A thin layer of oil was noticed in several of the BH during and after testing, indicating that the hydraulic system is leaking. However, we found no influence on the pressure recordings, and these matters are considered negligible in further interpretations of the data. It can also be seen from Figure 36 that the painting is about to disappear from the jack. We think this happens due to pressure acting back on the jack from the ice.

Table 1: Minimum and maximum measures of ice thickness, snow depth and freeboard for BH where tests were conducted in Grid AB.

Grid	h_i [cm]	h_s [cm]	FB [cm]
AB	30 to 65	7 to 41	-25 to 0

Figure 34: Picture of the core from A4.3 where the bottom points left.

Figure 35: Close-up of the skeleton layer. Brine pockets are present in the core.

Figure 36: The indentor twisted about 45°in Test 5, A1.5.

Figure 37: This picture shows one of the many BHs that were flooded with mud.

Figure 38: The core extracted from the BH shown in the figure above.

7.1.2 Grid CD

Upon the next arrival in Van Mijenfjorden several holes were drilled across Sveabukta to find an area where mud and surface water could be avoided. The location which was the best fit is shown in Figure 28, at 77.87 °N, 16.72 °E. We decided to establish two grids of different sizes to provide data on the spatial variability of the BH strength. Grid D (10 by 10 m) was situated within Grid C (100 by 100 m), see Figure 39 for grid setups. The center of Grid D was located the minimum distance recommended for full horizontal confinement, i.e. 1.5 m, East of the center in Grid C.

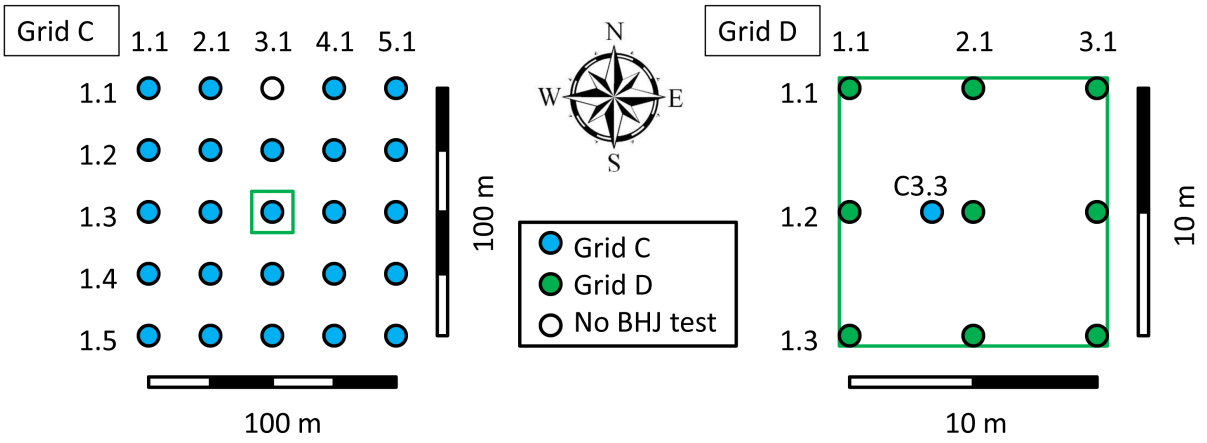

Figure 39: Setup for Grid C and D. BHJ test was not conducted in C3.1 due to mud encounter. C3.3 is located 1.5 m West of D2.2.

Figure 40: Picture of students drilling hole D2.2 and making ready the BHJ. Sveagruva is seen in the background.

A picture of AT307f students working in Grid D is seen in Figure 40. Table 2 shows how the ice thickness, snow depth and freeboard vary within each of the grids. Generally greater variations are found within Grid C than Grid D for all parameters. The initial plan of avoiding

surface water failed. All the tests in this area were attempted done in center of the ice floe to provide maximal vertical confinement in each BH. Figures 41 to 44 provide the spatial variation of ice thickness and temperatures of the two grids. The variations of these parameters are greater for Grid C than Grid D, in accordance with what was found in Table 2. The temperature measurements are done at indentor depth of the respective BHs.

Table 2: Minimum and maximum values of ice thickness, snow depth and freeboard of Grid C and D (Bencomo et al., 2012).

Grid	h_i [cm]	h_s [cm]	FB [cm]
C	38 to 52	25 to 51	-17 to -4
D	43 to 48	42 to 48	-18 to -14

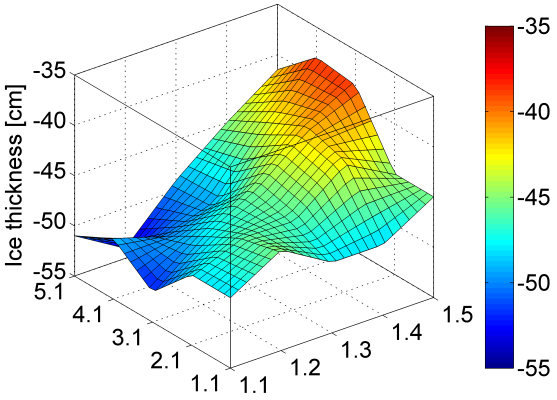

Figure 41: Ice thickness variation within Grid C. 25 m internal distance.

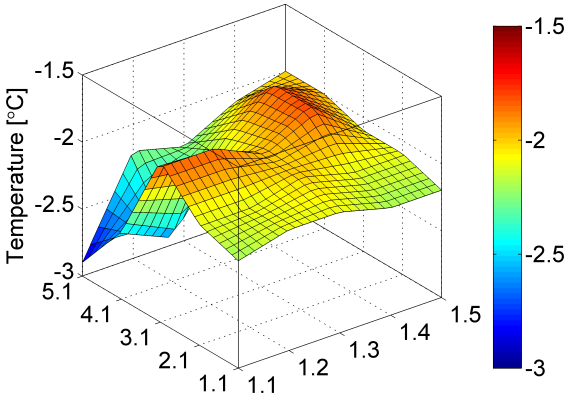

Figure 42: Temperature measurements at IDs within Grid C. 25 m internal distance.

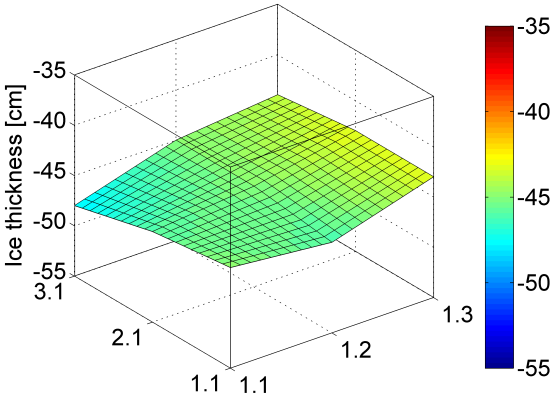

Figure 43: Ice thickness variation within Grid D. 5 m internal distance.

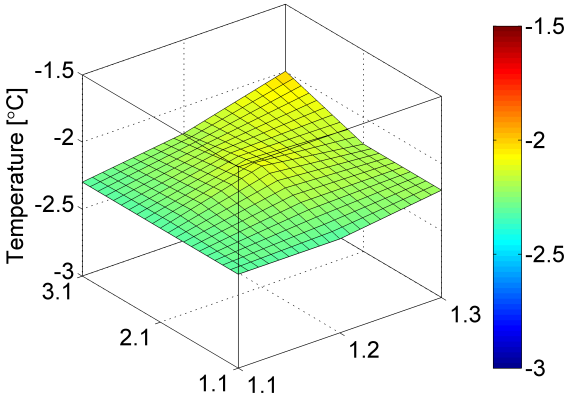

Figure 44: Temperature measurements at IDs within Grid D. 5 m internal distance.

Salinity and density profiles were made for each corner and the center of Grid C and are plotted in Figures 45 and 46. Considering only the test range, salinity varies from 3.9 to 5.2 ppt,

which is considered a narrow range. Density profiles for C5.1 and C5.5 indicate that porous ice is found in the Eastern parts of the grid. The three remaining profiles are go from 922.3 kg/m^3 to 978.9 kg/m^3 in test range. The salinity and density profiles established in C3.3 are considered to provide reliable information also for Grid D.

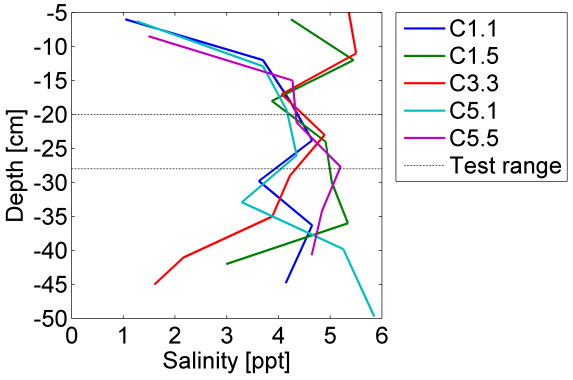

Figure 45: Salinity profiles from Grid C, where test range goes from 20 to 28 cm (Bencomo et al., 2012).

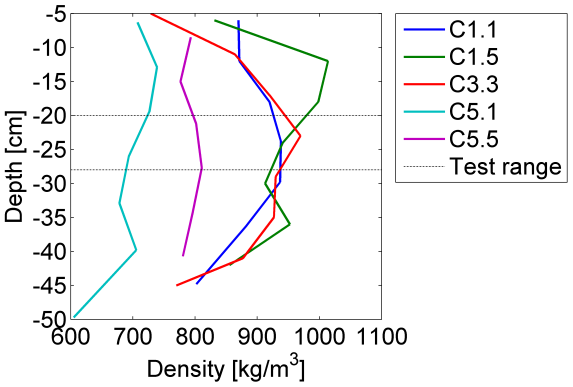

Figure 46: Density profiles from Grid C, where test range goes from 20 to 28 cm (Bencomo et al., 2012).

Figure 47: Slush preventing the BHJ crew from observing the failure (if any) in the ice surface of an arbitrary test.

From Figure 39 it is seen that only C3.1 was untested for BH strength. This was the only BH where mud was encountered. The surface water was however not avoided for any of the BHs, which prevented the BHJ crew from visually observing the ice during testing, example given in Figure 47. Oil was also seen on the water surface during and after the tests, meaning that the system continued to leak oil.

7.2 Barents Sea

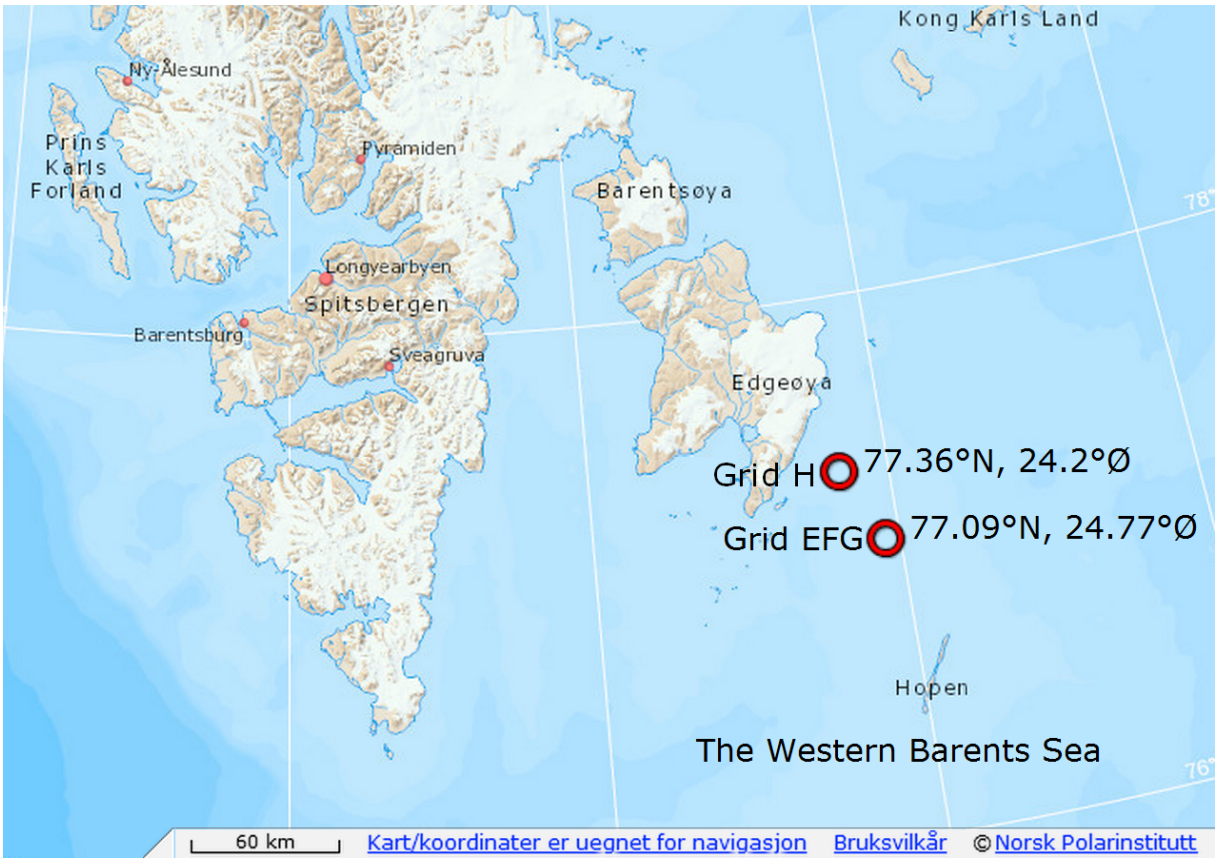

Figure 48: Map of parts of the Western Barents Sea with locations of Grid EFG and H (Norsk Polarinstitutt, 2012).

7.2.1 Grid EFG

The first stop for this expedition was rafted and young ice encountered at 77.09°N, 24.77°E between Hopen and Edgeøya, see map in Figure 48. The weather conditions during the stay were considered good fieldwork conditions with a stable air temperature at -12°C. Grid E was established 3 to 4 m from and parallel to R/V Lance, occupying an area of 20 by 20 m with internal distances 10 m between the BHs. A severe crack developed parallel to the vessel during Test 4 in E1.2, resulting in an ice floe of approximate 3.5 by 12.5 meters breaking loose. The grid was therefore expanded by adding a row of three new BHs to the opposite side as compensation. This way, the closest BHs were 10 m from open water. Grid F and G both had internal distances 2 m between BHs, and were established inside Grid E to provide information on the spatial variation, see Figure 49. The indentation direction was consistently kept towards R/V Lance for all tests, that is to the left in Figure 49. Figure 50 is a picture taken from the helideck of R/V Lance, providing an overview of the area where the grids were established. The FB varied from -1 to 1 in all three grids, while the snow depth ranged from 10 to 16 cm.

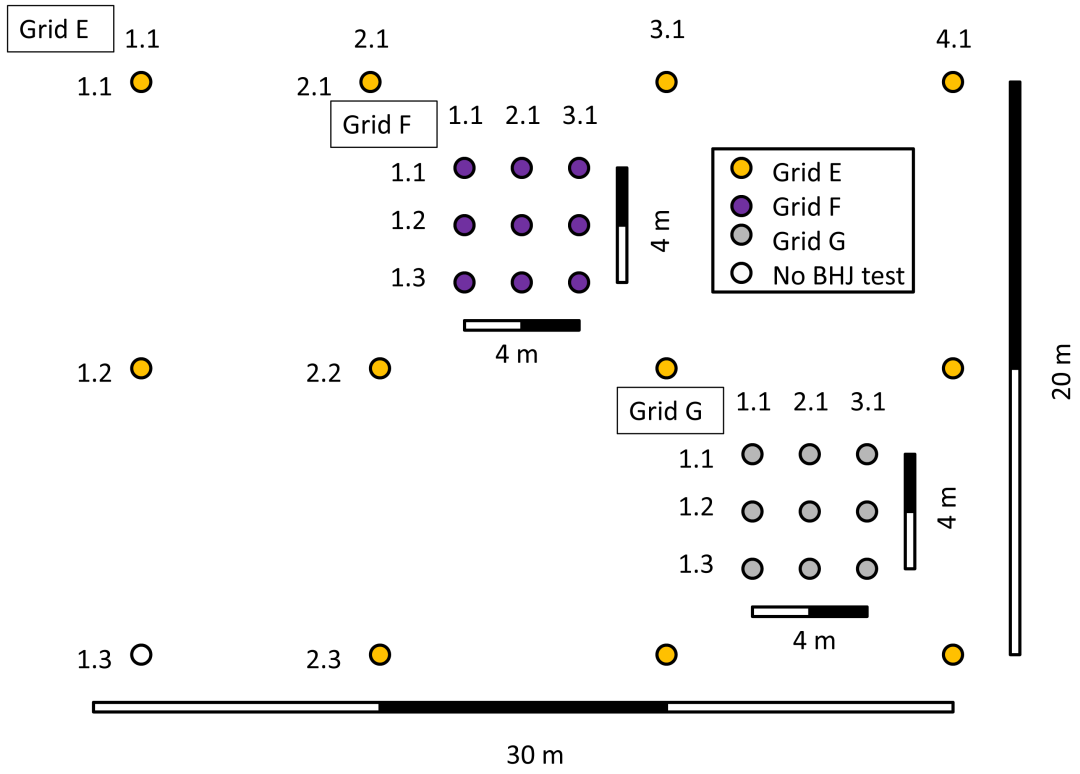

Figure 49: Grid E, F and G setup. The distance from the corner points of Grid F and G to the closest point of Grid E, e.g. F3.3 to E3.2, was 3 m.

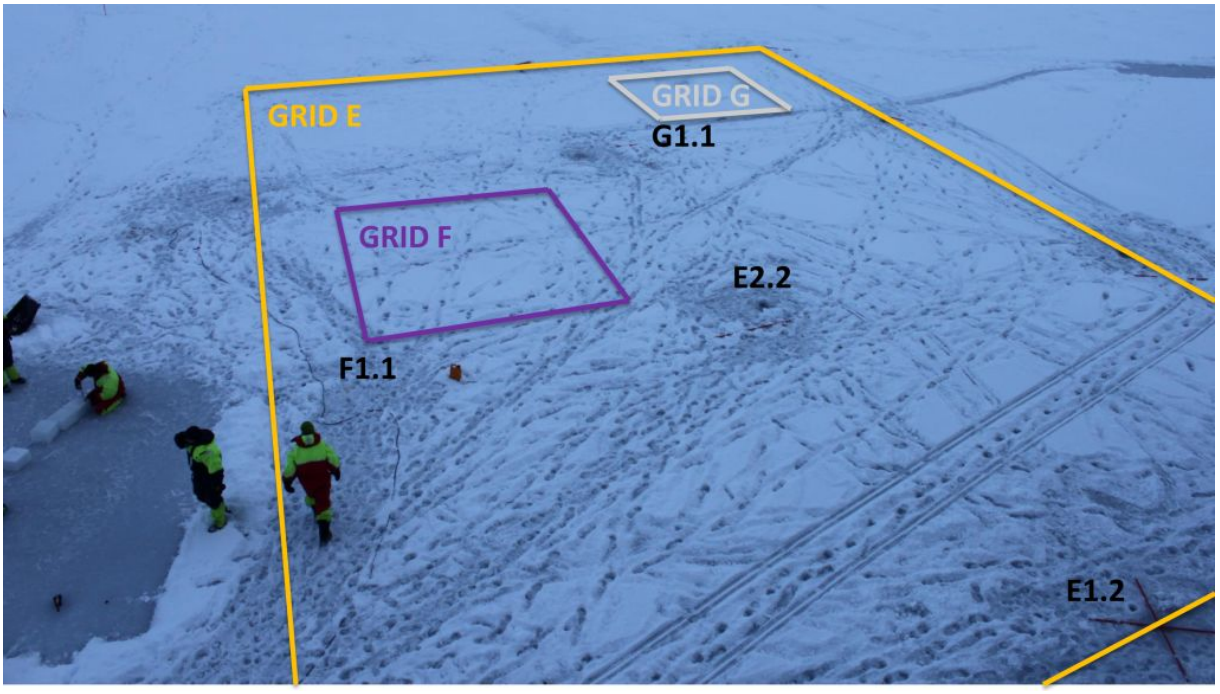

Figure 50: Grid E, F and G setup. The picture was taken before the holes of Grid F and G were drilled.

Figure 51, 53 and 54 indicate that Grid E, F and G are all partly established in young ice and partly in rafted ice. The ice thickness goes from relatively constant 20 cm down to 55 cm (F2.3). Temperatures were measured at indentor depth for all BHs in Grid E and are shown in Figure 52, where no clear dependence on ice thickness can be found when comparing to Figure 51.

The young ice proved perfect conditions for studying the failure mode of the ice and investigating the vertical confinement in BHJ tests. Elevation of the ice and cracking noises were noticed for several of the tests. Figure 55 illustrates fragments of ice that broke off during testing as results of spalling failures. Fragment A, see Figure 56, was not expected as it has not successfully been found described in other works. The inclination of the fragment varied between 45°as seen in the picture, to 90°seen in the sketch. Fragment B in Figure 57 is a result of downward breaking spalling failure, typically ranging from 5 to 15 cm in thickness. What characterized Fragment B was fracture parallel to the basal plane, as seen in the photo and illustrated in the sketch.

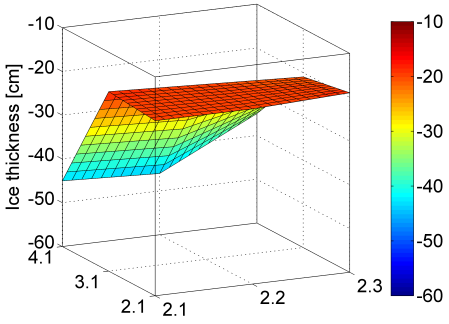

Figure 51: Ice thickness variation in Grid E with 10 m internal distance between BHs.

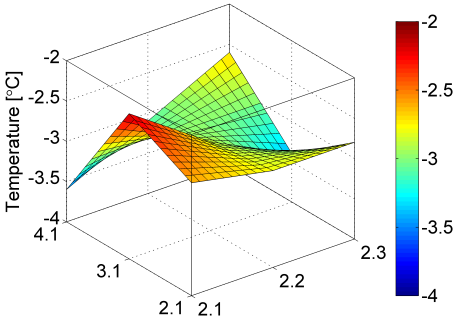

Figure 52: Temperature at IDs for Grid E with 10 m internal distance between BHs.

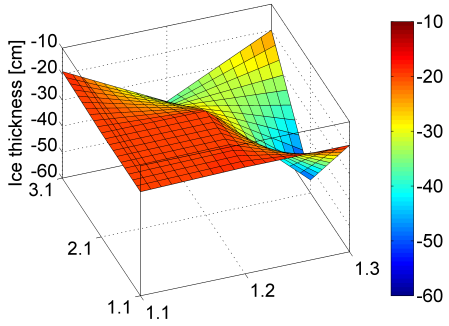

Figure 53: Ice thickness variation in Grid F with 2 m internal distance between BHs.

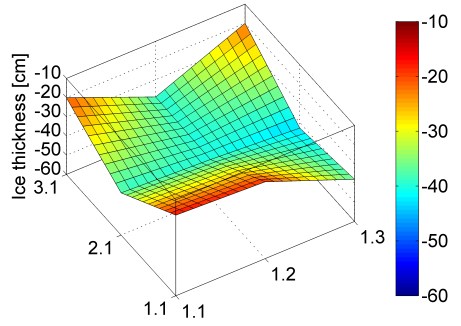

Figure 54: Ice thickness variation in Grid G with 2 m internal distance between BHs.

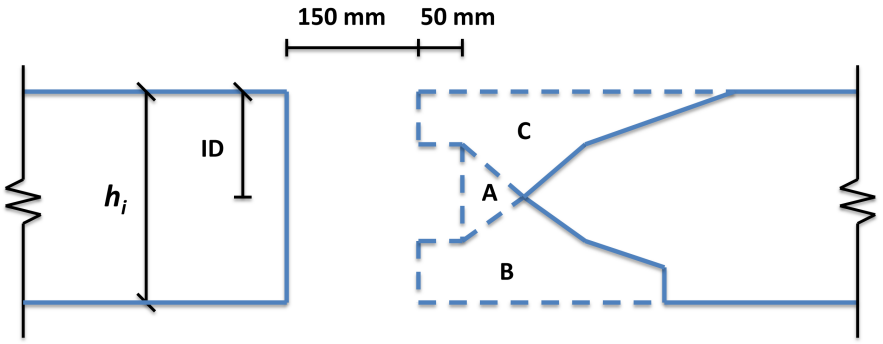

Figure 55: Vertical cross-section of BHJ test location illustrating spalling failure, which was frequently observed in Grid E, F and G. Fragment B and C could occur in separate or the same test, while A did not appear without B present. The indentor depth was consistently half the ice thickness for all three grids.

Figure 56: Fragment A recovered from BH G3.2.

Figure 57: Fragment B from BH E3.1.

Figure 58: Fragment C breaking upwards in BH E3.2.

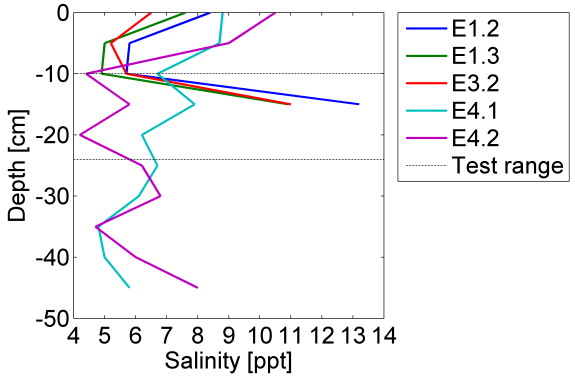

Figure 59: Salinity profiles from Grid E, where the test range is 10 to 24 cm (Elgaard et al., 2012).

Salinity profiles were found for five BHs in Grid E, see Figure 59, where the young ice profiles show an abrupt increase in salinity at bottom of the ice floe and the rafted show more or less steady tendencies.

One had previously only assumed that maximal displacement was reached in tests where capacity of the system induced limitations. This was confirmed in Test 5, E3.2, where a spalling failure occurred. An attempt of measuring the indentation with a meter stick was done while the jack was still stuck in the ice, see Figure 60, but turned out inconvenient as some ice was still in the way. We therefore decided to use an axe to chop the jack out of the ice without retracting the indentor. At the surface the displacement was measured to 50 mm, confirming the assumption. Figure 61 shows Fragment A from a different angle than shown before. The surface matched the curvature of the indentor perfectly and was very smooth.

Figure 60: An attempt of measuring the displacement of the indentor at BH E3.2.

Figure 61: Fragment A collected from BH G3.2.

7.2.2 Grid H

During the night to 20th of April, R/V Lance manoeuvred through level ice and ridges before mooring into the ice at 77.36°N, 24.20°E, map shown in Figure 48. 14 BH were made with internal distance 2 m parallel to one of the ridges, see Figure 62, where the snow depth ranged from 1 to 16 cm. The BHs were enumerated from H1 to H14, where H1 is closest in the photo. The distance to the top of the ridge at the right side is 9.1 m at H14, 6.1 m at H7 and 7.7 m at H1.

The ice thickness of the topmost layer varied from 50 to 120 cm. Aiming for testing this layer, IDs ranged 32 to 104 cm, with temperatures from -6.1 to -2.7°C. A full temperature profile was made for H4, Figure 63. The tendency is increasing temperature with increasing depth.

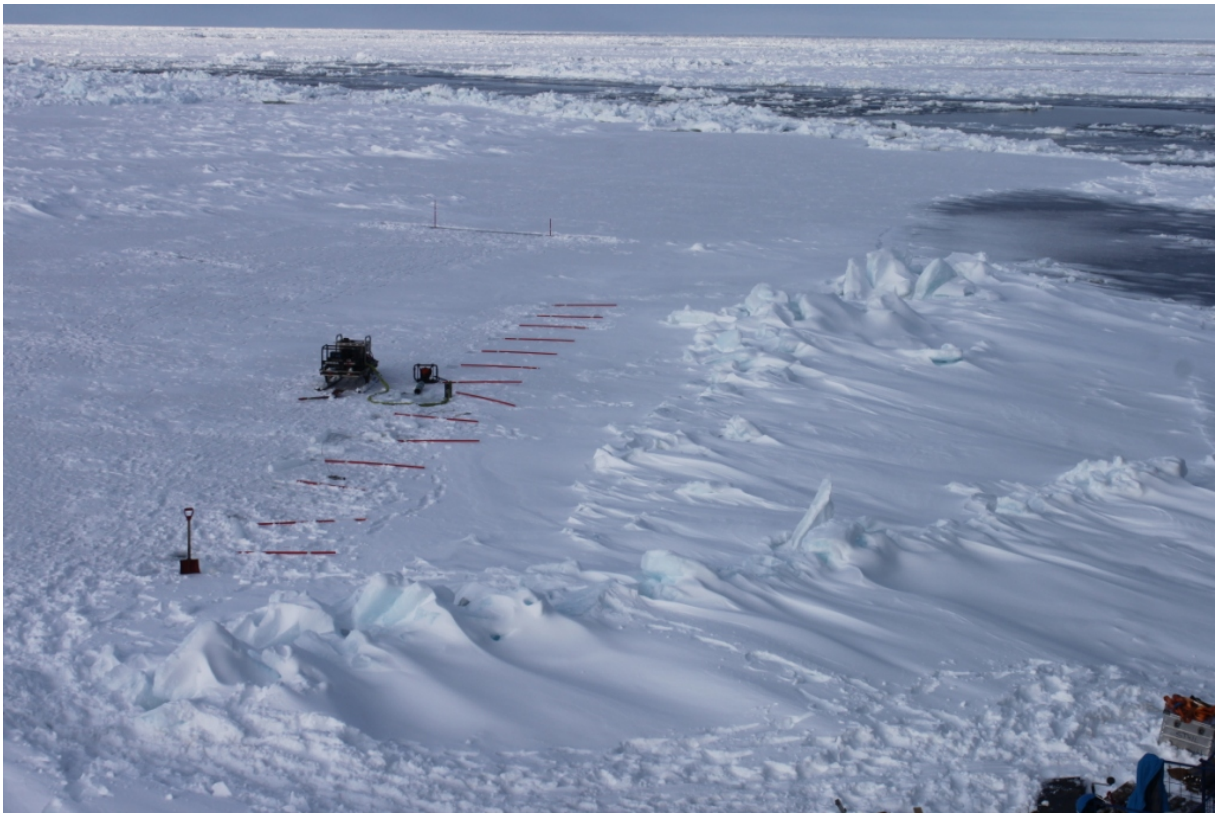

Figure 62: Picture of Grid H and surrounding ice conditions. 14 BH were made in line parallel to an ice ridge with internal distance 2 meters, each at left end of the red sticks.

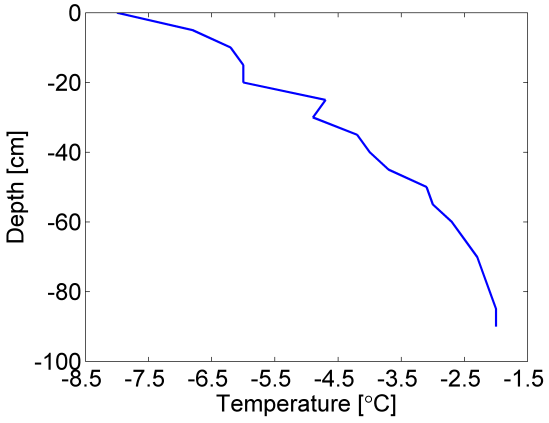

Figure 63: Temperature profile from BH H4 (Elgaard et al., 2012).

Some problems were experienced with the power supply from the 1.6 kWh generator at H9, and was here replaced by the generator of 3.6 kWh. However, data was not affected from this as no tests were running when the problems occurred. Also, the two generators were closely watched during testing and no problems were observed. Hence, the power supply was considered sufficient for all BHJ tests.

8 Results

This chapter presents an assortment of BHJ data collected from fieldwork done in Van Mijenfjorden and in the Barents Sea during March and April 2012. It is here focused on results that distinguishes from others due to observations during testing or to substantiate a certain classifications of tests. The BHJ records are shown as stress and stress rate - time curves with photos of failure modes where this is available. A summary of the data is found in the latter section of the chapter in form of statistical data in tables and figures. Supplementary data for all tests is found in Appendix C, D, E and F where tables and stress - time curves of Grid AB, CDE, EFG and H are given respectively.

The term minimal vertical confinement (C_{min}) is used consistently from here on instead of indentor depth and ice thickness when describing test depth. C_{min} refers to the shortest distance from the *ID* to either top or bottom surface of the ice. It is more convenient to use because a significant number of tests were done where the confinement was decisive for the outcome. Also, the fact that the tests in Grid CD and EFG were done in the center of the ice floe gives the term a second meaning, namely half the ice thickness.

8.1 Grid AB

Figure 64 show the two tests where the indentor twisted, and Figure 65 the successive tests where the indentor twisted back. Test 5 and 17 both have BH strength of 3.6 MPa

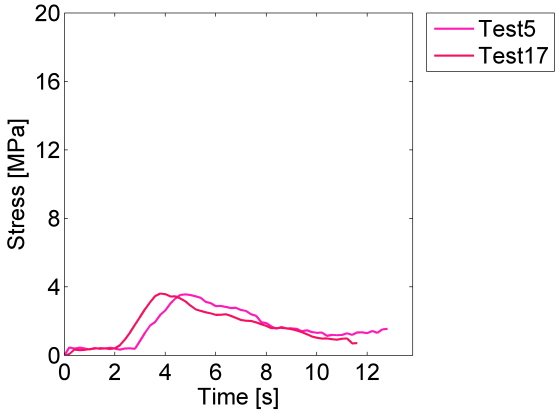

Figure 64: Stress - time curves for Test 5 (A1.5) and 17 (A3.3) classified UY4 and UY1 failure respectively.

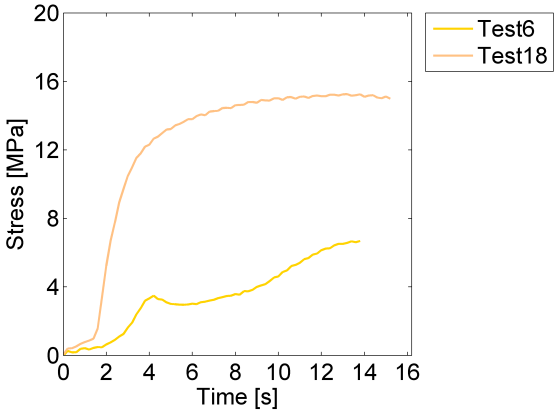

Figure 65: Stress - time curves for Test 6 (A1.6) and 18 (A3.4), classified UY3 and AS failure respectively.

Test 10 and 13, Figure 66 and 67, are both classified UY2 failures and are presented here to illustrate that common failure types may show significant differences in magnitude of failure stress and behavior of post-peak stress. Test 10 has a considerable drop in stress and stress rate at 6.6 s followed by an increase towards the later stages.

The main results obtained from the tests presented here are shown in Table 3.

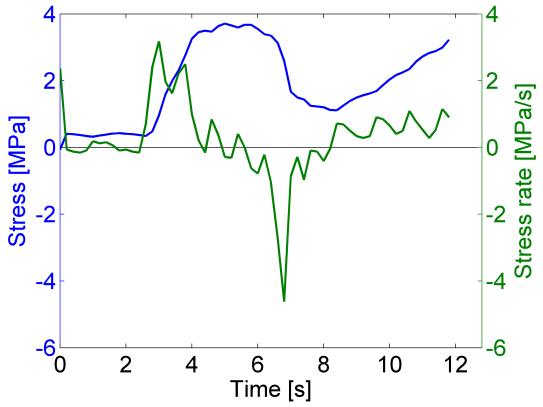

Figure 66: Stress and stress rate - time curves for Test 10 from A2.5, classified UY2 failure.

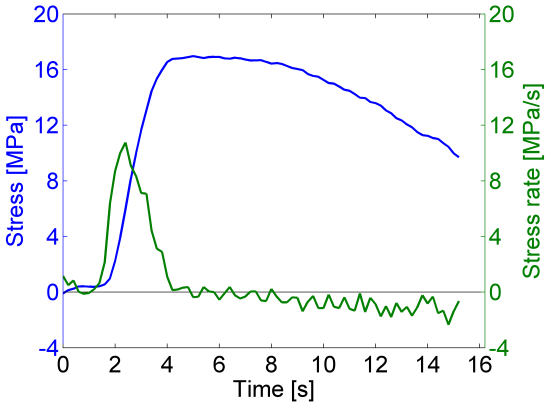

Figure 67: Stress and stress rate - time curves for Test 13 from A2.2, classified UY2 failure.

Table 3: Main results for Test 5, 6, 10, 13, 17 and 18 from Grid A.

Test	BH	FT	C_{min} [cm]	U/D [s$^-$1]	T [°C]	σ_f [MPa]	t_f [s]	$\dot{\sigma}_{af}$ [MPa/s]
5	A1.5	UY4	23	0.43	-	3.6	4.8	0.7
6	A1.6	UY3	30	0.40	-	3.5	4.2	0.8
10	A2.5	UY2	19	0.47	-	3.7	5.0	0.7
13	A2.2	UY2	23	0.37	-	17.0	5.0	3.4
17	A3.3	UY1	24	0.48	-	3.6	3.8	1.0
18	A3.4	AS	23	0.37	-	15.3	-	-

8.2 Grid CD

Fragment C and extracted core from Test 12, C3.4, can be seen in Figure 68 with accompanying stress and stress rate - time curves in Figure 69. A considerable drop in stress is found at 8.8 s. The bottom of the core points left in the picture and the characteristic white layer in top is a result of the ice growing upwards. Figure 70 and 71 represent the tests conducted in the center of Grid C and D respectively. From Table 4 it is found that the differences between the tests mainly rely on failure type and indentation rate. Spatial variation of failure stresses for Grid C and D in Figure 72 and 73, where 24 tests were conducted in the former and 9 in the latter. Failure/max stresses for the grids ranges from 10.1 to 19.1 and 16.5 to 17.3 MPa respectively. Lack of information leaves an open area in C3.1.

Table 4: Main results for Test 12, 13 and 25 from Grid C and D.

Test	BH	FT	C_{min} [cm]	U/D [s$^-$1]	T [°C]	σ_f [MPa]	t_f [s]	$\dot{\sigma}_{af}$ [MPa/s]
12	C3.4	UY4	20	0.49	-1.8	14.1	5.6	2.5
13	C3.3	UY1	21	0.39	-2.0	16.2	8.2	2.0
25	D2.2	AS	21	0.27	-2.1	16.5	-	-

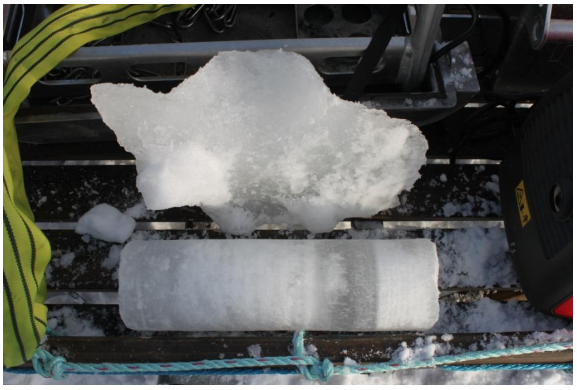

Figure 68: Core and Fragment C from spalling failure in Test 12 (C3.4).

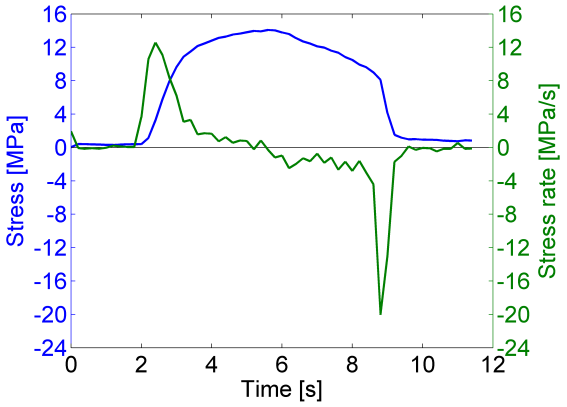

Figure 69: Test 12 (C3.4), UY4 failure.

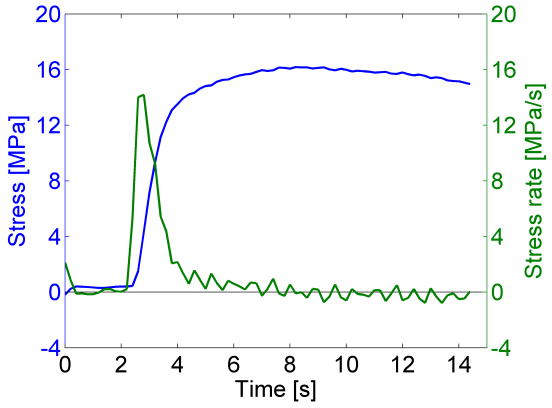

Figure 70: Stress and stress rate - time curves for Test 13 (C3.3), UY1 failure.

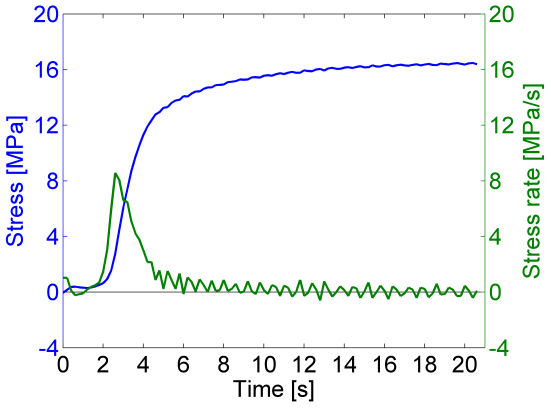

Figure 71: Stress and stress rate - time curves for Test 25 (D2.2), AS failure.

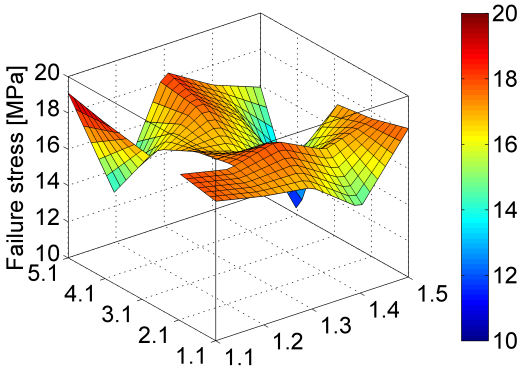

Figure 72: Spatial variation of failure stress of Grid C. The internal distance between BHs is 25 m.

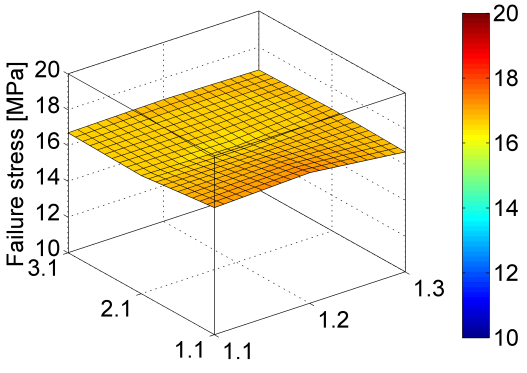

Figure 73: Spatial variation of failure stress of Grid D. The internal distance between BHs is 5 m.

8.3 Grid EFG

Test 1 and 4 from Grid E is omitted from the summary in Table 8 as the ice may have been disturbed in this area upon mooring of the vessel. Nevertheless, Test 4 is presented in this chapter, since its failure mode was exceptional.

Test 2 showed spalling failure in top, but was constrained in bottom. Fragment C is seen in Figure 74, with stress and stress rate - time plots in Figure 75.

Spalling failure top and bottom was the case for Test 3 (E2.2), shown in Figure 76 and 77. The indentor did a jump forward at about 10.5 s, causing severe drops in stress and stress rate. The circular shape of ice Fragment C is recognized from Figure 5 c) in Introduction.

For Test 7, (E.4.1), spalling failure took place only in the top of the ice, i.e. only Fragment C broke off, see Figure 78 and 79.

Figure 74: Spalling failure in top of the ice from BH E2.1 (photo courtesy of S. Løset).

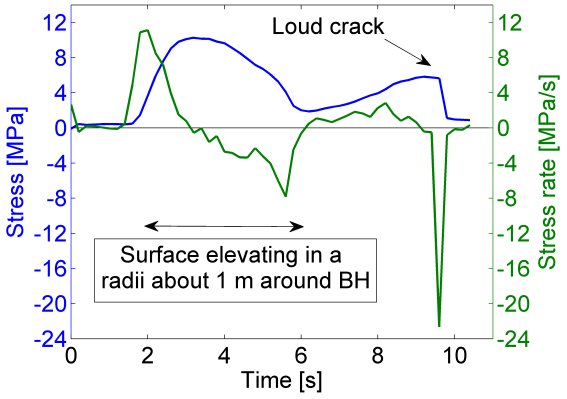

Figure 75: Stress and stress rate - time curves for Test 2 (E2.1), UY3 failure.

Figure 76: The ice conditions after Test 3 (E2.2). Spalling both Fragment B and C.

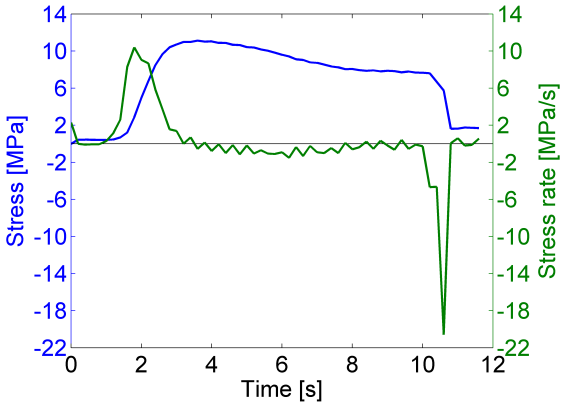

Figure 77: Stress and stress rate - time curves for Test 3 (E2.2), UY4 failure.

Figure 78: Test 7 (E4.1). Unconstrained top and constrained bottom.

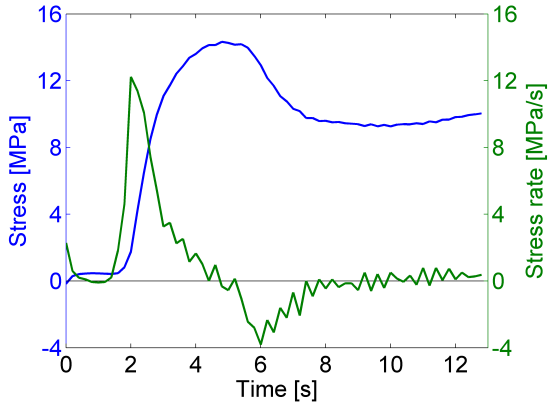

Figure 79: Stress and stress rate - time curves for Test 7 (E4.1), UY3 failure.

Figure 80 show radial cracks ±90° to the indentation direction at E1.2, Test 4, which was conducted 3.35 m from open water. The cracks propagated about 6 m to either side of the BH, where one deflected into the open water and the other abruptly stopped. The appurtenant stress and stress rate - time curves are shown in Figure 81. The cracks occurred at about 3 s, causing a P failure. The test was aborted shortly after.

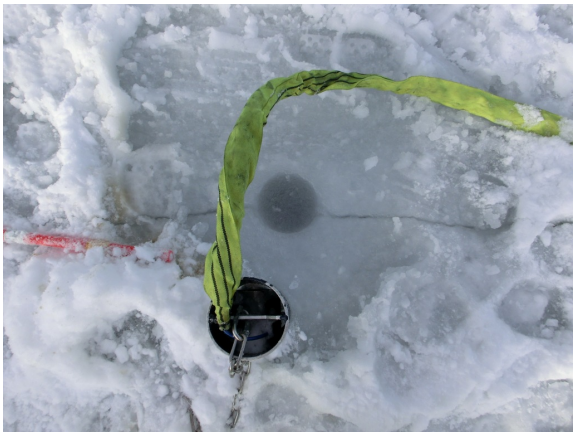

Figure 80: Radial cracks from Test 4, E1.2. Indenor directed upwards in the picture.

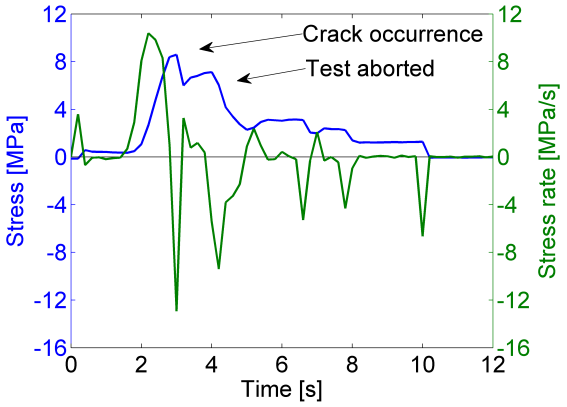

Figure 81: Stress and stress rate - time curves for Test 4 (E1.2), P failure.

Test 6, G2.3, was conducted in a block of rafted ice, see Figure 82, cracks formed at ±45°and -180° to indentation direction. Stress and stress rate - time curves is shown in Figure 83.

Supplementary data for tests conducted in BH E2, E3, E7, E4 and G6 is found in Table 5.

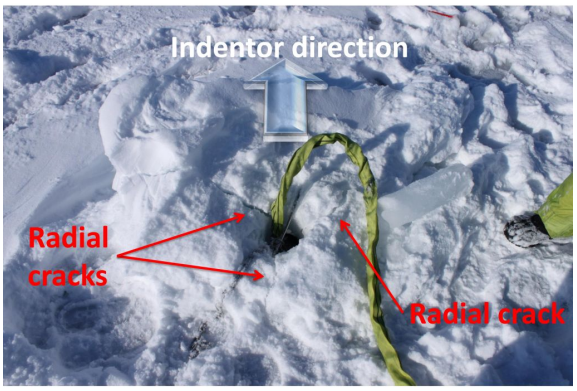

Figure 82: Test 6 (G2.3). Radial cracks from test performed in rafted ice block.

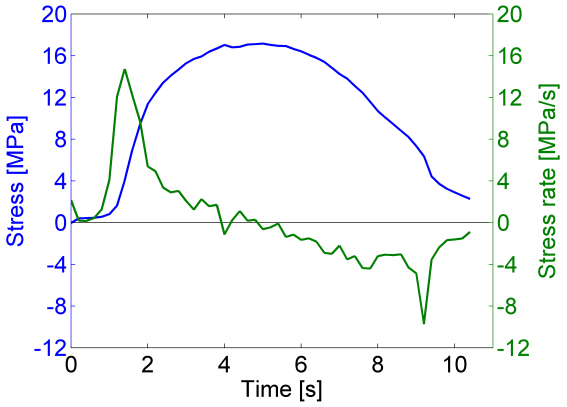

Figure 83: Stress and stress rate - time curves for Test 6 (G2.3), UY1 failure.

Table 5: Main results from Grid E and G.

Test	BH	FT	C_{min} [cm]	U/D [s$^-$1]	T [°C]	σ_f [MPa]	t_f [s]	$\dot{\sigma}_{af}$ [MPa/s]
2	E2.1	UY3	10	0.53	-2.6	10.3	3.2	3.2
3	E2.2	UY4	10	0.48	-2.8	11.1	3.6	3.1
4	E1.2	P	9	-	-2.9	8.6	3.0	2.9
7	E4.1	UY3	20	0.43	-3.6	14.3	4.8	3.0
6	G2.3	UY1	20	0.53	-	17.2	5.0	3.4

Figures 84 to 86 show how the failure stresses varied throughout Grid E, F and G respectively. It is seen that the lowest stresses are found closest to the vessel, and as approaching the ridged area the magnitudes increase.

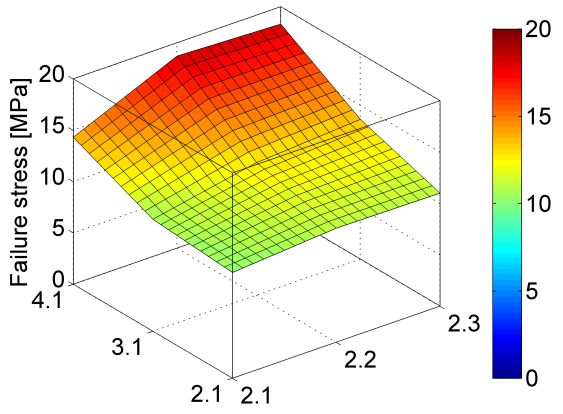

Figure 84: Spatial variation of failure stress in Grid E. Internal distances between BHs are 10 m.

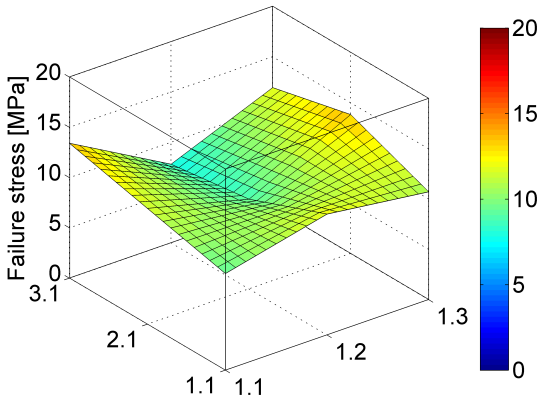

Figure 85: Spatial variation of failure stress in Grid F. Internal distances between BHs are 2 m.

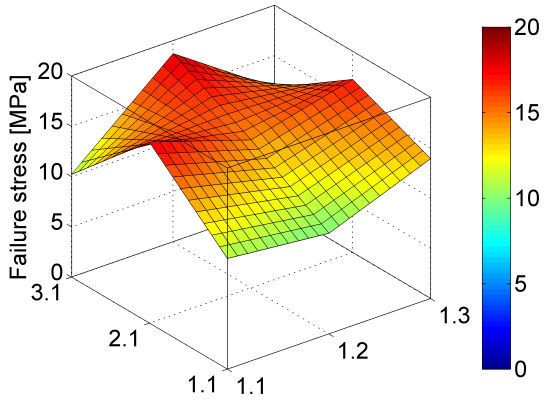

Figure 86: Spatial variation of failure stress in Grid G. Internal distances between BHs are 2 m.

8.4 Grid H

Figure 87: Bottom 30 cm of H3 extracted as one core. Large brine pocket (left) located at 105 cm depth.

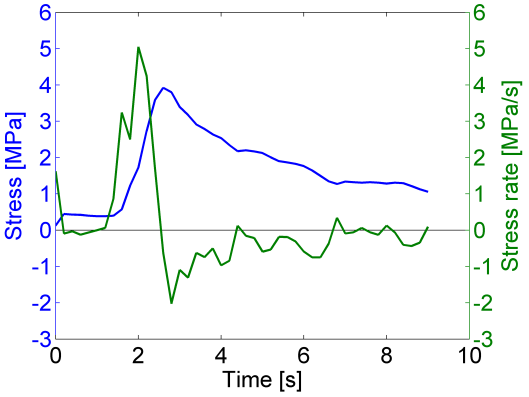

Figure 88: Stress and stress rate - time curves for Test 7 (H3), UY1 failure and conducted at 86 cm depth.

Extensions were needed here to extract the core shown in Figure 87. The core is from 70 to 110 cm depth and the brine pocket appeared at 105 cm. Test 7, H3, was done at 86 cm and had the second lowest failure stress in the grid, see Figure 88. Main parameters of the test are found in Table 6. Figure 89 shows the failure type, temperature, indentor depth and ice thickness across Grid H.

Table 6: Test 7 from Grid H.

Test	BH	FT	C_{min} [cm]	U/D [s^{-}1]	T [°C]	σ_f [MPa]	t_f [s]	$\dot{\sigma}_{af}$ [MPa/s]
7	H3	UY1	24	0.62	-2.6	3.9	2.6	1.5

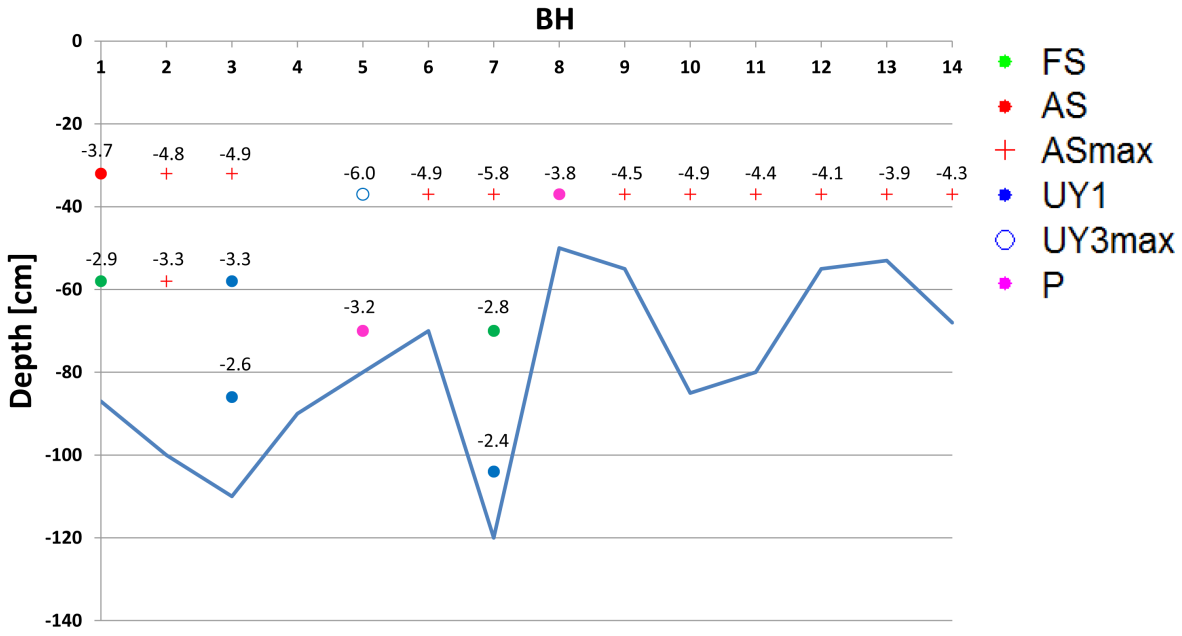

Figure 89: Failure types vs. test depth and ice thickness in Grid H. Temperatures at ID are shown in °C and the distances between BHs are 2 m. The blue line represents the profile of the ice.

8.5 General

Table 7 shows the frequency of failure types in total and within the respective grids given in percentage in parentheses. It is seen that UY1 is the most common failure type of all, and that

Table 7: Failure type sorted by grids with number of and percentage occurrence.

FT	Total	Grid AB	Grid C	Grid D	Grid E	Grid F	Grid G	Grid H
FS	5 (5%)	2 (7%)	1 (4%)	-	-	-	-	2 (10%)
AS	11 (10%)	4 (14%)	3 (13%)	2 (22%)	1 (11%)	-	-	1 (5%)
UY1	29 (27%)	8 (29%)	12 (50%)	4 (44%)	-	-	2 (22%)	3 (15%)
UY2	4 (4%)	2 (7%)	1 (4%)	1 (11%)	-	-	-	-
UY3	19 (18%)	3 (11%)	3 (13%)	1 (11%)	6 (67%)	5 (56%)	1 (11%)	-
UY4	16 (15%)	6 (21%)	2 (8%)	1 (11%)	2 (22%)	3 (33%)	2 (22%)	-
P	7 (6%)	-	-	-	-	1 (11%)	4 (44%)	2 (10%)
AS_{max}	16 (15%)	3 (11%)	2 (8%)	-	-	-	-	11 (55%)
$UY3_{max}$	1 (1%)	-	-	-	-	-	-	1 (5%)
Total	108	28	24	9	9	9	9	20

Table 8: Mean and standard deviation (STD) values of main parameters from all grids sorted by failure type (top) and grid (bottom). Temperature values are calculated from where available, that is Grid C, D, E and H.

FT	Total	C_{min} [cm]		U/D [s^{-1}]		T [°C]		σ_f / σ_{max} [MPa]		t_f [s]		$\dot{\sigma}_{af}$ [MPa/s]	
		Mean	STD	Mean	STD	Mean	STD	Mean	STD	Mean	STD	Mean	STD
FS	5	29.8	11.7	0.40	0.10	-2.6	0.4	-	-	-	-	-	-
AS	11	24.0	4.3	0.33	0.05	-2.4	0.6	17.3	1.3	-	-	-	-
UY1	29	22.3	6.7	0.46	0.08	-2.2	0.3	14.5	4.6	6.6	1.9	2.3	0.8
UY2	4	20.7	1.8	0.40	0.06	-2.1	0.1	14.0	6.9	6.8	2.1	2.1	1.1
UY3	19	16.0	6.9	0.49	0.07	-2.7	0.5	11.8	4.2	3.9	0.7	3.1	1.2
UY4	16	18.3	6.7	0.47	0.09	-2.4	0.5	10.9	5.2	4.4	1.7	2.7	1.4
P	7	12.4	6.6	0.55	0.04	-3.5	0.4	10.8	2.5	2.6	0.3	4.1	0.9
AS_{max}	16	29.0	7.8	-	-	-4.2	0.9	19.1	0.4	-	-	-	-
$UY3_{max}$	1	37.0	0.0	-	-	-6.0	0.0	19.3	0.0	5.0	0.0	3.9	0.0
Grid AB	28	24.0	4.7	0.41	0.05	-	-	11.1	6.0	5.7	2.1	1.5	0.9
Grid C	24	22.0	3.0	0.49	0.08	-2.1	0.3	16.8	1.9	6.9	1.7	2.7	0.7
Grid D	9	21.0	1.4	0.39	0.09	-2.2	0.1	16.8	0.3	6.8	2.0	2.7	0.8
Grid E	9	13.0	5.0	0.42	0.10	-2.9	0.4	13.0	3.2	3.8	0.7	3.2	0.3
Grid F	9	13.0	6.3	0.50	0.06	-	-	11.1	2.0	3.5	1.0	3.4	1.1
Grid G	9	14.7	5.2	0.54	0.05	-	-	14.0	3.4	3.3	0.9	4.3	0.7
Grid H	20	29.8	11.8	0.47	0.14	-4.0	1.0	16.3	5.8	4.3	2.9	2.5	1.4

FS and UY2 represented the most rare cases (considering AS_{max} and $UY3_{max}$ as one). No values of indentation rates are given where maximal capacity of the system is reached. The reason is that one does not know if the indentor is fully extracted in these tests. This can be found in the pressure recordings for the other failures, as the pressure will abruptly increase to 2150 mV (maximal capacity) when reached 50 mm displacement. Hence, the velocity is found by dividing the time lapse of the test by 50 mm.

It is also found that the maximal capacity of the system is reached in 16% of the tests, where 12 of these were done in Grid H. For Grid AB and C, which are also the grids of greatest span, all types but P are represented. Grid E and F are similar in the way that both have a majority of UY3 failures, where Grid G showed P failure in 44% of the tests. From Table 8 it is seen that the mean failure/max stresses of Grid C (100 by 100 m) and D (10 by 10 m) are both 16.8 MPa, where the standard deviation is 1.0 MPa for the former and 0.3 MPa for the latter. It is also noted that the mean values of failure/max stress of Grid H is not considered representative since a significant number (60%) of the tests reached maximal capacity of the system. In reality these tests would fail at higher stresses. As indicated earlier, max capacity have the highest value of C_{min} and the lowest T in terms of mean values. Low temperatures (-3.5°C on average) and low C_{min} (12.4 cm on average) provokes P failures.

Figure 90 to 95 show σ_f / σ_{max} plotted vs. T, t_f and $\dot{\sigma}_{af}$ in pairs for FT and grid in scatter diagrams. Figure 96 and 97 show how U/D varies with C_{min}.

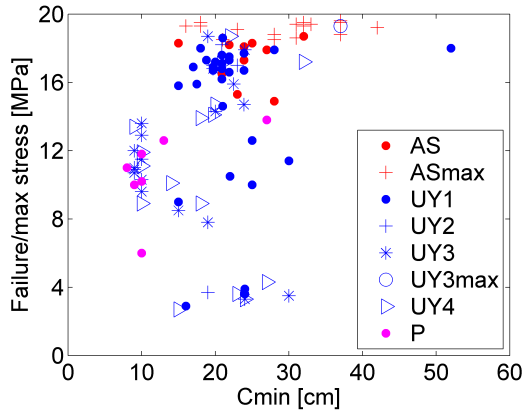

Figure 90: Failure stress vs. minimal confinement, highlighting failure types.

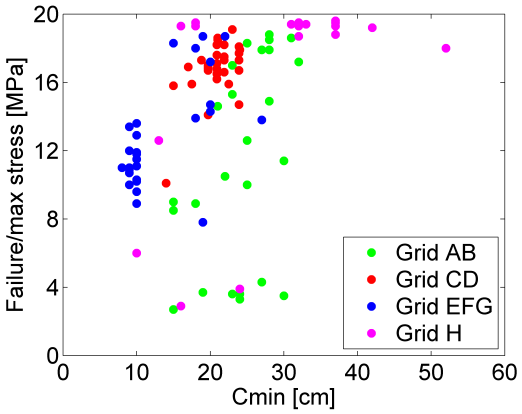

Figure 91: Failure stress vs. minimal confinement, highlighting grids.

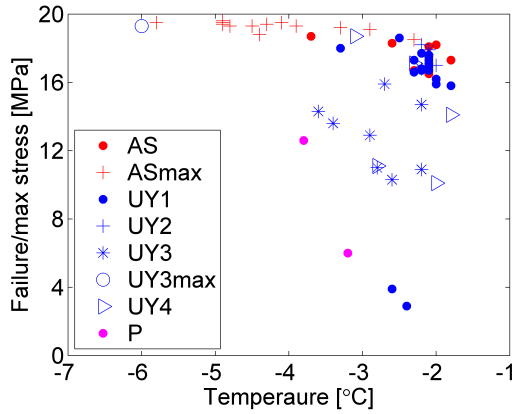

Figure 92: Failure/max stress vs. temperature, highlighting failure types.

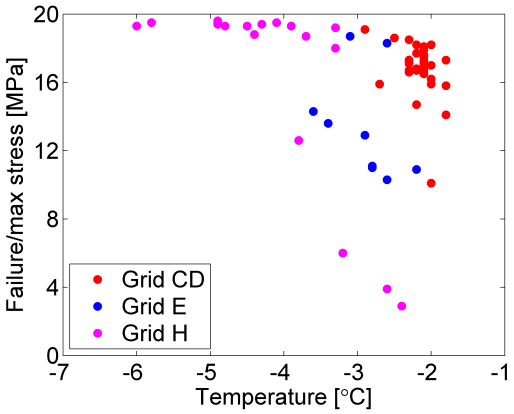

Figure 93: Failure/max stress vs. temperature, highlighting grids.

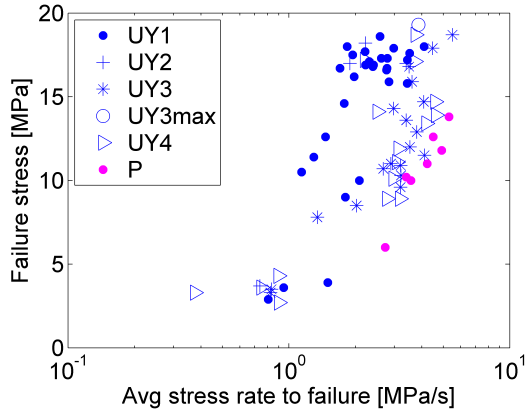

Figure 94: Failure stress vs. average stress rate to failure, highlighting failure types.

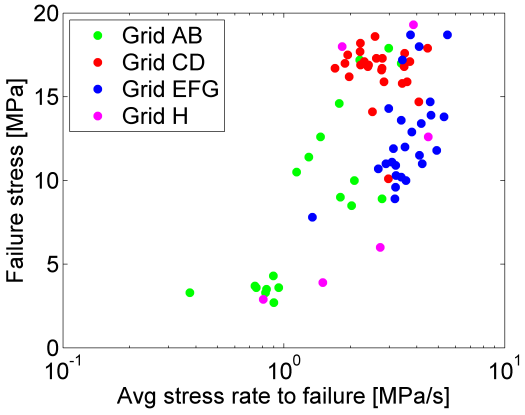

Figure 95: Failure stress vs. average stress rate to failure, highlighting grids.

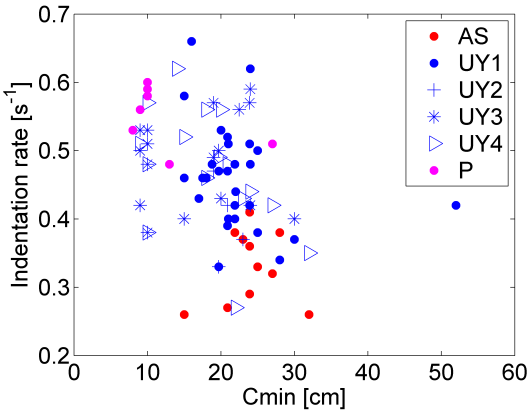

Figure 96: Indentation rate vs. C_{min} highlighting failure types.

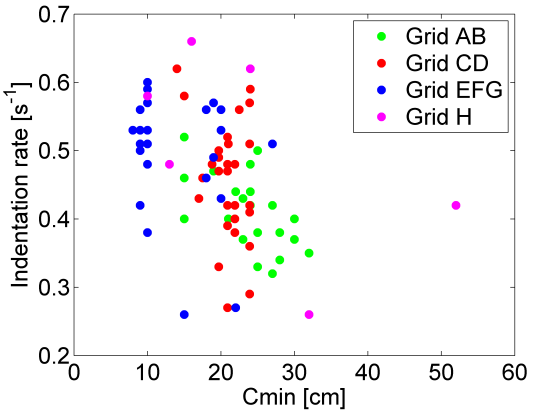

Figure 97: Indentation rate vs. C_{min} highlighting grids.

9 Discussion

The main goal of the fieldwork was initially to investigate the spatial variation of the BH strength. It turned out that the ice conditions that were encountered forced the focus towards the vertical confinement of UNIS-BHJ tests instead, as the BH strength is fundamentally based on confined tests. What appears as weak zones in the BHJ tests from Grid E, F and G may be results of the ice being allowed to expand in vertical direction. Until now, conservative values of minimal vertical confinement (37 cm) have been used to ensure full confinement. Uncertainties related to the confinement of the ice occurs when the thickness becomes less than 74 cm, hence the necessity of a more accurate value. Which do, like every other parameter in ice mechanics, depend on the physical properties.

The statistical data available here is not considered sufficient for drawing major conclusions, and the effect is magnified when dividing into subgroups, resulting in even fewer measurements to rely on. However, some tendencies are found and are addressed in this chapter.

9.1 Classification

Using the classification chart and definitions from Chapter 6, examples of each failure type are presented in Figure 98 to 105. Note that different scaling between the figures is used both for stress and stress rate at y-axes and time on x-axis. It is also seen that the stress rate is presented for all results to illustrate certain definitions.

Figure 98 shows a FS (*e-h*) failure. It is seen that the stress is continuously increasing throughout the test and that it takes between 2 and 3 s for full contact to be established between the indentor and the BH wall, which is typical for most tests. An example of AS (*e-h-c*) failure is given in Figure 99. From 0 to 10.2 s the ice is going through the elastic and hardening zones, before the stress stabilizes at about 15 MPa. Even though the stress rate is greater than 0.1 MPa/s and less than -0.1 MPa/s at times (as seen at 11.8 s) it is the general behavior of the ice after the hardening process has ended that defines the last part of the test as constant stress.

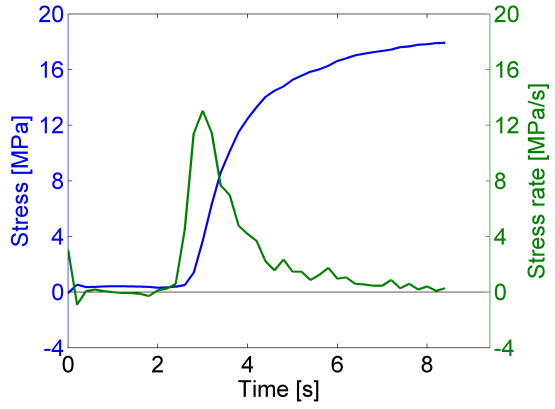

Figure 98: Example of FS failure. Test 4 from Grid C, Van Mijenfjorden 27.03.12.

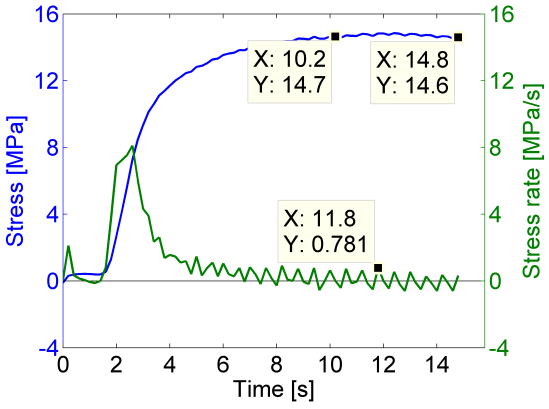

Figure 99: Example of AS failure. Test 19 from Grid A, Van Mijenfjorden 22.03.12.

UY1 (*e-h-s*) failure shown in Figure 100. The failure occurs at 8.2 s which is the transition between hardening plasticity and softening plasticity. Figure 101 shows an UY2 (*e-h-c-s*) failure

as constant stress is found from 4.2 to 7.8 s (-0.1 MPa/s < $\frac{0.21MPa}{3.6s}$ < 0.1 MPa/s), though it is seen also here that variations give stress rates outside the range.

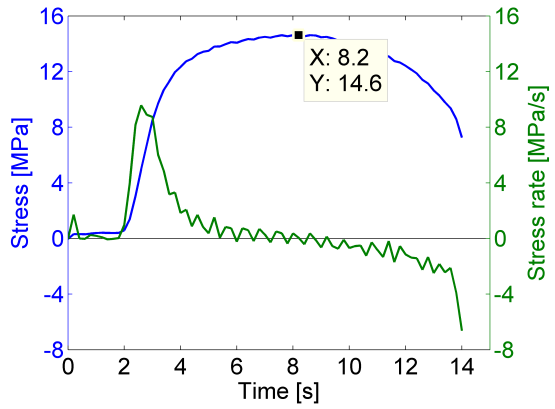

Figure 100: Example of UY1 failure. Test 29 from Grid B, Van Mijenfjorden 22.03.12.

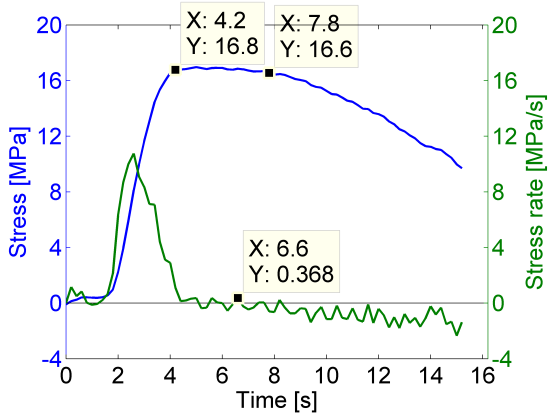

Figure 101: Example of UY2 failure. Test 13 from Grid A, Van Mijenfjorden 22.03.12.

A typical UY3 (*e-h-s-h*) failure is found in Figure 102, where the BH strength is obtained from the first peak at 4.6 s. It may be described as a combination of an UY1 and a FS failure if divided into two parts at about 6.5 s. Further it is noted that the lowest recorded stress rate is -2.2 MPa/s. For this to be categorized a P failure, the stress rate would have to be -2.5 MPa/s or less and occurring in transition hardening to softening, which neither are cases here. An example of UY4 (*e-h-s-c*) failure is given in Figure 103. The post-peak stress is here stabilizing at about 2 MPa.

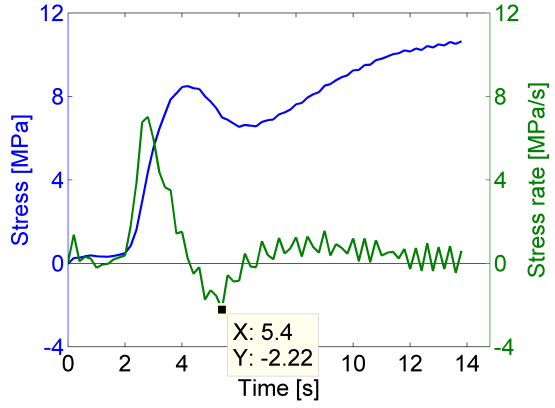

Figure 102: Example of UY3 failure. Test 28 from Grid B, Van Mijenfjorden 22.03.12.

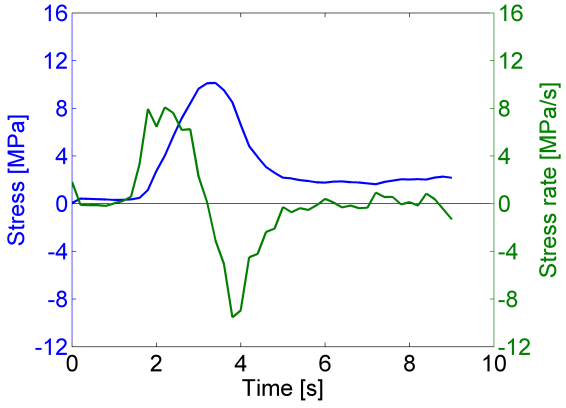

Figure 103: Example of UY4 failure. Test 10 from Grid C, Van Mijenfjorden 27.03.12.

Figure 104 show a P (*e-h-s*) failure since the stress rate is less than -2.5 MPa/s in the transition between hardening to softening. As there is only one P failure type, the post-peak behavior is not taken into account for further evaluation. The test also shows an example of the previously mentioned cycling process of hardening and softening, failing a number of times. Regardless of the magnitude of the failures, the BH strength is obtained from the first peak. The maximal

capacity of the system is reached for the test in Figure 105. Here an AS_{max} (*e-h-c*) is shown, but not considered a failure, because it is not known if the ice yields. For an evaluation of that, the displacement must be taken into account. However, as a significant number of tests reached this limit, the data is included here to illustrate effects of high confinements and low temperatures on BHJ records. It is seen that a magnitude of 18 MPa and about 13.5 MPa/s are reached within 5 s for stress and stress rate respectively, which per definition qualifies for maximal capacity being reached.

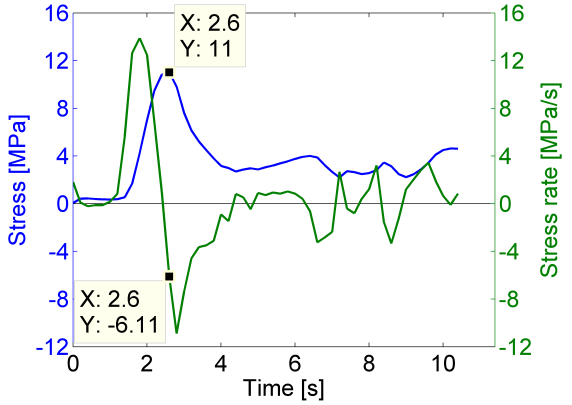

Figure 104: Example of P failure. Test 1 from Grid G, Barents Sea 19.04.12.

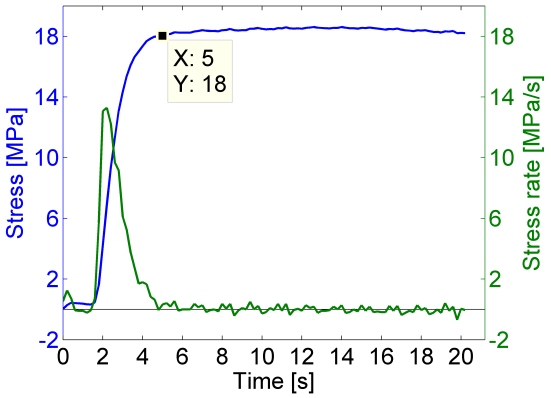

Figure 105: Example of AS_{max} failure. Test 20 from Grid A, Van Mijenfjorden 22.03.12.

9.2 Grid AB

Based on visual inspections, the ice was in general porous with a characteristic skeleton layer in bottom. The temperature profiles show that the ice within testing range varies between -2.3 and -1.3°C for the measured BHs, which is considered warm ice. The deep snow in the area has at least two effects; 1) it acts as an insulating layer on top of the ice and 2) it submerges the ice, resulting in higher salinity content. These are factors that point towards low failure stresses and weak zone encountering, which was the case for the majority of the tests here. Figure 91 shows that the recorded failure stresses from Grid AB are widely spread for C_{min} from 15 to 30 cm. This is substantiated in Table 8 where it is seen that the failures stresses have the highest standard deviations among all grids. This may be due to the BHJ crew not double checking the ice thickness. The measurements on ice thickness were more or less trusted blindly from the first group.

In Test 5 and 17 the indentor twisted. The stress - time curves, Figure 64, are remarkably similar concerning stress development and magnitude of failure stress. However, it is not understood how this relates to the incidents. An explanation to the twisting may be that the jack was not exactly vertical oriented in the BH (perhaps due to non-vertical drilling), or that ice fragments got stuck between the indentor and BH wall when the tests started. Both scenarios could result in a moment on the piston, which in turn may have caused the twisting. A thorough check will be performed at M-Tech's premises during Summer 2012. The successive tests, Test 6 and 18 are shown in Figure 65. Test 18 has an untraditional stress development during the first 1.6 s as pressure increases earlier than most other tests, presumably because contact was established

at an earlier stage. This becomes natural since the curvature of the indentor did not fit the BH wall. With that said, the rest of the test seem to have a rather normal stress development, and it is believed that the twisted indentor was aligned at an early stage and had a negligible effect on the stress development after 1.6 s. Test 6 does not differ from any other test and is also evaluated on similar terms as the rest.

The fact that painting showed signs on vanishing rose questions regarding the design of the equipment. The UNIS-BHJ differs from the original, seen in Figure 4 in Introduction, since minimal expansion of the ice is allowed in horizontal direction above and below the indentor during testing. A test where a strap was placed in approximately 45°angle to the indentor direction between the BH wall and the jack to check if contact truly was established. The diameter of the cylinder and that of the BH leaves an opening of 10 mm, allowing the strap sufficient spacing to be inserted with the jack into the BH. The test proved that the strap was impossible to extract when the piston had reached maximal displacement, hence contact must have been established at this angle. As both the strap and jack is easily taken out of the BH both before and after testing, it is suspected that the elastic deformation plays a key role in preventing the strap from being extracted. A possible change of the design of the jack will be discussed between M-Tech and NTNU in near future.

Test 10 and 13, shown in Figure 66 and 67 make good examples of the tests classified the same failure type and yielding significantly different stresses. The figures also emphasizes the difference after the 4th term of description (both being *e-h-c-s*), as Test 10 clearly has a stress increase in the later stages. However, it is believed that more than 4 terms would lead to confusingly many failure types (which may be the case for 4 subgroups of UY failures as well).

Unfortunately Grid AB did not provide the wanted results on spatial variability due to mud encountering in several of the BHs. However, experience in organizing students and equipment, as well as familiarizing with the ice and mud conditions in the area, was considered of great value.

9.3 Grid CD

Test 12, C3.4, showed spalling failure mode as the ice above the indentor broke off. It is believed that this happens after 8.8 s, where an abrupt decrease in stress is registered. Comparing Tests 13 and 22 (C3.3 and D2.2), which are tests conducted 1.5 m apart, minimal differences are found in failure stress. However, Test 13 indicate a weak layer distant from the indentor, and this may be the reason for the stress rate upon contact with the BH wall and indentation rate being greater than for Test 22. If the observations are related to each other, it is unknown how and to what extent. It should also be mentioned that 1.5 m seem sufficient for full horizontal confinement also for the UNIS-BHJ, as no weak zones (no influence from Test 12) is detected in the latter test.

From Figures 72 and 73 for Grid C and D it is seen that the variability in Grid C is larger than that found for failure stresses in Grid D, which is reasonable since the former is significantly larger in size. Considering the failure/max stresses found in Table 8, it is striking to see that the mean values both are 16.8 MPa, where also the STDs substantiate the larger variations found in Grid C. It may be argued that a grid of size 10 by 10 m reflects the same failure stresses as a 100 by 100 m grid when established in FYLI, given uniform ice thickness and temperature. However, more data is required for verification.

What recognizes many of the tests in Grid C and D are substantial decreases in stresses in the softening zone. It was mentioned that the distance to the weak zones influences both the magnitude of the UY stress and the time to failure (Shkhinek et al., 2010). From Table 8 it is found that Grid C and D on average have the longest time to failures and greatest failure stresses among all grids, which would indicate weak zones in considerable distances to the indentor, but does not explain the rapidly decreasing stresses in the post-peak zones. Therefore, it not unthinkable that this phenomenon is partly explained by the ice being allowed to expand in vertical direction or even spalling failures. Elevation of the ice surface could not be registered here due to the considerable amount of snow and surface water covering it. If this is the case, the tests conducted here (C_{min} from 14 to 24 cm) are in what may be categorized the transition zone to full vertical confinement.

9.4 Grid EFG

Similarities between Test 2 and 3 are seen at the later stages of the tests where considerably drops in stress and stress rates occur. It is possible that the spalling failures occur here. If so, it would be convenient to have this expressed in the respective failure types. Perhaps this would be possible if the system relied on the stress rate - time curve for classification, where the magnitude of failure also could be quantitatively measured. This is however a system that would rely much on indentation rate and logging frequency, and may not be easily compared across different BHJs.

No significant drops in stress or stress rate were registered during Test 7, E4.1. In fact, the post-peak stress is significantly greater than that of the other two examples shown here, which is possibly related to the thicker ice encountered. Its failure type was UY4 as the softening process per definition stops at about 10 s. It may however be better described as an UY3 failure, since the softening is very modest at the later stages (7 to 10 s).

Common for Test 4, E1.2, and Test 6, G2.3, is that both resulted in radial crack failures. However, the BHJ records show distinct stress and stress rate - time curves, where the former shows a P failure and the latter an UY1 failure. The differences are emphasized in Table 5. It is not possible to read from the stress - time curves of Test 6, Figure 83, at which time the cracks form. This may require an assessment of the acoustic emissions through accelerometers installed in the ice, as was shown by Sinha et al. (2012). However, the stress rate is perhaps indicating failures in the ice at about 4 and 9 s. The stress rate - time curve expose changes in the stress - time curve, which may be better intercepted with higher logging frequencies. For the UNIS-BHJ system it is possible to program the transducer to increase the logging frequency from 5 Hz to 50 Hz. Running tests parallel with acoustic measurements would tell if it is possible to identify crack formation from stress - time or stress rate - time curves.

Grid E, F and G covers young and rafted ice. The three tests with the greatest confinements are also the tests with the greatest failure stresses in Grid E. The trend is also present in Grid F and G.

Failure stresses of 13.0, 11.1 and 14.0 MPa in Grid E, F and G respectively, showed that the ice encountered was weaker than that of FYLI in Van Mijenfjorden, which is likely related to the ice thickness on average being thinner at this location. STD values also suggest that a larger variation is found here, which is natural since both young ice and rafted ice are represented. It is also reminded that the grids are smaller, 20 by 20 m and two times 4 by 4 m. This implies that the

randomness of mechanically deformed sea ice is harder to estimate than the FYLI encountered in a fjord. It can also be mentioned that the temperatures are generally colder in Grid C and D, which emphasize the effect of confinement on failure stresses.

For Grid E and F all failures at 10 cm are classified UY3 or UY4, while the same is true for P failures in Grid F for 8 and 10 cm. Considering Figure 93 it is found that the failure stress increases linearly with decreasing temperature for 7 out of the 9 tests in Grid E. Test 8 and 9 stand out probably due to the greater minimal confinements encountered here. Spalling failures are frequently found, especially for young ice, but also in other cases, e.g. in F3.2 where elevation of the surface was observed. From the salinity profile shown in Figure 59 a more narrow estimate of salinity was encountered at 10 cm depth than at 20 cm. This could imply that the variations in failure stresses are thereafter. Such a relation was however not found, and demonstrates that the BH strength is dependent on more than one variable.

9.5 Grid H

Test 7 and 13, in H3 and H7 respectively, both show UY1 failure with low failure stresses. Throughout the grid inspections of cores revealed that large brine pockets often were found in these parts of the ice, which may well be the cause for the low stresses found here. However, the data recorded for Test 7 is not expected to be a direct consequence of the brine pocket shown in the photo, for that the distance is probably too far. The two tests are also those with the highest measured temperatures. From Table 7 it is seen that UY1 failures appear most frequently for high temperatures. The high standard deviation found in Table 8 can be explained by Test 7, 13 and 9, the two former mentioned earlier and Test 9 the test with the least confinement in the Grid, resulting in a spalling (downward breaking) premature failure.

Figure 89 shows the failure types across Grid H with corresponding temperatures, indentor depth and ice thickness for the different BHs. A proper investigation of the confinement would have to include tests closer to the surface since it is evident that 35 and 37 cm are conservative values. In fact, tests in BH 9, 12 and 13 show that maximal capacity is also reached for 18, 18 and 16 cm respectively. Premature failures are expected encountered if tests are done closer to the surface, as these seem prominent for low confinement and low temperatures, see Figure 8.

9.6 General

From Table 7 it is seen that UY1 failures are most common for FYLI, appearing in 29% (Grid AB), 50% (Grid C) and 44% (Grid D) of the tests. UY2 failures did only occur in 4% on total, which means its applicability will have to be evaluated in possible future classification systems. UY3 (67% in Grid E), UY4 (56% in Grid F) and P (44% in Grid G) failures dominated in young sea ice of 10 cm confinement, while maximal capacity of the system was reached in 60% of the tests in colder rafted ice. AS failures were represented at every site and showed an average appearance of 10%. It is surprising to see that FS failures only occurred in 5% of the tests, as this failure type was expected frequently found in warm first-year ice. It may be that the system overrules appearances as a 0.5 MPa drop in stress qualifies for failure, and a re-evaluation of the definition may come necessary. The indentation rate is also relatively high for the current BHJ system and may provoke such failures. This low ratio of FS failures underlines that the statistical data collected here is not sufficient of drawing conclusions (among others) on failure

type appearance. It also amplifies the suspicion that the low-confined ice encountered conduced to more frequent UY appearances.

The standard deviations of failure stresses are relatively high, both among FTs and within grids respectively, see Table 8. This is substantiated in Figures 90 to 97. However, there are exceptions. AS failures have the lowest STD of all FTs, disregarding AS_{max} and $UY3_{max}$, which are classified partly based on the criteria. AS failure is typical for low indentation rate and confinement greater than 18 cm. It is also seen that UY1 failures show a distinct greater failure stress than UY3 and UY4 failures. This is probably due to the generally higher C_{min} found in UY1 that is related to ice features mentioned above. Hence, it seems to be a greater coherence between FT and C_{min} than FT and failure stress. The latter being exemplified in Chapter 8.

It is seen in Figure 91 that the general trend is increasing failure stress with increasing confinement until 32 cm, from where the maximal capacity is reached for all tests. Based on the many spalling failures observed in the young ice (C_{min} of 10 cm) in the Barents Sea, it is obvious that full confinement was not obtained for all tests here. Also, the FYLI encountered in Grid CD is suggested to be in the transition zone for vertical confinement. Therefore, one can only assume that full confinement is obtained in range 14 to 32 cm, where the value depends on the physical properties encountered in the ice. This is verified by the tests conducted with C_{min} of 18 and 16 cm reaching the maximal capacity of the system for colder ice in Grid H. Hence, deeper investigations on the matter are required.

Figure 93 and 92 show that failure stresses increase with decreasing temperature, also within each grid respectively. This is in accordance with what was discussed in Literature by Blanchet et al. (1997). Below -3.8°C maximal capacity is reached for every test, where all are found in Grid H.

From Figure 94 and 95 it is seen that the magnitudes of $\dot{\sigma}_{af}$ are generally greater than what was reported in Literature (0.01 to 3.0 MPa/s). In fact, the mean values of the respective FTs are in range 2.3 to 4.1 MPa/s. One explanation may be that the NTNU-BHJ has a high indentation rate, which means a generally shorter time to failure. The fact that the failure stresses are of lower magnitudes, which is partly due to many tests conducted in low-confined ice and that failure stresses greater than 18.5 MPa could not be recorded, should lead to a reduced $\dot{\sigma}_{af}$. Evidently, sufficient compensation was not obtained. Considering Figure 94 it is also seen that UY1, UY3, UY4 and P occurs in distinct areas of the plot. P failures dominate for the greater values of $\dot{\sigma}_{af}$, closely followed by UY4 and UY3, and later UY1.

The advantage with the classification system is that the definitions are clear and the opinions of the person utilizing the system are of lesser importance. This means that the system can be globally used, and comparisons across different BHJ results become feasible.

10 Conclusions

The fieldwork investigations can be divided into three groups; spatial variability of BH strength, classification of BHJ records and vertical confinement in BHJ tests. The most important findings from each group are listed in the following sections.

10.1 Spatial variability

- Grids of sizes 100 by 100 m and 10 by 10 meters were established in FYLI in Van Mijenfjorden. Both concluded mean failure stresses of 16.8 MPa with STD of the larger grid equal to 1.9 MPa and the smaller 0.3 MPa.
- Young and first-year rafted ice were encountered the Barents Sea. Three grids of sizes 20 by 20, 4 by 4 and 4 by 4 m introduced average failure stresses of 13.0, 11.1 and 14.0 MPa with STDs 3.2, 2.0 and 2.4 MPa, emphasizing larger variability in a more complex environment.

10.2 The classification system

- The classification system proved convenient to use and is applicable for all BHJs, allowing comparisons of data to be made regardless of the BHJ used.
- A further development of the classification system will not benefit from more terms of description. An approach that rather quantifies stress decreases throughout tests is preferable as this may detect failures (and possible crack occurrences) in the ice. This will have to be verified by accelerometers installed in the ice.
- BHJ tests in young ice of 20 cm thickness were classified UY3, UY4 or P failure curves, which often resulted in spalling ice fragments upwards and/or downwards.

10.3 Vertical confinement

- A general trend of increasing failure stress was found for increasing vertical confinement.
- It is reason to believe that the transition to full minimal vertical confinement for FYLI and rafted ice is in range 14 to 32 cm. The range is susceptible to temperature variations.
- A direct link between stress - time plots and occurrence of spalling and radial cracking failures was not obtained. But there are indications that abrupt decreases in failure stresses took place at the moment of crack formation for spalling failures.

11 Further work

This chapter is divided into three parts. The first section concerns parts of the UNIS-BHJ and supplementary equipment that needs repair or improvements. The second part carries some suggestions on how to improve the classification system, and the third lists ideas on how to improve interpretation of BHJ data.

11.1 BHJ and field equipment

- The indentor tends to twist from time to time. Currently it cannot be said to be a big problem as the results seem relatively unaffected. However, it is not known if the effect will escalate and eventually render the BHJ broken.
- The BHJ leaks oil both during testing and transportation. However, the pressure recordings do not show any signs of being affected, yet.
- The CR1000 Wiring Panel records noise from the pressure sensor that is hard to discover. Luckily, the Short Cut script reveals the corrupted data where "pressure" is significantly different from "raw pressure".
- A Zarges box or similar is required for protection of the core drill (mainly the knives) upon transportation and storage.
- The design of the jack may prevent the ice from deforming "naturally". Paint vanishing from the front reveals that there are stresses from the ice that acts on the jack surface both below and above the indentor.
- The maximal capacity of the hydraulic system (300 bar) is here reached for a significant number of tests. Especially this has proven a problem in ice colder than -3.8°C. A solution may be replacing the indentor with one of smaller area to induce higher stresses in the ice, without exposing the hydraulic system further. It is of great importance that a new indentor has a smooth surface. The disadvantage by doing so is that comparisons to works by the NRC and the AARI, where indentor surfaces of 6.50 x 10^3 and 6.40 x 10^3 mm^2 are used, as well as previous work with this indentor, 6.36 x 10^3 mm^2, becomes inconvenient. It is also kept in mind that a reduced area of indentation means a reduced volume of ice tested, which in turn means reducing one of the main advantages of the BHJ system; its applicability of measuring the bulk properties of the ice.
- Installing a control lever that allows experiments to be repeated at reduced, but constant, oil flow rate. (Ideally, it is the indentation rate that should be constant.) Currently, this BHJ system (6.7 mm/s in air) also exceeds the indentation rates that of NRC (0.005 to 0.5 mm/s) and AARI (4.2 mm/s constant in ice).
- The logging frequency may be increased from 5 Hz to its maximum of 50 Hz using Short Cut.
- The BHJ is not ready for new missions before the displacement sensor is replaced.

- Currently, it is not known if the transducer is logging when conducting experiments. This is at best inconvenient. A CR1000KD, digital display from Campbell Scientific Inc., should accompany the BHJ as standard equipment, so that displacement and stress can be monitored throughout experiments. Alternatively, an improvised voltmeter could be connected to the CR1000 Wiring Panel to be certain that data is logging at all.

11.2 The classification system

- A system that is able to take several failures into account would be an advantage when attempting to relate failure types to failure modes.
- Based on the stress rate - time curve a system could be established for coping with the case mentioned above, as it allows failures to be quantified. The system would however be susceptible to indentation rate and logging frequency and a global system applicable for all BHJs thus become hard to establish.
- The definition of failure may need a re-evaluation. The value of 0.5 MPa could be increased, or expressed in percentage decrease instead.

11.3 Interpretation of BHJ records

- With a new displacement sensor installed it becomes feasible to investigate if the ice is creeping when the maximal capacity is reached.
- Further investigations can also be done regarding the vertical confinement of the ice, by reducing the uncertainty related to full vertical confinement (for various ice features and physical properties). An evaluation of what should be the minimum distance between tests in the same BH would also be useful.
- Working diagrams are commonly used in concrete technology for e.g. measuring the fracture energy. Introducing the concept to interpretation of stress - displacement curves of BHJ records can allow for new ways of evaluating the data, e.g. on classifying failure types, post-peak stress behavior, energy to failure (BH energy), etc. Useful parameters on the subject may be ready for adoption to the field of ice mechanics. It is however believed that the necessity of a constant indentation rate becomes more urgent here.

References

Barrault, S. and Strub-Klein, L. (2009). An experimental set-up for measuring stress propagation in sea ice, *Proceedings of 20th International Offshore on Port and Ocean Engineering under Arctic Conditions*, pp. 445 – 452.

Bencomo, A., Bertheussen, L., Bulakh, M. and Byrne, E. M. (2012). Report from field work in the van Mijenfjord 27 – 29 march 2012. Unpublished report: AT307f course at UNIS.

Blanchet, D., Abdelnour, R. and Comfort, G. (1997). Mechanical properties of first-year sea ice at Tarsiut Island, *Cold regions engineering* .

Ekeberg, O. C. and Shestov, A. (2011). Data report describing the work and the results of expedition. Unpublished report: Fram Strait expedition August-September 2011.

Elgaard, J., Hassel, T. A., Karlsen, E. and Eriksen, M. (2012). Kompis and TDS - Lance cruise. Unpublished report: AT-208 course at UNIS.

Frederking, R. and Johnston, M. (2002). Testing the compressive strength of sea ice with a borehole jack, *Technical report*, Canadian Hydraulics Centre, National Research Council of Canada.

Johnston, M., Frederking, R. and Timco, G. (2001). Decay of first-year sea ice.

Johnston, M., Timco, G. W. and Frederking, R. (2003). In situ borehole strength measurements on multi-year sea ice, *Proceedings of The Thirteenth (2003) International Offshore and Polar Engineering Conference*, pp. 445 – 452.

Karlsen, E., Elgaard, J., Eriksen, M. and Hassel, T. A. (2012). Measurements of ice thickness, salinity, temperature and density. Unpublished report: AT-208 course at UNIS.

Lønøy, C. (2010). State of the art on borehole jack testing and some recent data from the old ice in the fram strait. Unpublished report: Course AT323 at UNIS.

Løset, S. (1998). At-208. Compendium: AT-208 course at UNIS.

Løset, S., Shkhinek, K. N., Gudmestad, O. T. and Høyland, K. V. (2006). *Actions from ice on arctic offshore and coastal structures*, LAN.

Masterson, D. M. (1996). Interpretation of in situ borehole ice strength measurement tests, *Canadian Journal of Civil Engineering* .

Masterson, D. M. and Graham, W. (1994). Development of the original ice borehole jack, *Canadian Journal of Civil Engineering* .

Norman Einstein (2012). Barents Sea Map, `http://www.eoearth.org/article/Barents_Sea`. Accessed 06.06.12.

Norsk Polarinstitutt (2012). TopoSvalbard, `http://toposvalbard.npolar.no/`. Accessed 06.06.12.

Reyes, A. (2006). Plasticity theory. Lecture material: KT8306 course at NTNU.

Sanderson, T. J. O. (1988). *Ice Mechanics*, Graham and Trotman Limited.

Scharffcher, M. and Scharffcher, P. (2012). Meeting 18th of January at M-Tech premesis, Trondheim.

Shkhinek, K. N., Jilenkov, A. G., Smirnov, V. N. and Thomas, G. A. N. (2010). Analysis of borehole jack records, *20th IAHR International Symposium on Ice*.

Sinha, N. K. (1986). The Borehole jack: Is it a useful arctic tool?, *Proceedings of the Fifth (1986) International Offshore Mechanics and Arctic Engineering Symposium*, Vol. IV, NRC Publications Archive (NPArC), pp. 328 – 335.

Sinha, N. K. (2011). Borehole indentor - A tool for assessing in-situ bulk ice strength and micromechanics, *Cold Regions Science and Technology* .

Sinha, N. K., Shkhinek, K. and Smirnov, V. (2012). On borehole indentor BHI measurements and analysis, *Cold Regions Science and Technology* .

Timco, G. W. and Weeks, W. F. (2009). A rewiew of the engineering properties of sea ice, *Cold Regions Science and Technology* .

Appendices

A Equipment check-list

A.1 Drilling

1. Stihl engine and fuel.
2. 150 mm core drill.
3. 150 mm auger.
4. Connector and safety pin between 1 and 2/3.
5. Allen key.

A.2 The borehole jack

1. BHJ (jack, engine, pump, sledge, cover).
2. Chain and pin.
3. Strops.
4. CR1000 Wiring Panel (Data logger).
5. 2x 12 V batteries (charged) for 4.
6. Generator (capacity depending on ice conditions).
7. Extension cord.
8. Laptop w/ Com Port cable.
9. CR1000KD (Data display).
10. Fuel for Stihl engine (mixed with oil).
11. Fuel for generator (not mixed with oil).

A.3 Optional

1. Waterproof gloves.
2. Sledge (for transporting BHJ and generator).
3. Meter stick (pref. w/ hook in end).
4. Slide caliper for young ice accurate ID.
5. Tape line (25 m if large grid).
6. Spade.

7. Sieve (to remove slush in hole).
8. Iron bar (to knock loose cores).
9. Axe (make room for pincers).
10. Pincers (to extract cores).
11. Manual small drill (for temp. measurements of core).
12. Thermometer.
13. Sampling bags.
14. Salinity boxes.
15. Scale.
16. Slide caliper for precise measurements of test depth if close to the surface.

A.4 Standard

1. Pen and paper.
2. Headlight.
3. Camera.
4. Memory stick.
5. Watch.

B Calibration data

Table B.1: Data from calibration 6th of March 2012.

CR1000 [mV]	Knekkis [kN]
12	0
80	5
163	10
333	20
505	30
680	40
860	50
1025	60

C Grid AB

Table C.1: Main results from Grid AB.

Test	BH	FT	C_{min} [cm]	U/D [$s^{-}1$]	T [°C]	σ_f [MPa]	t_f [s]	$\dot{\sigma}_{af}$ [MPa/s]
1	A1.1	FS	22	0.39	-	-	-	-
2	A1.2	UY3	24	0.42	-	3.3	4.0	0.8
3	A1.3	UY1	30	0.37	-	11.4	8.8	1.3
4	A1.4	UY4	27	0.42	-	4.3	4.8	0.9
5	A1.5	UY4	23	0.43	-	3.6	4.8	0.7
6	A1.6	UY3	30	0.40	-	3.5	4.2	0.8
7	A1.7	FS	22	0.41	-	-	-	-
8	Fail	-	-	-	-	-	-	-
9	A2.6	UY4	24	0.44	-	3.3	8.8	0.4
10	A2.5	UY2	19	0.47	-	3.7	5.0	0.7
11	A2.4	AS	25	0.33	-	18.3	-	-
12	A2.3	UY1	22	0.44	-	10.5	9.2	1.1
13	A2.2	UY2	23	0.37	-	17.0	5.0	3.4
14	A3.1	UY1	28	0.34	-	17.9	6.0	3.0
15	A2.1	UY4	32	0.35	-	17.2	7.8	2.2
16	A3.2	UY1	25	0.38	-	12.6	8.6	1.5
17	A3.3	UY1	24	0.48	-	3.6	3.8	1.0
18	A3.4	AS	23	0.37	-	15.3	-	-
19	A3.5	AS	28	0.38	-	14.9	-	-
20	A4.3	AS_{max}	31	-	-	18.6	-	-
21	A4.2	UY4	15	0.52	-	2.7	3.0	0.9
22	A4.1	UY1	25	0.50	-	10.0	4.8	2.1
23	A5.1	UY4	18	0.46	-	8.9	3.2	2.8
24	Fail	-	-	-	-	-	-	-
25	A5.4	UY1	15	0.46	-	9.0	5.0	1.8
26	A5.5	AS_{max}	28	-	-	18.8	-	-
27	A6.2	AS	27	0.32	-	17.9	-	-
28	B1.2	UY3	15	0.40	-	8.5	4.2	2.0
29	B2.1	UY1	21	0.40	-	14.6	8.2	1.8
30	B3.2	AS_{max}	28	-	-	18.5	-	-

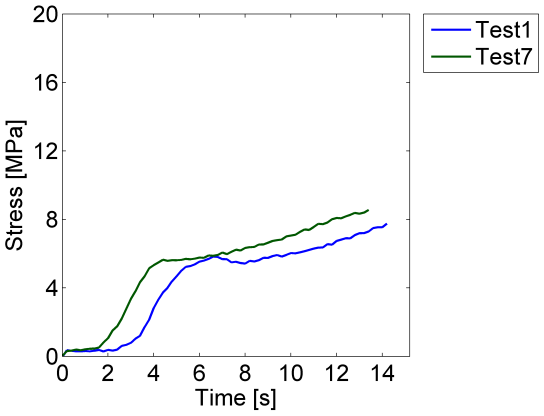

Figure C.1: FS failures of Grid AB.

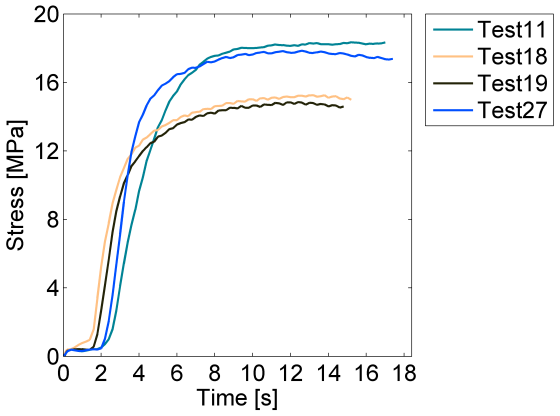

Figure C.2: AS failures of Grid A and B.

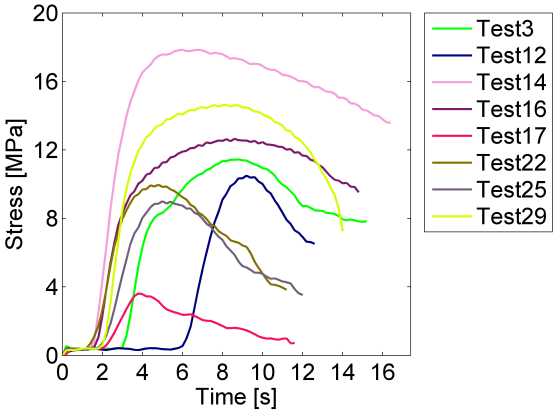

Figure C.3: UY1 failures of Grid AB.

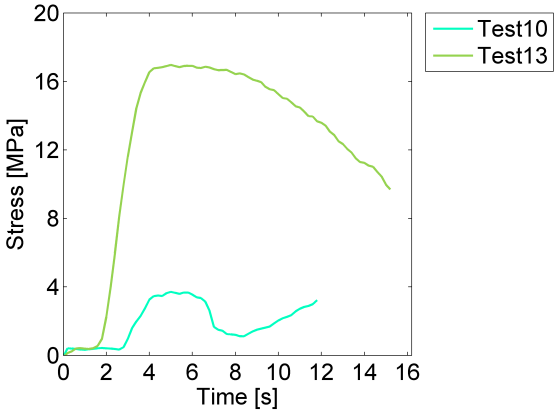

Figure C.4: UY2 failures of Grid AB.

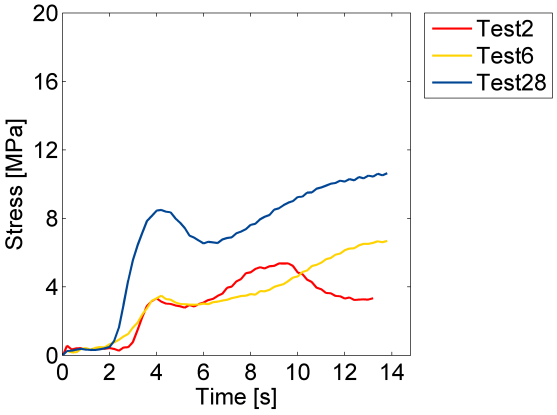

Figure C.5: UY3 failures of Grid AB.

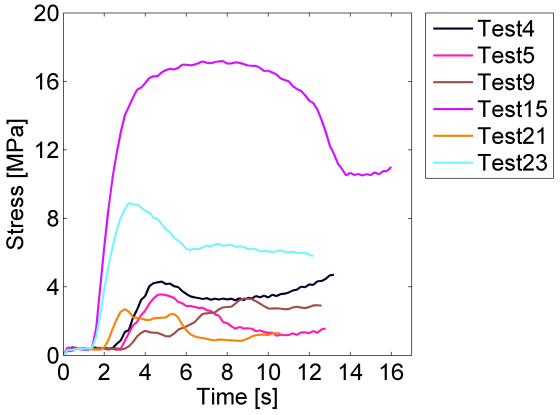

Figure C.6: UY4 failures of Grid AB.

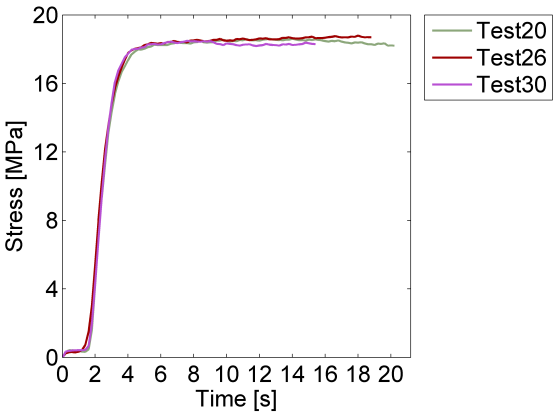

Figure C.7: AS_{max} failures of Grid AB.

D Grid CD

Table D.1: Main results from Grid C.

Test	BH	FT	C_{min} [cm]	U/D [s$^-$1]	T [°C]	σ_f [MPa]	t_f [s]	$\dot{\sigma}_{af}$ [MPa/s]
1	C5.5	UY1	18	0.46	-2.0	15.9	5.6	2.8
2	C5.4	UY1	17	0.43	-2.1	16.9	7.0	2.4
3	C5.3	AS_{max}	21	-	-2.3	18.5	-	-
4	C5.2	FS	26	0.67	-2.2	-	-	-
5	C5.1	AS_{max}	23	-	-2.9	19.1	-	-
6	C4.1	UY1	21	0.51	-2.5	18.6	7.2	2.6
7	C4.2	UY3	23	0.56	-2.7	15.9	4.4	3.6
8	C4.3	UY3	24	0.59	-2.1	17.9	4.0	4.5
9	C4.4	UY1	15	0.58	-1.8	15.8	4.6	3.4
10	C4.5	UY4	14	0.62	-2.0	10.1	3.4	3.0
11	C3.5	UY1	19	0.48	-2.1	17.3	6.2	2.8
12	C3.4	UY4	20	0.49	-1.8	14.1	5.6	2.5
13	C3.3	UY1	21	0.39	-2.0	16.2	8.2	2.0
14	C3.2	AS	24	0.41	-1.8	17.3	-	-
-	C3.1	-	-	-	-1.8	-	-	-
15	C2.1	AS	24	0.36	-2.1	18.1	-	-
16	C2.2	UY1	22	0.42	-2.1	17.5	9.0	1.9
17	C2.3	AS	22	0.38	-2.0	18.2	-	-
18	C2.4	UY1	20	0.47	-2.1	16.9	7.6	2.2
19	C2.5	UY1	21	0.52	-2.1	17.6	5.0	3.5
20	C1.5	UY2	21	0.42	-2.2	18.2	8.2	2.2
21	C1.4	UY3	24	0.57	-2.2	14.7	3.6	4.1
22	C1.3	UY1	24	0.51	-2.1	16.7	6.0	2.8
23	C1.2	UY1	21	0.47	-2.1	17.1	7.4	2.3
24	C1.1	UY1	24	0.42	-2.2	17.7	8.0	2.2

Table D.2: Main results from Grid D.

Test	BH	FT	C_{min} [cm]	U/D [s$^-$1]	T [°C]	σ_f [MPa]	t_f [s]	$\dot{\sigma}_{af}$ [MPa/s]
25	D2.2	AS	21	0.27	-2.1	16.5	-	-
26	D3.1	AS	24	0.29	-2.3	16.7	-	-
27	D1.3	UY1	20	0.33	-2.2	16.7	9.8	1.7
28	D3.3	UY2	20	0.33	-2.0	17.0	9.0	1.9
29	D1.2	UY1	22	0.40	-2.3	17.3	6.6	2.6
30	D1.1	UY4	21	0.48	-2.3	17.1	4.6	3.7
31	D2.3	UY3	20	0.50	-2.2	16.8	4.8	3.5
32	D3.2	UY1	21	0.47	-2.2	16.8	7.0	2.4
33	D2.1	UY1	22	0.48	-2.3	16.6	6.0	2.8

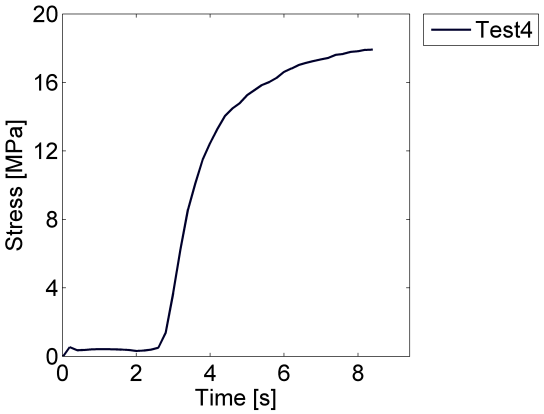

Figure D.1: FS failure of Grid C.

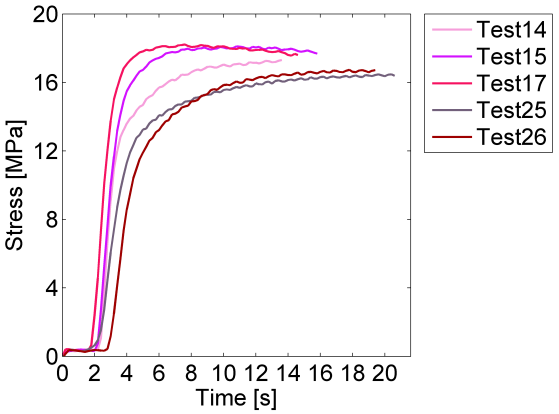

Figure D.2: AS failures of Grids CD.

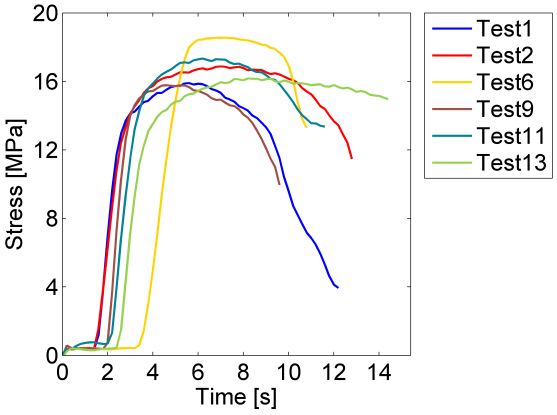

Figure D.3: UY1 failures of Grid C.

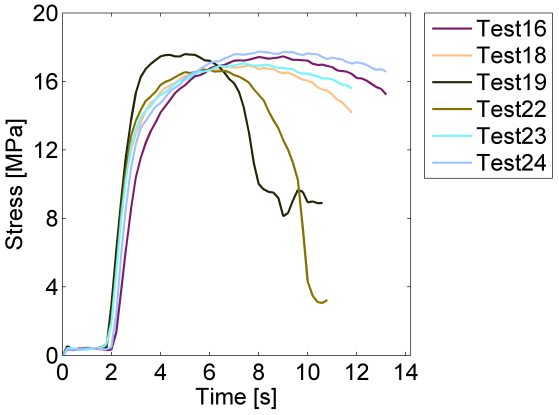

Figure D.4: UY1 failures of Grid C.

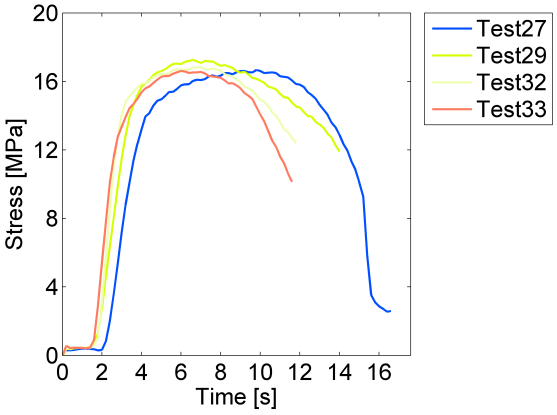

Figure D.5: UY1 failures of Grid D.

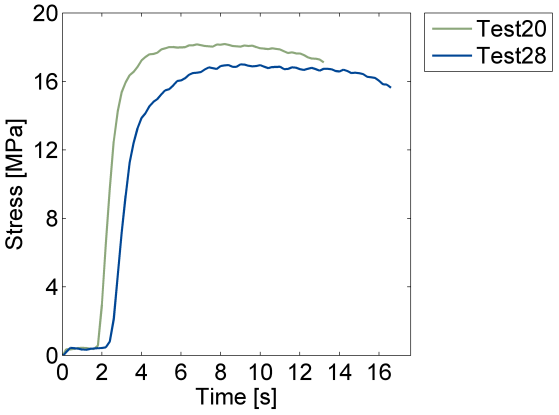

Figure D.6: UY2 failures of Grid C and D.

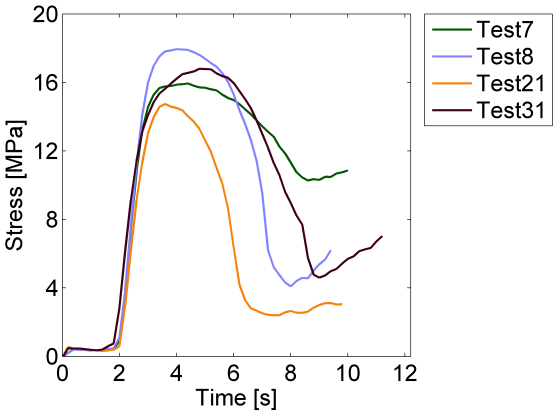

Figure D.7: UY3 failures of Grid C and D.

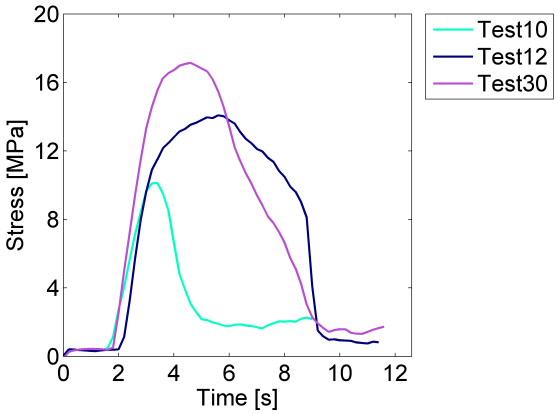

Figure D.8: UY4 failures of Grid C and D.

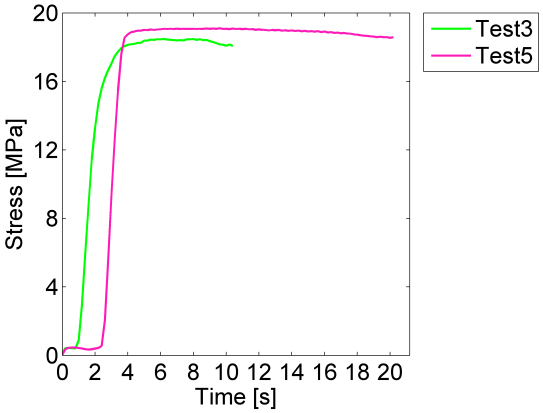

Figure D.9: AS_{max} failures of Grid C and D.

E Grid EFG

Table E.1: Main results from Grid E.

Test	BH	FT	C_{min} [cm]	U/D [s^{-}1]	T [°C]	σ_f [MPa]	t_f [s]	$\dot{\sigma}_{af}$ [MPa/s]
1	E1.1	FAIL	-	-	-	-	-	-
2	E2.1	UY3	10	0.53	-2.6	10.3	3.2	3.2
3	E2.2	UY4	10	0.48	-2.8	11.1	3.6	3.1
4	E1.2	P	9	-	-2.9	8.6	3.0	2.9
5	E3.2	UY3	10	0.51	-2.9	12.9	3.4	3.8
6	E3.1	UY3	9	0.50	-2.2	10.9	3.4	3.2
7	E4.1	UY3	20	0.43	-3.6	14.3	4.8	3.0
8	E4.2	UY4	22	0.27	-3.1	18.7	5.0	3.7
9	E4.3	AS	15	0.26	-2.6	18.3	-	-
10	E3.3	UY3	10	0.38	-3.4	13.6	4.0	3.4
11	E2.3	UY3	9	0.42	-2.8	11.0	3.8	2.9

Table E.2: Main results from Grid F.

Test	BH	FT	C_{min} [cm]	U/D [s^{-}1]	T [°C]	σ_f [MPa]	t_f [s]	$\dot{\sigma}_{af}$ [MPa/s]
1	F3.3	UY4	10	0.38	-	11.9	3.8	3.1
2	F1.3	UY3	9	0.42	-	10.7	4.0	2.7
3	F1.1	UY3	10	0.48	-	9.6	3.0	3.2
4	F3.1	UY4	9	0.51	-	13.4	3.2	4.2
5	F2.1	UY3	10	0.53	-	11.5	2.8	4.1
6	F1.2	UY3	9	0.53	-	12.0	3.4	3.5
7	F2.2	UY4	10	0.57	-	8.9	2.8	3.2
8	F2.3	P	27	0.51	-	13.8	2.6	5.3
9	F3.2	UY3	19	0.57	-	7.8	5.8	1.3

Table E.3: Main results from Grid G.

Test	BH	FT	C_{min} [cm]	U/D [s^{-}1]	T [°C]	σ_f [MPa]	t_f [s]	$\dot{\sigma}_{af}$ [MPa/s]
1	G1.1	P	8	0.53	-	11.0	2.6	4.2
2	G2.1	UY1	18	0.46	-	18.0	4.4	4.1
3	G3.1	P	10	0.59	-	10.2	3.0	3.4
4	G3.2	UY3	19	0.49	-	18.7	3.4	5.5
5	G3.3	P	10	0.60	-	11.8	2.4	4.9
6	G2.3	UY1	20	0.53	-	17.2	5.0	3.4
7	G1.3	UY4	18	0.56	-	13.9	3.0	4.6
8	G1.2	P	9	0.56	-	10.0	2.8	3.6
9	G2.2	UY4	20	0.56	-	14.7	3.2	4.6

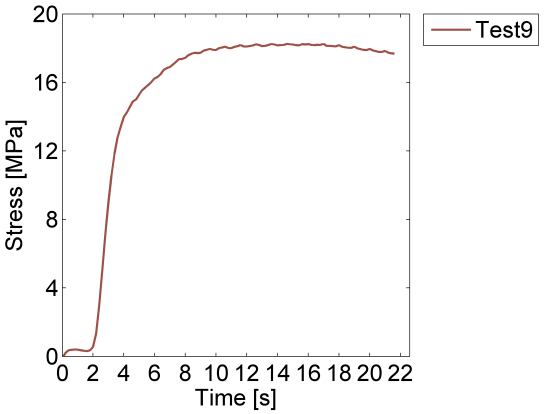

Figure E.1: AS failure of Grid E.

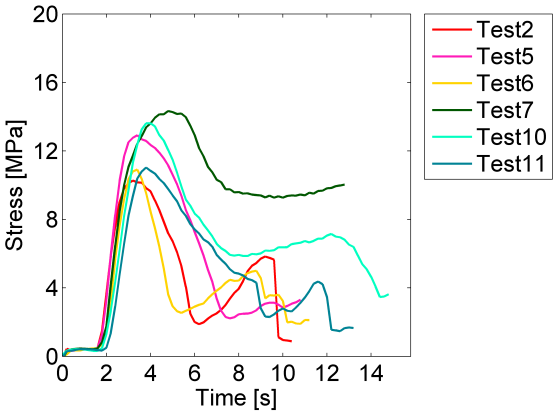

Figure E.2: UY3 failures of Grids E.

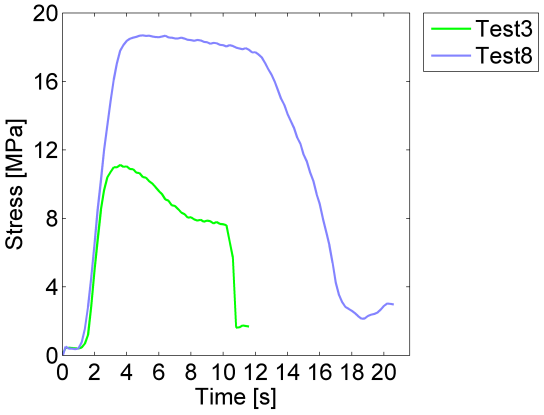

Figure E.3: UY4 failures of Grid E.

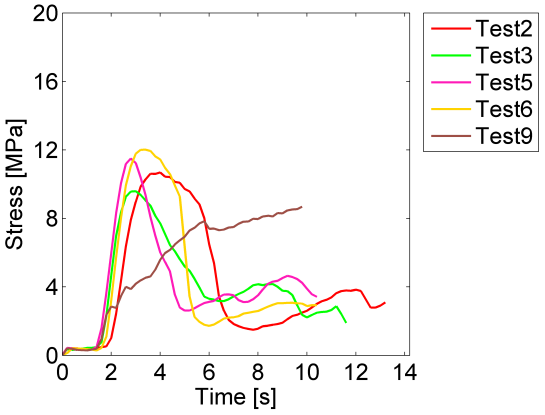

Figure E.4: UY3 failures of Grid F.

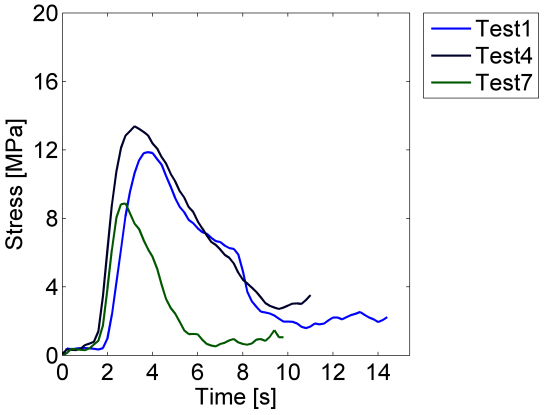

Figure E.5: UY4 failures of Grid F.

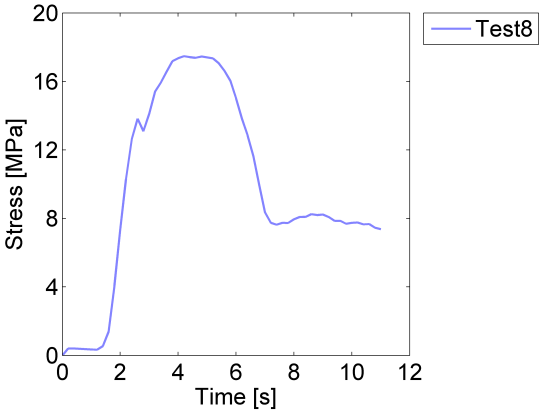

Figure E.6: P failure of Grid F.

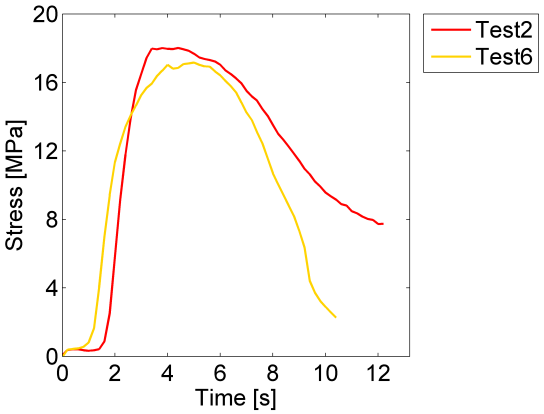

Figure E.7: UY1 failures of Grid G.

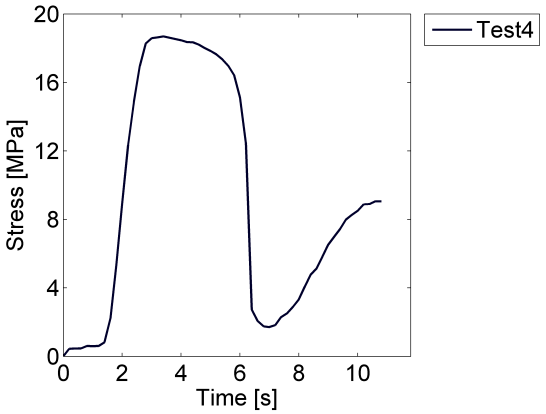

Figure E.8: UY3 failure of Grid G.

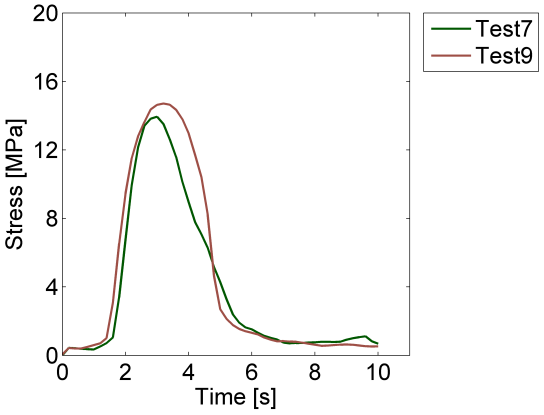

Figure E.9: UY4 failures of Grid G.

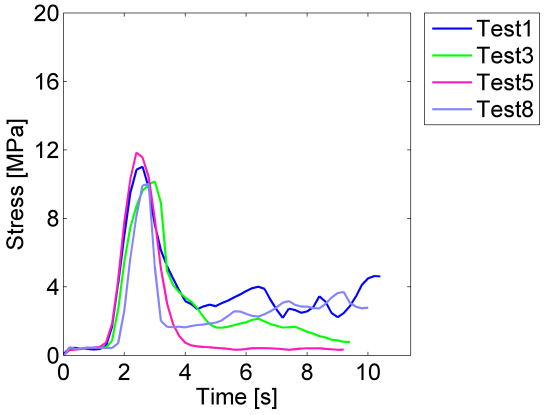

Figure E.10: P failures of Grid G.

F Grid H

Table F.1: Main results from Grid H.

Test	BH	FT	C_{min} [cm]	U/D [s^{-}1]	T [°C]	σ_f [MPa]	t_f [s]	$\dot{\sigma}_{af}$ [MPa/s]
1	H1	FS	29	0.33	-2.9	-	-	-
2	H1	AS	32	0.26	-3.7	18.7	-	-
3	H2	AS_{max}	32	-	-4.8	19.3	-	-
4	H2	AS_{max}	42	-	-3.3	19.2	-	-
5	H3	AS_{max}	32	-	-4.9	19.5	-	-
6	H3	UY1	52	0.42	-3.3	18.0	9.8	1.8
7	H3	UY1	24	0.62	-2.6	3.9	2.6	1.5
8	H5	$UY3_{max}$	37	-	-6.0	19.3	5.0	3.9
9	H5	P	10	0.58	-3.2	6.0	2.2	2.7
10	H6	AS_{max}	33	-	-4.9	19.4	-	-
11	H7	AS_{max}	37	-	-5.8	19.5	-	-
12	H7	FS	50	0.41	-2.8	-	-	-
13	H7	UY1	16	0.66	-2.4	2.9	3.6	0.8
14	H8	P	13	0.48	-3.8	12.6	2.8	4.5
15	H9	AS_{max}	18	-	-4.5	19.3	-	-
16	H10	AS_{max}	37	-	-4.9	19.6	-	-
17	H10	FAIL	-	-	-	-	-	-
18	H11	AS_{max}	37	-	-4.4	18.8	-	-
19	H12	AS_{max}	18	-	-4.1	19.5	-	-
20	H13	AS_{max}	16	-	-3.9	19.3	-	-
21	H14	AS_{max}	31	-	-4.3	19.4	-	-

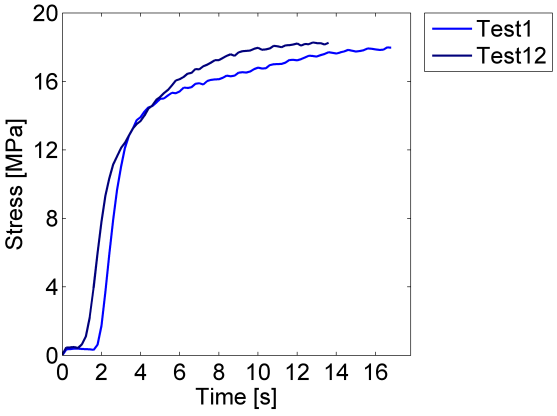

Figure F.1: Flow stress failures of Grid H.

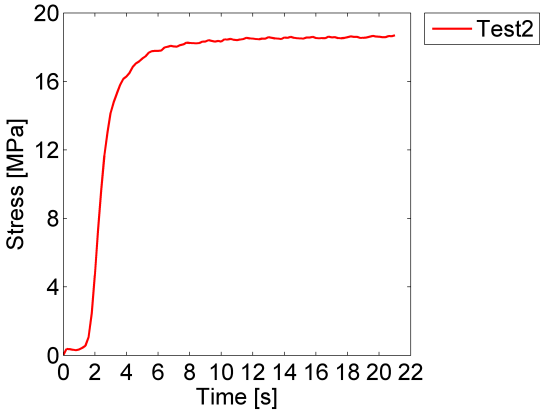

Figure F.2: Asymptotic failure of Grid H.

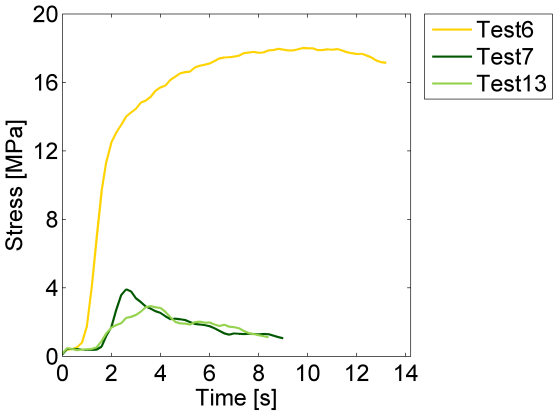

Figure F.3: UY1 failures of Grid H.

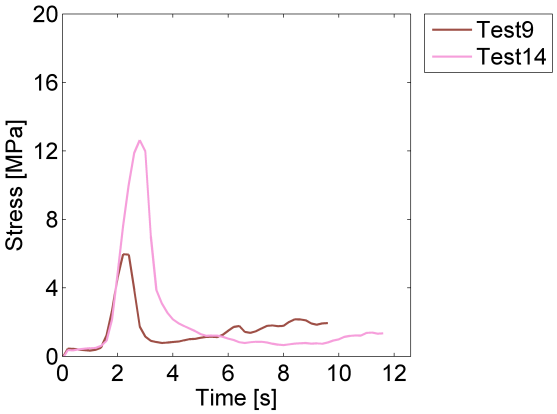

Figure F.4: P failures of Grid H.

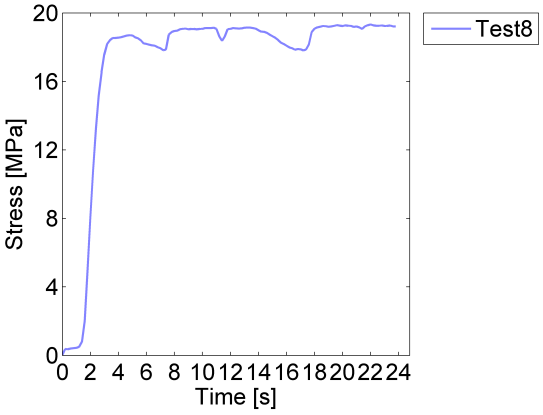

Figure F.5: UY3$_{max}$ failure of Grid H.

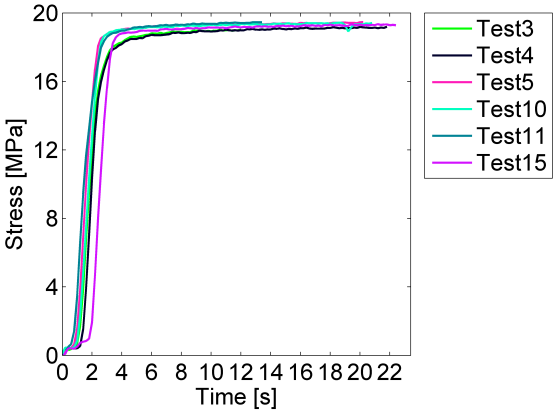

Figure F.6: AS$_{max}$ failures of Grid H.

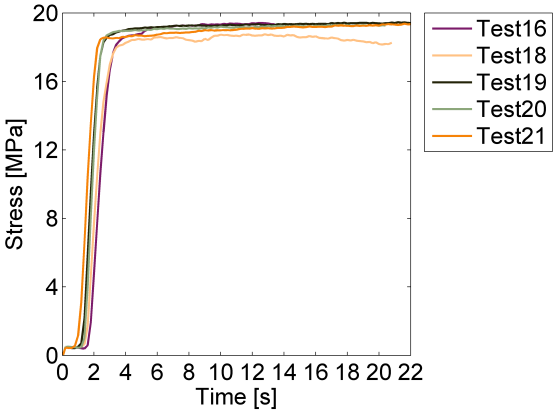

Figure F.7: AS$_{max}$ failures of Grid H.